6-2011

Elasto-Plastic Lateral Torsional Buckling of Steel Beams with Perforated Web

Mohammad Iqbal Mohammad Hesham Martini

جامعة الإمارات العربية المتحدة
United Arab Emirates University

UAEU

Master Program of Civil Engineering
Department of Civil and Environmental Engineering
Faculty of Engineering
United Arab Emirates University

Thesis Title:

Elasto–Plastic Lateral Torsional Buckling of Steel Beams with Perforated Web

Author's Name:

Mohammad Iqbal Mohammad Hesham Martini

Principal Supervisor:

Dr. Amr Mahmoud Sweedan
Assistant Professor of Structural Engineering
Department of Civil and Environmental Engineering
Faculty of Engineering
United Arab Emirates University

Co–Supervisor:

Dr. Khaled Mahmoud El-Sawy
Associate Professor of Structural Engineering
Department of Civil and Environmental Engineering
Faculty of Engineering
United Arab Emirates University

جامعة الإمارات العربية المتحدة
United Arab Emirates University

UAEU

Certificate of Examination

Examination Committee

Dr. Michael J. Tait (External Examiner)
Associate Professor of Structural Engineering
Faculty of Engineering
McMaster University, Canada
Hamilton, Ontario, Canada.

Dr. Bilal El-Ariss (Internal Examiner)
Associate Professor of Structural Engineering
Faculty of Engineering
United Arab Emirates University
Al-Ain, Abu Dhabi, UAE.

Dr. Amr Sweedan (Principal Supervisor)
Assistant Professor of Structural Engineering
Faculty of Engineering
United Arab Emirates University
Al-Ain, Abu Dhabi, UAE.

Dr. Khaled El-Sawy (Co-Supervisor)
Associate Professor of Structural Engineering
Faculty of Engineering
United Arab Emirates University
Al-Ain, Abu Dhabi, UAE.

The thesis by
Mohammad Iqbal Mohammad Hesham Martini

Entitled:
Elasto–Plastic Lateral Torsional Buckling of Steel Beams with Perforated Web

is accepted in partial fulfillment of the
requirements for the degree of
Master of Science in Civil Engineering

June 1 ,2011

ABSTRACT

I–shaped steel members represent the basic structural element in the majority of steel structures. Perforated–web I–shaped steel sections have been used as structural members since the Second World War in an attempt to enhance the flexural behavior of traditional solid–webbed I–shaped steel sections without increasing the cost of the material. In general, two types of web perforations are commonly used in engineering practice; hexagonal and circular. Although, the main intent of the perforation process is to produce stiffer I–sections by increasing the web height and providing higher major–axis flexural capacity than solid–webbed members of the same weight, it also provides access to services and optimizes the use of the costly structural steel material. Moreover, the appealing aesthetical appearance of perforated–web members make them essential elements in construction of exposed steel structures. These advantages, combined with the significant development in computerized manufacturing equipments, have led to the wide spread use of perforated steel members with a variety of geometries suitable for various loading conditions in different structural applications.

Structural designs are always attracted by the fact that the augmentation of the cellular section height, compared to its original solid counterpart, enhances its in–plane structural characteristics. It should be noted, however, that the non–uniformity in the beam's cross section due to the presence of web perforations may have an adverse effect on the in–plane flexural capacity of cellular beams in case of instability failure before reaching their full flexural capacity. Web perforations are also expected to influence the response of these beams and the associated potential failure modes. The elastic lateral stability of cellular steel beams is typically a concern during the construction stage when lateral bracing elements are

not yet installed. However, the inelastic lateral buckling behavior of cellular beams is more likely to be faced in practice, as a result of yielding in the outmost fibers of the beam before commencement of buckling. The load carrying capacity of these beams is influenced by its global buckling, local buckling of cross section elements and also by the discontinuities in the cross section due to the web perforations. Unfortunately, current design codes do not provide direct guidelines to address lateral torsional buckling of perforated steel beams.

The present research work is concerned with the lack of information pertaining to lateral stability of cellular steel beams subjected to flexure. This research presents a literature survey for experimental and numerical studies related to structural behavior of perforated steel beams with emphasis on the buckling response of castellated and cellular I–shaped steel beams. The study is carried out numerically using a detailed three dimensional finite element modeling using the general purpose software package ANSYS. The developed model takes into consideration material and geometrical non–linearities. The adopted mesh is selected to allow various deformations and rotations associated with global and local buckling modes of such beams to be captured (simulated). The developed model is validated by simulating various analytical and experimental case studies that have been reported in the literature. The validated finite element model is utilized to perform extensive buckling analyses of simply supported cellular steel beams subjected to equal end moments, mid–span concentrated load, and uniformly distributed load. Conducted buckling analyses cover a wide spectrum of practical geometrical dimensions and perforation patterns of I–shaped cellular beams.

A total of 11,340 cases of analyses are performed to investigate the influence of load application location on the elastic lateral torsional buckling of I–shaped cellular beams. Conducted analyses consider various cases of loading that are applied at the top and bottom

flange levels of the modeled beams. The impact of various cross sectional dimensions, beam slenderness, and web openings size and spacing on the elastic buckling capacity is investigated under different types of loads. Results of conducted analyses are utilized to evaluate the variation of the moment gradient factor C_b relative to a non–dimensional factor k_e that relates the warping rigidity to the torsional rigidity of cellular beams. Results are compared with those reported in the literature for loading at the shear center of beams. The comparison reveals a clear destabilizing effect for loads applied at the top flange level. On the contrary, loads applied at the bottom flange level enhance the lateral stability of cellular beams. Long span cellular beams are shown to buckle with pure lateral torsional buckling mode (LTB). Buckling of intermediate span beams is controlled by lateral distortional buckling (LDB) where web distortion occurs simultaneously with lateral deformations. Buckling of short span beams is dominated by a high level of web distortion due to the high shear stresses induced in the web. This particular behavior is shown to be consistently coupled with a significant reduction in the C_b value.

The study also covers the inelastic lateral buckling of cellular beams loaded at their shear center. A single steel material type is considered; namely A36 according to the American standards AISC 360–05. A comprehensive parametric study that includes 2,268 cases of analyses is conducted to evaluate the impact of various cross section dimensions, beam slenderness, different types of loads, and web openings size on the inelastic buckling capacity and their associated modes for cellular steel beams. Consistent with the case of elastic buckling, outcomes of the inelastic investigation are discussed by presenting the variation of the moment gradient factor C_b with respect to the non–dimensional factor k_e. Similar to the observed elastic buckling response, long span cellular beams are shown to experience inelastic lateral buckling due to lateral torsional buckling (LTB) or lateral

distortional buckling (LDB). Cellular beams with intermediate span length experience interaction between lateral buckling and local web shear deformations at buckling. The buckling of short span cellular beams is governed by high level of web distortion that results from the high shear stresses induced in the web. In such a case, no lateral buckling occurs and significant reduction in C_b values takes place. Several moment gradient factor C_b ranges that correspond to various buckling modes experienced by the wide range of dimensions considered in the simulation study are identified. This categorization takes into consideration possible interaction between global buckling modes and localized deformations of the cross section elements.

Keywords: cellular beam, castellated beam, perforated web, lateral torsional buckling, lateral distortional buckling, elastic buckling, inelastic buckling, major–axis moment capacity, moment–gradient factor, finite element method, buckling modes, load application location.

ACKNOWLEDGEMENTS

The author would like to start by expressing his truly thanks for the almighty God, Allah, for showering us with his countless favors, endless kindness and vast mercy. Without his right and straightforward guidance, this study would never be produced. The author hope that almighty God, Allah, strengthen our belief and trust in him, accept our good deeds and purify them from any duplicity.

The author would like to express his sincere gratitude and gratefulness to his thesis supervisors, Dr. Amr M ahmoud Sweedan and Dr. Khaled Mahmoud El-Sawy, for their valuable guidance, precious advice, supportive assistance, helpful cooperation and unlimited time he received throughout his graduate studies. Without their noble approach, this study would never be completed. Their precious efforts made this dissertation possible.

Particular thanks are due to the faculty and staff members of the Civil and Environmental Engineering Department at UAEU for their support and encouragement.

The author wishes to express his gratitude to his family including his brothers, sisters and relatives for their constant encouragement and morale support that gave him the strength and confidence to complete his master degree.

The author would like to extend his acknowledgment to his wife for her dedication, faith in him, patience, and continuous encouragement during the period of this study.

Finally, the author would like to take this opportunity to express his sincere gratitude and appreciation to the most important people in his life, his father and mother. He is truly thankful for their untold blessing, which have always been the source of motivation in achieving any success in his life. He would like to thank them from the bottom of his heart for their immeasurable sacrifices, continuous genuine love and immense help. Last but not least, the author prays to Allah to bless and award them by his enormously generosity, honestly forgiveness and heavenly Paradise.

TABLE OF CONTENTS

Page

LIST OF TABLES

LIST OF FIGURES

Figure **Page**

LIST OF NOTATIONS

A_f: Area of flange plate (mm^2)

A_w: Area of web plate (mm^2)

b: Width of each element of I–shaped cross–section (mm)

b_f: Flange width of beam (mm)

b_f/t_f: Flange width–to–thickness ratio (flange aspect ratio)

b_i: Width of the rectangular components of the I–beam's cross section (mm)

C_b: Moment gradient factor

C_w: Warping torsional constant of the cross section (mm^6)

d: Diameter of web hole (hole size) of castellated beams (mm)

d_h: Diameter of circular web hole (hole size) of cellular beams (mm)

d_h/h_w: Hole diameter–to–web height ratio

$\mathrm{d}\{F\}$: Load increment (N)

$\{\mathrm{d}F\}$: Change in nodal forces (load) (N)

$\|d\{F\}\|$: Norm of change in nodal forces (load) (N)

$\{\mathrm{d}u\}$: Change in nodal displacements (mm)

$\frac{du}{dz}$: Derivative of lateral (horizontal) deflection of cross section with respect to length

$\frac{dv}{dz}$: Derivative of vertical deflection of cross section with respect to length

$\frac{d\phi}{dz}$: Derivative of twist angle of cross section with respect to length (mm^{-1})

$\frac{d^3\phi}{dz^3}$: Third derivative of twist angle of cross section with respect to length cube (mm^{-3})

E: Young's modulus of elasticity (N/mm^2 or MPa)

E_t: Strain hardening modulus (N/mm^2 or MPa)

E_T: Tangent Young's modulus (N/mm^2 or MPa)

EC_w : Warping rigidity (N.mm^4)

$\{F\}$: Nodal forces (or nominal load vector) (N)

$\{F_n\}$: Nodal forces (loads) of increment n (N)

F_r: Material residual stress (N/mm^2 or MPa)

F_u: Ultimate stress (N/mm^2 or MPa)

F_y: Yield stress (N/mm^2 or MPa)

G: Shear modulus of elasticity (N/mm^2 or MPa)

G_T: Tangent shear modulus (N/mm^2 or MPa)

GJ: Saint–Venant's torsional rigidity (N.mm^2)

h: Total height (depth) of beam (mm)

h_o: Height between centers of top and bottom flanges of beam (mm)

h_w: Web height of beam (mm)

h_w/t_w: Web height–to–thickness ratio (web slenderness)

I_f: Second moment of area for one flange about the y–axis of the beam (mm^4)

I_y: Minor–axis moment of inertia of the cross section of the beam (mm^4)

i: Iteration index

J: Torsional constant of the cross section (mm^4)

J_{net}: Torsional constant of net cross section at center of the web hole (mm^4)

j: Counter variable

$[K]$: Total stiffness matrix of the structure (N/mm)

$[K_E]$: Constant elastic small–strain stiffness matrix (N/mm)

$[K_G]$: Geometrical stiffness matrix (N/mm)

$[K_T]$: Tangent stiffness matrix (N/mm)

$[K_T]_i$: Tangent stiffness matrix of iteration i (N/mm)

$[K_T]_1$: New tangent stiffness matrix of iteration 1 (N/mm)

$[K_T]_o$: Tangent stiffness matrix at the end of the previous load increment (N/mm)

$[K_\sigma]$: Stress stiffness matrix of the structure (N/mm^2)

k_e: Non–dimensional factor relates the warping rigidity to the torsional rigidity of cellular beams

L: Unbraced span length of the beam (mm)

L_b: Laterally unbraced length of the beam (mm)

L_p: Unbraced length for the limit state of yielding (mm)

L_r: Unbraced length for the limit state of inelastic lateral torsional buckling (mm)

LDB: Lateral distortional buckling mode

LTB: Lateral torsional buckling mode

M: Uniform bending moment case due to pure end moments (N.mm)

M_{cr}: Critical lateral torsional buckling moment for an I–shaped beam under uniform bending moment case (N.mm)

M_{FE}: Finite element moment resulted from finite element analysis (N.mm)

M_{FE-M}: Finite element buckling moment due to uniform moment distribution (N.mm)

M_{FE-P}: Finite element buckling moment due to concentrated mid–span load (N.mm)

M_{FE-W}: Finite element buckling moment due to uniformly distributed load (N.mm)

M_{inel}: Inelastic lateral torsional buckling strength of an I–shaped beam (N.mm)

M_n: Nominal lateral torsional buckling moment of an I–shaped beam subjected to a specific transverse load (N.mm)

M_{n-el}: Nominal elastic critical lateral torsional buckling moment of an I–shaped beam subjected to a specific transverse load (N.mm)

$M_{n-el(max)}$: Maximum elastic lateral torsional buckling moment strength of an I–shaped beam subjected to a specific transverse load (N.mm)

$M_{n\text{-}inel}$: Nominal inelastic critical lateral torsional buckling moment of an I–shaped beam subjected to a specific transverse load (N.mm)

M_o: Constant (uniform) moment acting in the plane of an I–shaped beam's web (N.mm)

M_{o-cr}: Critical buckling moment acting in the plane of the beam's web (N.mm)

M_p: Plastic moment capacity of an I–shaped beam (N.mm)

M_r: Maximum elastic lateral torsional buckling moment of the beam (N.mm)

M_{SV}: Saint–Venant's pure torsion moment (N.mm)

M_T: Total torsional moment (N.mm)

M_w: Warping torsion component (N.mm)

M_x: External constant bending moment (N.mm)

$M_{x'}$: Moment component about the x' axis (N.mm)

$M_{y'}$: Moment component about the y' axis (N.mm)

$M_{z'}$: Moment component about the z' axis (N.mm)

n: Increment index or counter

P: Mid–span concentrated load case (N)

P_{cr}: Critical buckling load for mid–span concentrated load case (N.mm)

P_{exp}: Experimental conducted buckling load for mid–span concentrated load case (N)

$\{R_i\}$: Residual force vector of iteration index i (N)

$\|\{R_i\}\|$: Norm of the residual forces (N)

$\{R_1\}$: Residual forces vector of iteration index 1 (N)

S_x: Elastic section modulus about x axis (mm^3)

s: Spacing between successive two holes (mm)

t: Thickness of each element of the I–shaped cross–section (mm)

t_f: Flange thickness of beam (mm)

t_f : Thickness of the rectangular components of the I–beam's cross section (mm)

t_w: Web thickness of beam (mm)

U_x: Out–of–plane displacements (mm)

U_y: Vertical displacements (mm)

U_z: Longitudinal displacements (mm)

u: Variable length in x axis direction (mm)

$\{u\}$: Nodal displacements vector (mm)

$\{u_i\}$: Total incremental nodal displacements vector at the end of iteration i (mm)

$\{u_n\}$: Nodal displacements vector of increment n (mm)

v: Variable length in y axis direction (mm)

W: Uniformly distributed load case (N/mm)

W_{cr}: Critical buckling load for uniformly distributed load case (N.mm)

W_y: Uniformly distributed load applied in the direction of y axis (N/mm)

W_z: Uniformly distributed load applied in the direction of z axis (N/mm)

WLB: Web local buckling mode

x_e: Distance between edge of castellated beams and center of first web hole (mm)

x' : Transformed x–coordinate of the buckled section

y' : Transformed y–coordinate of the buckled section

z: Variable length in z axis direction (mm)

z' : Transformed z–coordinate of the buckled section

$\Delta\{u_1\}$: Total incremental deformation (mm)

$\|\Delta\{u_i\}\|$: Norm of total incremental deformation (mm)

$\delta\{u_i\}$: Iterative deformation vector (mm)

$\delta\{u_1\}$: First iterative solution for the deformations (mm)

$\|\delta\{u_i\}\|$: Norm of the iterative deformation (mm)

ε: Strain in the element

ϕ: Angle of twist of the cross section (radian)

λ: Eigenvalue or load multiplier

λ_1: Lowest eigenvalue

$\lambda\sigma$: Stress level (N/mm^2)

$\lambda\{F\}$: Load vector (N)

ν: Poisson's ratio

σ: Existing stresses in the element (N/mm^2)

$\{\sigma\}$: Element stresses vector (mm)

σ_{cr}: Critical stress level in the element (N/mm^2)

CHAPTER 1

INTRODUCTION

1.1 PROBLEM STATEMENT

Perforated–web I–shaped steel sections have been used as structural members since the Second World War in an attempt to enhance the flexural behavior without increasing the cost of the material. In general, two types of web perforations are commonly used in engineering practice; hexagonal and circular. The hexagonal perforation pattern occurs during the typical manufacturing of castellated members by cutting the web longitudinally and reassembling it by welding. On the other hand, the circular web openings require special computerized cutting systems to create the cellular I–shaped members. Nowadays, with the advancement in computer–controlled cutting and welding technology, steel sections with circular web perforations are produced in a wide variety of geometries suitable for various loading conditions.

Beams are structural members that resist the applied load primarily by bending (flexure) and shearing actions. I–shaped beams subjected to flexure have much greater strength and stiffness in the plane of load application (i.e.; when bent about their major axis) than in the plane of minor axis. When a beam, with a solid or perforated web, is bent about its axis of greater flexural rigidity, out of plane bending and twisting (i.e., instability) will occur when the applied load reaches a critical value. This instability is referred to as lateral torsional buckling where the top flange and portion of the web act as a compression element that tends to buckle laterally resulting in twisting of the beam's cross section as shown in Fig.1.1. Unless these beams are properly braced against lateral deformation and twisting, they are subjected to the aforementioned instability mechanism, which is referred to as lateral

torsional buckling, prior to the attainment of their full flexural capacity when bent about their major axis. Lateral torsional buckling is a limit state of structural usefulness where the deformation of a beam changes from predominantly in plane deflection to a combination of lateral deflection and twisting while the load capacity remains first constant, before dropping off due to large deflection and yielding.

In the case of an I–shaped beam with a solid web, when a varying bending moment profile acts along the longitudinal axis of the beam, the lateral torsional buckling (LTB) moment is greater than when the beam is under uniform bending moment. This is reflected in the value of the moment gradient factor C_b, which is always greater than unity as specified by various international design codes and standards where C_b is defined as

$$C_b = \frac{\text{LTB Moment for the Case of Varying Bending Moment Profile}}{\text{LTB Moment for the Case of Uniform Bending Moment Profile}} \qquad (1.1)$$

For perforated beams, the non–uniformity in cross section properties d ue to the existence of web perforations increases the level of complexity of the behavior of these beams. Web perforations are also expected to influence the response of these beams and the associated potential failure modes. However, current design codes do not provide direct guidelines to address lateral torsional buckling of perforated steel beams.

1.2 OBJECTIVES OF THE STUDY

The present research work is concerned with the lack of information pertaining to stability of non–composite cellular steel beams. The load carrying capacity of these beams is influenced by global buckling, local buckling of cross section elements and discontinuities in the cross section due to the web perforations. In current practice, an approximate conservative approach is used where the properties of the weakest section, at the centre line

of the web holes, are considered to represent the behavior of the entire beam. In this study, the finite element method is employed to investigate the elasto–plastic lateral torsional buckling characteristics of cellular steel beams. A detailed three dimensional non–linear elasto–plastic (i.e., inelastic) finite element model is developed to simulate the behavior of such beams. The developed model is validated by comparing finite element predictions with other theoretical, numerical and experimental counterparts available in the literature. The validated finite element model is used to conduct extensive parametric analyses to assess the impact of various geometrical design parameters on the elasto–plastic stability of cellular steel beams. These parameters include the dimensions of the beam cross–section; flange width and thickness b_f and t_f, web height and thickness h_w and t_w, hole size d_h, and hole spacing s. Besides, the influence of load application level on the elastic stability of cellular beams is investigated. The study assesses the critical buckling load of all modeled beams along with the corresponding buckling modes. Several moment gradient factor C_b ranges that correspond to various buckling modes experienced by the wide range of dimensions considered in the simulation study are identified. Such assessment takes into consideration possible interaction between global buckling modes and localized deformations of the cross section elements.

The outcomes of the this study are expected to provide more insight into the behavior of cellular steel beams, which would enhance the level of understanding of the influence of the circular web perforations on the global stability of steel sections. In addition, findings of this research will enhance the effectiveness of the design of cellular steel beams by providing more realistic estimates of the moment gradient factor C_b associated with the various buckling modes.

1.3 HISTORICAL BACKGROUND

1.3.1 Castellated Beams

The concept of improving the material behavior and practices of design and construction is one of the main targets of structural engineers. Many attempts have been made to improve ways to reduce the cost of steel structures since the Second World War, where the shortage in construction material significantly increased its cost . The limited availability of materials led to the development of castellated beams. The term castellated stems from the external appearance of the castellated beam and its similarities with the castle battlements [Boyer (1964)]. This type of open–web beam is made by modifying a standard rolled shape by creating a regular pattern of holes in the web. Castellated beams are manufactured by using a typical rolled I–shaped steel beam and cutting a saw tooth (zigzag) pattern through its web, separating the two portions, staggering the top and bottom elements, and welding the member back together [Watson et al., (1974)] as shown in Figs. 1.2(a) through 1.2(c). Different geometries of castellation holes can be produced based on the sloping sides (the angle of the cut) and the length of the horizontal portion (welded joint length) as shown in Fig. 1.2(b).

A major advantage of castellated beams is the improved flexural strength due to the increased depth of the section without any additional weight of steel in order to enhance the structural performance against bending such as the enhancement of moment of inertia, section modulus, bending stiffness, flexural resistance and load carrying capacity of the section. Furthermore, the web openings allow easy, flexible, fast, and less expensive installation of building services. These services include heating, ventilating, and air conditioning (HVAC) ductwork, plumbing pipelines, and electrical conduits. These may pass through the structural depth of the beam rather than being hung from the bottom of the

structural elements (or access holes being cut in the web) which, in turn, reduces the floor–to–floor height.

1.3.2 Cellular Beams

Cellular beams are the modern style of the traditional castellated beams. They are open–web expanded steel beams. Their webs are perforated by large closely spaced circular openings over almost the full span with a variety of specified opening configurations. Unlike castellated beams, cellular beams have more flexibility in opening pitch, diameters and location. Due to their design and construction advantages, cellular beams have been widely used in steel construction for the last two decades. Like its predecessor, castellated beams, the cellular steel beams can be manufactured by cutting two semicircular sections (to form regular circular openings pattern) through the web of a rolled I–shaped beam section along its centerline and then separating, offsetting and welding the tips of the long cuts of the two halves as shown in Figs. 1.3(a) through 1.3(c). While castellated beams require only one cut through the web and produce minimal waste, the cellular beams require two cuts as illustrated in Fig. 1.3(a). The first cut creates the top semi–circular boundary of the perforation cells while the second cut creates the bottom semi–circular boundary of the cells. The circular shape of the openings is attainable after trimming the excess steel parts (waste) indicated in Fig. 1.2(a). The resulting holes are of regular circular openings pattern over the full span of the beam with a variety of specified opening configurations (i.e., hole diameter and spacing). In some instances, this process increases the overall beam depth to be up to 1.6 times deeper than of the root (parent) solid section. The diameter of the openings can reach 80% of the total height of the beam and it is possible to leave only a small distance between the openings which allow a high level of transparency. Nowadays, built–up sections constructed of steel plates are used to produce steel plate girders with circular web openings [Shanmugam et al.

(2002), Hagen (2004)]. Besides, the advancement in computer–controlled cutting and welding technology enables production of perforated steel sections in a wide variety of geometries suitable for various applications.

Despite the tremendous advantages of perforated steel beams, their reduced shear capacity as a result of the web openings make them more susceptible to shear failure and lateral torsional buckling under the applied loads. These added openings, however, also result in a different stress distribution within the web and new failure modes associated with the perforated beam. As a result, and given the recent increase in usage of cellular beams, the need for additional relevant research is emphasized.

1.4 THESIS ORGANIZATION

The thesis includes six chapters. Chapter 2 introduces the problem studied in the current research. It also presents a brief review for the theory of lateral torsional buckling and its application to conventional I–shaped beams with solid webs. A literature review is provided for relevant research work conducted on castellated and cellular steel beams. Chapter 3 explains the development of a three dimensional linear elastic and non–linear elasto–plastic (inelastic) finite element models to simulate the buckling behavior of cellular beams. Validation of the developed finite element model is discussed in detail. Chapter 4 investigates elastic analysis of lateral buckling of cellular steel beams with a wide range of geometrical dimensions. A study on the influence of the type and application level/position of the load on the lateral stability of cellular beams is also included in the chapter. Chapter 5 studies the inelastic lateral buckling of cellular steel beams. The critical buckling loads along with the corresponding buckling modes are assessed for a wide spectrum of cellular beams geometries. The correlation between various buckling modes, including interaction of

potential modes, on the moment gradient factor C_b is discussed. The moment gradient factor ranges that correspond to the resulting buckling modes are also identified. In chapter 6, summary and conclusions that are drawn from the outcomes of the elastic and elasto-plastic (inelastic) finite element analyses are presented. Suggestions for future research areas are also proposed.

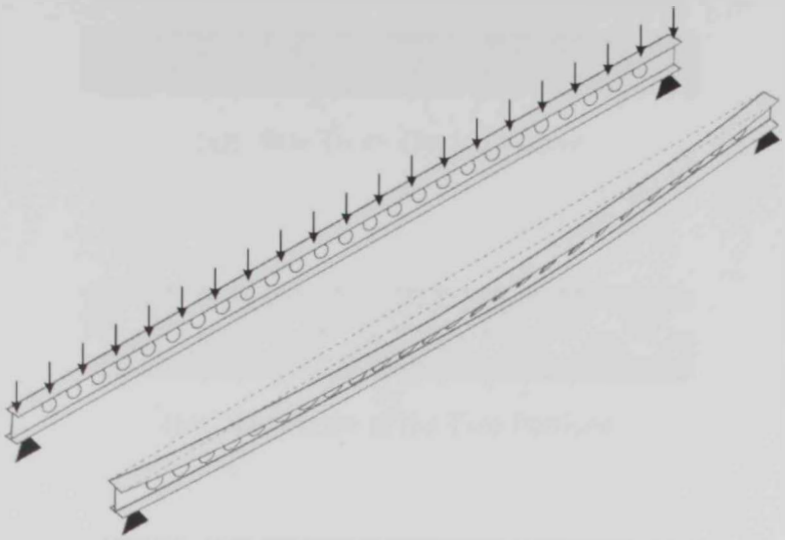

Figure 1.1: Example of Lateral Instability of a Cellular Beam Subjected to Uniformly Distributed Load

(a): Saw Tooth Cutting Pattern

(b): Separation of the Two Portions

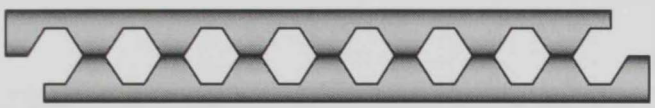

(c): Staggering and Welding of the Two Halves

Figure 1.2: Manufacturing of Castellated Steel Beams

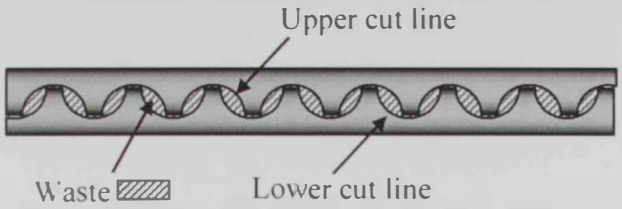

(a): Cutting of Two Semicircular Sections

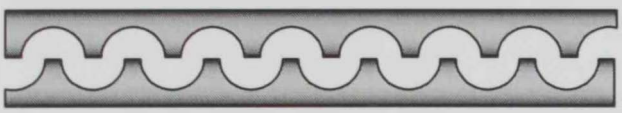

(b): Separation of the Two Portions

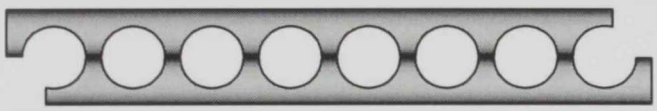

(c): Offsetting Staggering and Welding of the Two Halves

Figure 1.3: Manufacturing of Cellular Steel Beams

CHAPTER 2

PROBLEM DEFINITION AND BACKGROUND

2.1 INTRODUCTION

Beams are structural members that resist the applied load primarily by flexure and shearing actions. I–beams subjected to flexure have much greater strength and stiffness in the plane in which the loads are applied (i.e.; about their major axis) than in the plane of minor axis. When beams are bent about their major axis, unless proper lateral bracing is provided, out of plane bending and twisting will occur leading to failure by lateral torsional buckling prior to the attainment of full in–plane flexural capacity of such beams. Lateral torsional buckling is a limit state of structural usefulness in which the top flange and portion of the web act as a compression member, and tend to buckle laterally, which, in turn, tends to twist the cross section as presented in Fig. 2.1.

In general, design of structural members is often based on strength and stiffness considerations. While strength is related to the ability of the member to withstand the applied load and its associated internal forces, stiffness is the resistance to deformation (i.e., the member is sufficiently stiff not to deform beyond permissible limits). However, a structural member may become unstable far before the strength and stiffness criteria are reached. In this case, the buckling capacity governs the design (i.e., buckling is more critical than the strength criterion). Instability failure that prevents achieving the full strength of solid beams can be attributed to buckling of the compression flange of the beam (referred to as flange local buckling), buckling of the web (called web local buckling) or lateral torsional buckling of the entire beam.

2.2 TORSIONAL STRESSES IN SOLID I–SHAPED BEAMS

Lateral torsional buckling of solid I–shaped steel beams is always associated with the development of two torsional–related stresses namely; Saint–Venant's torsion and warping torsion stresses. The former stress represents pure torsion that assumes that the plane cross section of the beam remains plane with element rotations occurring due to in–plane twisting only as shown in Fig. 2.2(a). Saint–Venant's pure torsion moment M_{SV} can be expressed as [Timoshenko and Gere (1961), Salmon et al. (2009)]:

$$M_{SV} = GJ\frac{d\phi}{dz} \tag{2.1}$$

where

GJ is the Saint–Venant's torsional rigidity,

G is the shear modulus of elasticity $= \frac{E}{2(1+\nu)}$, in which E is Young's modulus and ν is Poisson's ratio,

J is the torsional constant of the section $\approx \sum \frac{1}{3} b_t t_t^3$, in which b_t and t_t are the width and thickness, respectively, of the rectangular components of the I–beam's cross section, and

ϕ is the angle of twist of the cross section.

Meanwhile, warping torsion represents the out–of–plane lateral bending effect that develops when the flanges are laterally displaced with the compression and tension flanges bent laterally in opposite directions leading to a non–planar section as shown in Fig. 2.2(b). The warping torsion component M_w is given by [Timoshenko and Gere (1961), Salmon et al. (2009)] as:

$$M_w = -EC_w\frac{d^3\phi}{dz^3} \tag{2.2}$$

where

EC_w is the warping rigidity,

E is Young's modulus, and

C_w is the torsional warping constant $= \frac{1}{2} I_f h_o^2$, in which I_f is the second moment of area for one flange about the y–axis of the beam and h_o is the height between centers of top and bottom flanges.

The total torsional moment M_T can then be obtained in accordance with the following expression:

$$M_T = M_{SV} + M_w = GJ\frac{d\phi}{dz} - EC_w\frac{d^3\phi}{dz^3} \tag{2.3}$$

It should be noted that the term $\left(\frac{d^3\phi}{dz^3}\right)$ has a negative magnitude and, therefore, Eq. (2.3) will end up being a direct summation of the two torsional moment components M_{SV} and M_w.

2.3 LATERAL TORSIONAL BUCKLING OF SOLID I–BEAMS UNDER PURE END MOMENTS

In the development of beam design equations, the case of constant (uniform) moment along a laterally unbraced length is usually used as the basic case for lateral torsional buckling of beams. Using the analogy of the compression flange as a column, the uniform moment causes constant compression in one flange over the entire unbraced length. On the contrary, when there is a moment gradient (variation in moment) the compression force in the flange varies along the unbraced length, resulting in a lower average compression force over that length. In other words, when the moment is not constant along the unbraced length of the

beam, the lateral torsional buckling moment is greater than the same moment in pure bending. This is reflected in the value of the moment gradient factor C_b, which is always greater than unity. The elastic and inelastic lateral torsional buckling of solid I–shaped beams under uniform moment is discussed in the following subsections.

2.3.1 Elastic Lateral Torsional Buckling

This section presents the basic information related to the derivation of the elastic lateral torsional buckling strength M_{cr} of an I–shaped beam under the action of constant (uniform) moment M_o acting in the plane of the web as shown in Fig. 2.3 [Timoshenko and Gere (1961)]. In this figure, x', y' and z' represent the transformed coordinates of the buckled section. The figure also shows the beam in its buckled position, where the applied moment M_o in the (z–y) plane will give rise to moment components $M_{x'}$, $M_{y'}$ and $M_{z'}$, about the x', y' and z' axes, respectively. The x' and y' axes coincide with the principal axes of the cross section while the z' axis is always tangent to the center line of the deflected position. The beam is subjected to an external constant bending moment $M_x = M_o$. Under the assumption of small deformations, the external bending moments about the transformed axes are related to M_o as follows:

$$M_{x'} = M_x \cos\phi = -M_o \tag{2.4}$$

$$M_{y'} = M_x \cos(\phi + 90) = -M_x \sin\phi = -M_o\phi \tag{2.5}$$

$$M_{z'} = M_o \cos\left(90 - \frac{du}{dz}\right) = M_o \sin\frac{du}{dz} = M_o \frac{du}{dz} \tag{2.6}$$

The governing equilibrium differential equations at the deformed state for the I–section under pure torsion are given by:

$$\left(EI_x \frac{d^2v}{dz^2} - M_{x'}\right) = \left(EI_x \frac{d^2v}{dz^2} + M_o\right) = 0 \tag{2.7}$$

$$\left(EI_y \frac{d^2u}{dz^2} - M_y\right) = \left(EI_y \frac{d^2u}{dz^2} + \phi M_o\right) = 0 \tag{2.8}$$

$$\left(GJ\frac{d\phi}{dz} - EC_w \frac{d^3\phi}{dz^3} - M_{z'}\right) = \left(GJ\frac{d\phi}{dz} - EC_w \frac{d^3\phi}{dz^3} - \frac{du}{dz}M_o\right) = 0 \tag{2.9}$$

By differentiating Eq. (2.9) with respect to the variable z:

$$GJ\frac{d^2\phi}{dz^2} - EC_w \frac{d^4\phi}{dz^4} - M_o \frac{d^2u}{dz^2} = 0 \tag{2.10}$$

The equilibrium differential equations describing the behavior of the beam at lateral torsional buckling is obtained by substituting Eq. (2.8) into Eq. (2.10) to give:

$$EC_w \frac{d^4\phi}{dz^4} - GJ\frac{d^2\phi}{dz^2} - \frac{M_o^2}{EI_y}\phi = 0 \tag{2.11}$$

The solution of this fourth order differential equation requires the application of the following four boundary conditions:

- No twisting (rotation about z) occurs at the left support:

  $$\phi(z = 0) = 0 \tag{2.12}$$

- No twisting (rotation about z) takes place at the right support:

  $$\phi(z = L) = 0 \tag{2.13}$$

- The beam is not restrained against warping. Therefore, no warping moment will be developed at the left support:

  $$\frac{d^2\phi}{dz^2}(z = 0) = 0 \tag{2.14}$$

- No warping moment will be developed at the right support:

$$\frac{d^2\phi}{dz^2}(z = L) = 0 \tag{2.15}$$

The solution of the differential equation which satisfies the above boundary conditions results in the critical value of M_o as:

$$M_o = M_{cr} = \frac{\pi}{L}\sqrt{EI_y GJ + \left(\frac{\pi E}{L}\right)^2 I_y C_w} \tag{2.16}$$

which provides the value of the critical elastic lateral torsional buckling moment for a simply supported I–shaped solid beam subjected to pure equal end moments.

2.3.2 Inelastic Lateral Torsional Buckling

Lateral torsional buckling of an intermediate length beam always occurs after some fibers of the cross section reach yield stress. Once these fibers become inelastic, their stress–strain modulus decreases and, hence, buckling strength decreases. The maximum elastic moment that can be attained by a beam is given by:

$$M_r = S_x(F_y - F_r) \tag{2.17}$$

where

S_x is the elastic section modulus,

F_y is the steel yield stress, and

F_r is the material residual stress

In Eq. (2.17), residual stresses are those self–equilibrated stresses that remain in a member after it has been formed into a finished product. Such stresses result from plastic deformations, which in structural steel may result from several sources. These sources include uneven cooling which occurs after hot rolling of structural shapes, cold bending or cambering during fabrications, punching of holes and cutting operations during fabrications,

and welding. Under ordinary conditions those residual stresses resulting from uneven cooling and welding are the most important. In fact, the important residual stresses due to welding are the result of uneven cooling. The typical value of the residual stresses F_r as adopted by the AISC 360–05 (2005) is approximately 70% of the yielding stress F_y (i.e., $M_r = 0.7 F_y S_x$).

A tangent modulus theory of inelastic buckling has been developed where the elastic moduli E and G are replaced by the tangent values E_T and G_T for all yielded parts of the beam [Galambos (1968), Trahair and Kitipornchai (1972), Nethercot and Trahair (1976)). A simplified expression has been proposed by Nethercot and Trahair (1976) for estimating the inelastic buckling strength M_{inel} for a simply supported beam under uniform moment:

$$M_{inel} = M_p \left[0.7 + 0.306 \left(1 - \frac{0.7 M_p}{M_{cr}} \right) \right] \leq M_p \tag{2.18}$$

where

M_p is the plastic moment capacity of the beam, and

M_{cr} is the elastic buckling moment for the beam as given by Eq. (2.16).

2.4 AISC CODE PROVISIONS FOR LATERAL TORSIONAL BUCKLING OF SOLID I–BEAMS

Beams in practical situations will be subjected to a wide variety of loadings, thus producing non–uniform moment along the length of the beam. In such cases, the governing equilibrium differential equations at the deformed state will have variable coefficients. For such cases, closed form solutions are not available and the critical loads are obtained through approximate numerical solutions [Chen and Lui (1987)]. When there is a moment gradient

(variation in bending moment profile) the compression force in the flange varies along the unbraced length, resulting in a lower average compression force over that length. The lower average compression force results in an increase in the lateral torsional buckling moment value. In other words, when the moment is not constant throughout, the lateral torsional buckling moment is greater than the same moment in pure bending. This is reflected in the value of the moment gradient factor C_b, which is always greater than unity. Current design codes account for the influence of moment gradient on the beam moment carrying capacity through a modification coefficient that is referred to as moment gradient factor C_b. This factor relates the nominal moment M_n for the beam subjected to a specific transverse load to the corresponding critical buckling moment M_{cr} of the same beam under uniform moment:

$$M_n = C_b M_{cr} \tag{2.19}$$

Table 2.1 summarizes the various values of moment gradient factors adopted by four major international design codes and standards [the American steel construction manual AISC 360–05 (2005), the new European standards EC3 (2005), the Australian design standards SA (1998), and the British Standards Institution BSI (2005)] for beams subjected to mid–span concentrated load and uniformly distributed load. As indicated by Eq. (2.19), all codes assign a C_b value of unity for beams subjected to equal end moments (i.e.; uniform moment distribution along the span of the beam). The moment–gradient factor, C_b, is applied to the exact lateral buckling solution of beams under uniform moment in order to account for the variable moment along the unbraced steel girder length. As such, the nominal elastic critical moment M_{n-el} can be expressed in accordance with Eq. (2.16) as

$$M_{n-el} = \frac{C_b \pi}{L} \sqrt{EI_y GJ + \left(\frac{\pi E}{L}\right)^2 I_y C_w} \tag{2.20}$$

The upper limit for M_{n-el} provided by Eq. (2.20) is the maximum elastic moment strength when extreme fiber reaches the yield strength. The maximum elastic moment strength is defined by [AISC 360–05 (2005)] as:

$$M_{n-el(\max)} = C_b M_r = C_b\left(0.7F_y S_x\right) \tag{2.21}$$

where the 0.7 factor accounts for the effect of residual stresses on the onset of yielding.

For inelastic lateral torsional buckling, the AISC 360–05 (2005) adopts a simplified approximation for the moment strength M_{n-inel} that assumes a linear variation of M_{n-inel} between the highest possible flexural strength (plastic moment) of the section M_p and the maximum elastic moment strength M_r as depicted in Fig. 2.4:

$$M_{n-inel} = C_b\left[M_p - \left(M_p - M_r\right)\left(\frac{L_p - L_r}{L_r - L_p}\right)\right] \le M_p \tag{2.22}$$

where

L_b is the laterally unbraced length of the beam,

L_p is the limiting unbraced length for the limit state of yielding, and

L_r is the limiting unbraced length for the limit state of inelastic lateral torsional buckling.

2.5 FAILURE MODES OF CASTELLATED BEAMS

The structural behavior of conventional solid web I–shaped beams is complicated due to its susceptibility to several buckling modes. For the particular case of castellated beams, the non–uniformity in cross section properties due to the existence of web openings increases the level of complexity in the behavior and the associated failure modes. This fact has attracted the attention of many researchers who investigated the response and stability of beams with perforated webs. Research investigations on the behavior of castellated beams

revealed that characterization of the failure in such beams may involve any combination of seven failure modes [Kerdal and Nethercot (1984), Chung et al. (2000), Mohebkhah (2004), Zirakian and Showkati (2006)]. Three of these modes are classified as strength failure modes and are listed as:

1. Flexural mechanism,
2. Vierendeel or shear mechanism, and
3. Rupture of welded web joints.

While the remaining four are instability–related modes and are described as:

1. Lateral torsional buckling (LTB),
2. Lateral Distortional buckling (LDB),
3. Shear buckling of the web post, and
4. Compression buckling of the web post.

The following sections present description of the potential failure modes along with a summary of previous research studies on these modes. More emphasis is given to stability modes that are related to the focus of this thesis.

2.5.1 Flexural Mechanism

Formation of a flexural mechanism mode of failure is most probable to occur in laterally supported I–shaped beams with stocky cross–sections subjected to significant bending moment and negligible shear. Under these conditions, the failure due to global or local instabilities is eliminated due to the existence of adequate lateral restraint and the low width–to–thickness ratio of the cross section elements. In such a case, the tee sections above and below the web openings yield in tension and compression until they become fully plastic as shown in Fig. 2.5 [Toprac and Cooke (1959), Halleux (1967)]. Thus, the beam can reach

its maximum in–plane moment carrying capacity. Ward (1990) recommended that the maximum moment capacity of the beam should not exceed the plastic moment capacity of the reduced section taken through the vertical centerline of the hole.

2.5.2 Vierendeel or Shear Mechanism

Formation of a Vierendeel mechanism is always associated with high shear forces acting on beams with relatively short spans. Stress concentration at the four re–entrant corners of the web castellation leads to the formation of plastic hinges at these corners leading to deformation of the hole (Fig. 2.6) as was first reported by Altifillisch et al. (1957) and Toprac and Cooke (1959). When a castellated beam is subjected to shear, the tee sections above and below the web opening must carry the shear and moment applied to the beam. Additionally, the tee sections also carry the secondary moments on the beam resulting from the action of the shear force over the horizontal length of the opening. As a result, secondary moments are more pronounced in beams with bigger opening size.

2.5.3 Rupture of Welded Web Joints

In this mode of failure, the mid depth weld joint of the solid web post between two consecutive openings may rupture when horizontal shear stresses exceed the yield strength of the welded joint (Fig. 2.7). Hosain and Speirs (1973) conducted experimental investigation on six beams with short welded joints. Results indicated that beams with shorter width of web posts are more vulnerable to this failure mode. Thus, it should be noted that reducing the spacing between the openings (i.e., reducing the width of the web–posts) may cause the web–post to become more susceptible to weld rupture in the web joints.

2.5.4 Lateral Torsional Buckling

Lateral torsional buckling mode (LTB) is characterized by combined rigid body lateral translation and rotation of the cross section of the beam as shown in Fig. 2.8(a). It can be noted from Fig. 2.8(a) that this rigid body mode does not involve any noticeable local changes in the cross section geometry. Lateral torsional buckling usually occurs in longer span beams with inadequate lateral support to the compression flange. The reduced torsional stiffness of the web, as a result of relatively deeper and slender section of castellated beams, causes such beams to be more susceptible to lateral torsional buckling. Lateral torsional buckling behavior of castellated beams was investigated experimentally by Nethercot and Kerdal (1982) who indicated that failure by lateral torsional instability of castellated beams is similar to that of solid web beams. However, a more recent study by Mohebkhah (2004) has shown a significant influence of beam's slenderness on the moment–gradient factor of castellated beams. Such influence was more apparent in beams that buckle inelastically. Alternative equations have been proposed for evaluating the moment–gradient factor as a function of the beam's modified slenderness instead of using the constant factors provided by current codes for solid beams.

2.5.5 Lateral Distortional Buckling

Unlike lateral torsional buckling mode of failure, lateral distortional buckling mode (LDB) involves localized distortion of the cross section leading to unequal angle of twist for the two flanges as presented in Fig. 2.8(b). As a result, the final buckling mode combines lateral displacement and twist, together with localized web distortion. This interaction usually occurs in intermediate length I–beams with slender webs. In beams with perforated web, existence of web openings results in a reduction in the stiffness of the web plate which increases the level of web deformations. As a result, local web distortions are more likely to

accompany the lateral torsional buckling deformations leading to the occurrence of lateral distortional buckling mode. Recently, experimental investigations of the distortional buckling of castellated beams have been conducted by Zirakian and Showkati (2006) and Zirakian (2008). Test results indicated that all beams underwent lateral torsional buckling accompanied by localized web distortion. Experimental outcomes were then used to develop several extrapolation techniques that have been reported to provide accurate predictions of critical buckling loads of castellated beams undergoing lateral distortional buckling.

2.5.6 Shear Buckling of the Web Post

In case of failure of the web post due to shear buckling mode, the horizontal shear force in the web post is associated with double curvature bending over the height of the post. As shown in Fig. 2.9, one inclined edge of the opening will be stressed in tension, and the opposite edge in compression and buckling will cause a twisting effect of the web post along its height. Several cases of web post buckling have been reported in the literature [Sherbourne (1966), Haileux (1967), Bazile and Texier (1968)].

Many analytical studies on web post buckling have also been reported to predict the web post buckling load due to shearing force. Based on finite difference approximation for an ideally elastic–plastic–hardening material, Aglan and Redwood (1974) produced some graphical design approximations for a wide range of beam and hole geometries. Some correlations between experimental and non–linear finite element analysis (FEA) estimations were found in the works of Redwood and Zaarour (1996). Redwood and Demirdjian (1998) conducted elastic finite element analysis to identify buckling loads. They found a good agreement between their numerical predictions and the experimental counterpart available in

literature. The study by Redwood and Demirdjian concluded that the results of Aglan and Redwood (1974) should not be used for very thin webs.

2.5.7 Compression Buckling of the Web Post

Compression buckling of web post results from direct application of a concentrated load/reaction over the web post. This mode was reported in the experiments conducted by Toprac and Cooke (1959) and Hosain and Speirs (1973). This mode is similar to crippling failure of web plates in solid beams [Kerdal and Nethercot (1984)]. Unlike webs of solid beams, this buckling mode is not considerably sensitive to the size of the loaded area [Okubo and Nethercot (1985)]. In general, this failure mode could be prevented if adequate web stiffeners are provided. A strut approach was proposed by Dougherty (1993) to apply standard column equations to determine the strength of the web post under the effect of concentrated load.

2.6 LITERATURE REVIEW ON CELLULAR BEAMS

Very limited number of resources was found available in the literature related to the behavior and response of cellular beams. This may be attributed to the recent wide use of cellular beams in building construction following the advancement in computerized manufacturing technology. M oreover, research on cellular beams is less developed than castellated beams, since cellular beams are more complicated to analyze due to their continuously changing section properties around the cell. In 1963, Barbarito investigated stress concentrations in cellular beams in pure bending as a function of varying cell diameters and spacing. Based on the photo–elasticity experimental outcomes, a ratio of hole diameter to beam depth not exceeding 0.5 was recommended to maintain the flexural capacity of the beam nearly unchanged from its solid web counterpart. Knowles (1991), Lawson (1987),

Darwin (1990) and Redwood and Cho (1993) have studied the strength of beams with circular web openings and proposed some formulae for strength design of such beams.

Ward (1990) showed the load carrying capacity of a cellular beam is the smaller of its overall strength in flexure and lateral torsional buckling and the local strength of the web posts and the upper and lower tees. Surtees and Liu (1995) conducted an experimental study on cellular beams and concluded that failure was controlled by local web post buckling and lateral torsional buckling. More recently, Aloi (2002) and Reiter (2002) investigated general behavior characteristics of cellular beams. They found that the governing mode of failure for all specimens was due to combined buckling of the end connection and the first web post at the connection. More experimental and numerical studies were carried out by Hennessey et al. (2004) and Reither et al. (2005) to characterize the effect of end connection type on the buckling behavior of cellular beams.

Chung et al. (2000) conducted analytical and numerical analyses to assess the load carrying capacity of cellular beams related to the Vierendeel failure mechanism. The coupled influence resulting from the combined effect of the moment and shear on steel beams with web opening with various shapes has been also investigated numerically by Liu and Chung (2003). The study focused on flexural failure associated with the Vierendeel mechanism along with shear failure. Results of this finite element investigation has been used by Chung et al. (2003) to develop a generalized moment–shear interaction curve for determining the load carrying capacities of steel beams with web openings of various shapes and sizes.

In a recent study on the lateral stability of cellular steel beams, Sweedan (2011) investigated numerically the influence of cellular web holes on elastic lateral stability of steel beams. Results of a comprehensive parametric analyses revealed that the moment gradient

factor is significantly influenced by beam geometry and slenderness. The study also showed that as the beam slenderness decreases web distortion increases leading to lateral distortional buckling mode which is associated with lower moment gradient factor (i.e., lower C_b value) than those values recommended by design codes for solid beams.

The previous review demonstrates the lack of information related to the influence of circular web perforations on the lateral torsional buckling of cellular steel beams. This may be attributed to the limited production of such structural members in the past. The current study is motivated by the lack of rational design procedure pertaining to stability of cellular beams under lateral buckling. It presents a comprehensive study to quantify the effect of circular web perforations on the load carrying capacity of laterally unrestrained cellular steel beams.

Table 2.1: Moment Gradient Factor Recommended by International Design Codes.

Case of Loading	American Code (AISC 360–05 [4])	European Standards (EC3 [16])	Australian Code (AS4100 [42])	British Standards (BSI5950–1 [9])
Mid–Span Concentrated Load	1.32	1.365	1.35	1.18
Uniformly Distributed Load	1.14	1.132	1.13	1.08

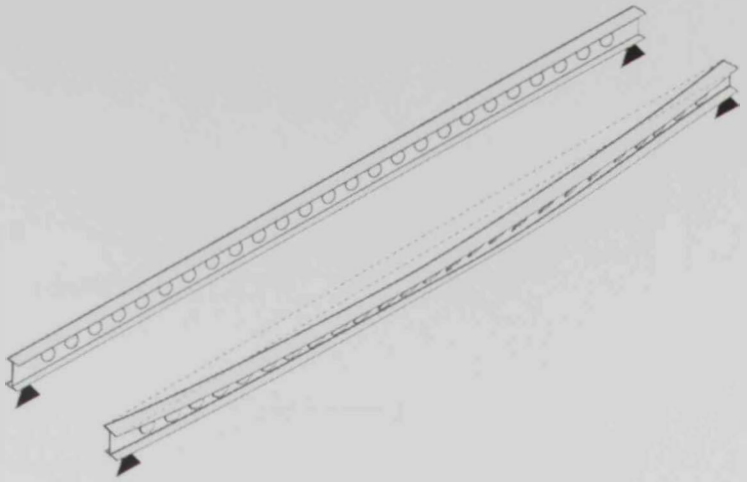

Figure 2.1: Lateral Torsional Buckling of a Cellular Beam

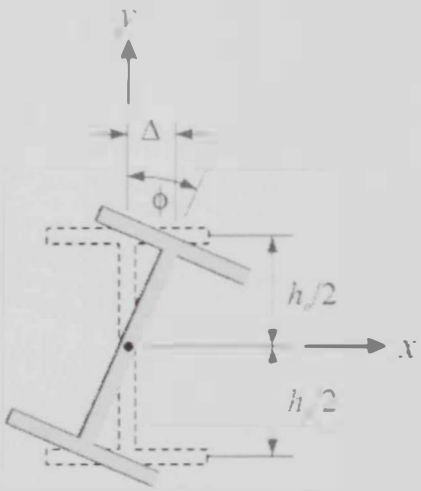

2.2(a): In–Plane Twisting

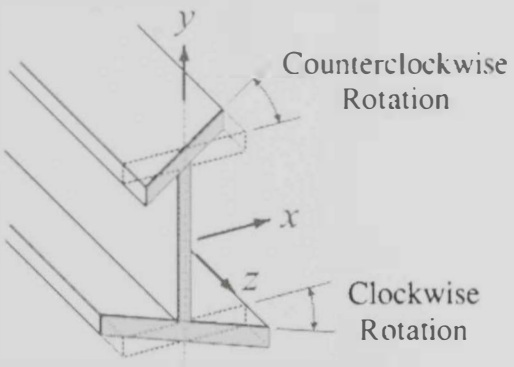

2.2(b): Out–of–Plane Warping

Figure 2.2: In–Plane Twisting and Out–of–Plane Warping of an I–Shaped Cross–Section

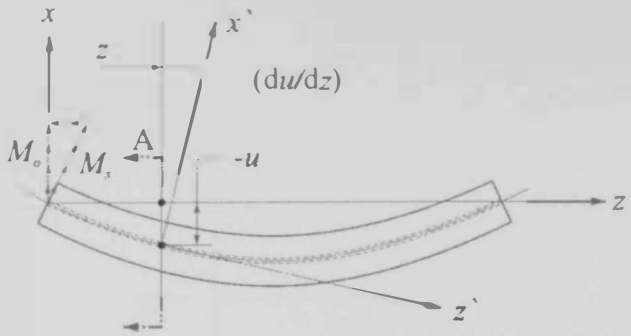

(a): Plan (Top) View of Buckled Beam

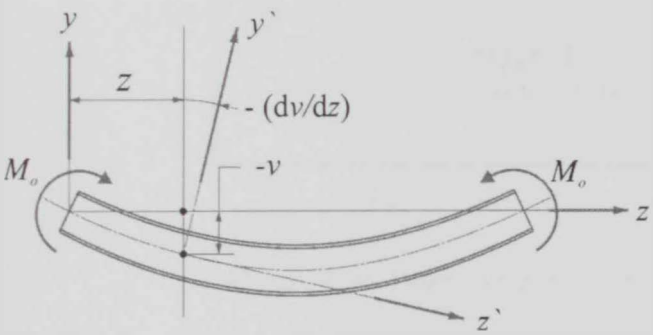

(b): Elevation of Buckled Beam

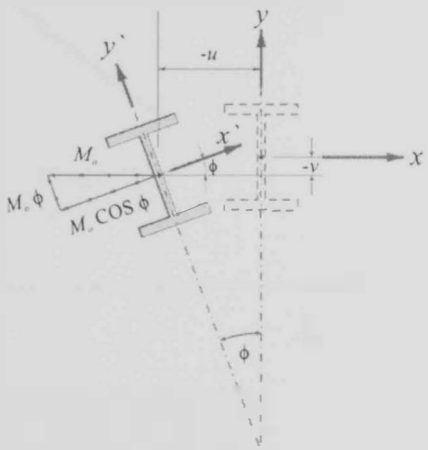

(c): Section A–A

Figure 2.3: Lateral Torsional Buckling (LTB) of I–Shaped Beam

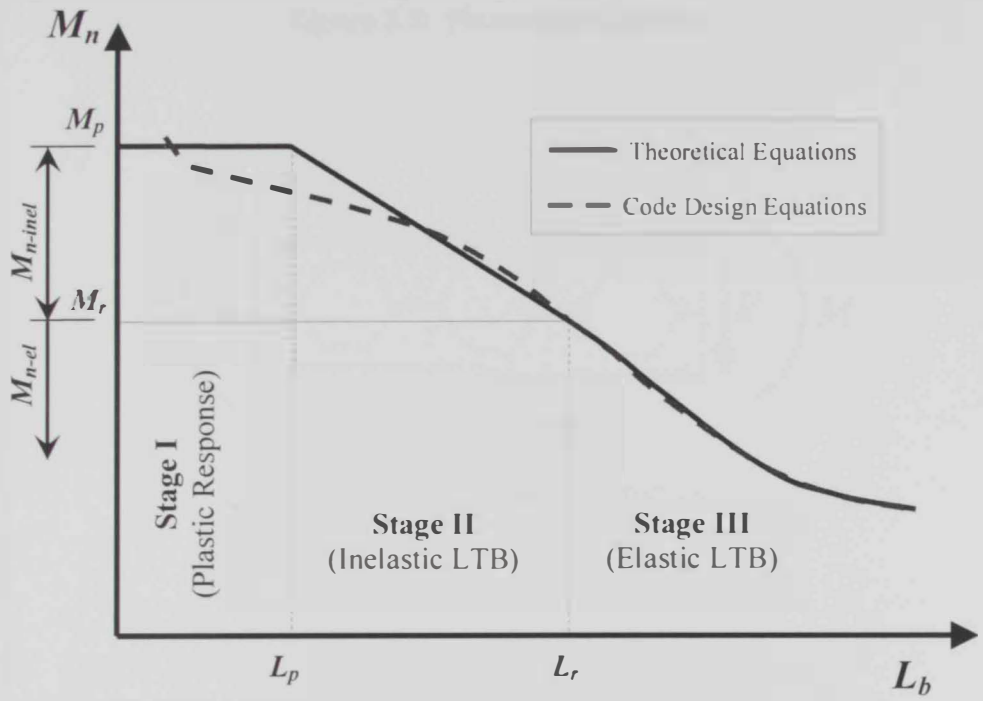

Figure 2.4: Beam Behavior as Related to Lateral Support

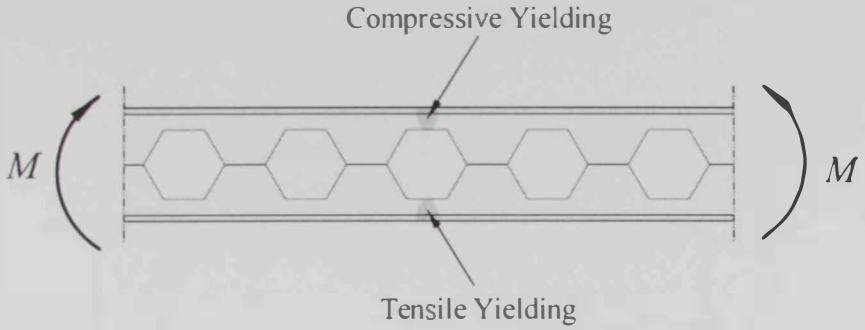

Figure 2.5: Flexural Mechanism

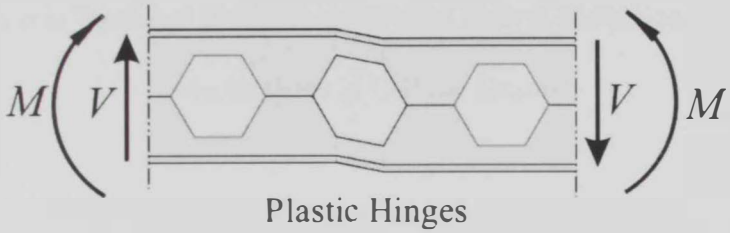

Figure 2.6: Virendeel Mechanism

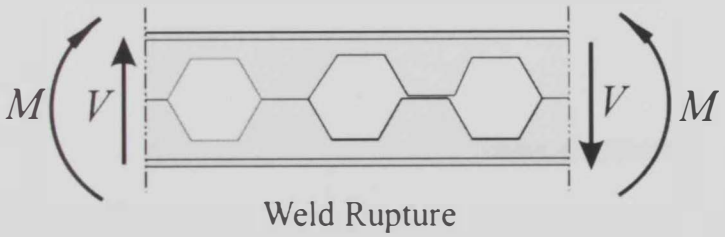

Figure 2.7: Web Rupture Mechanism

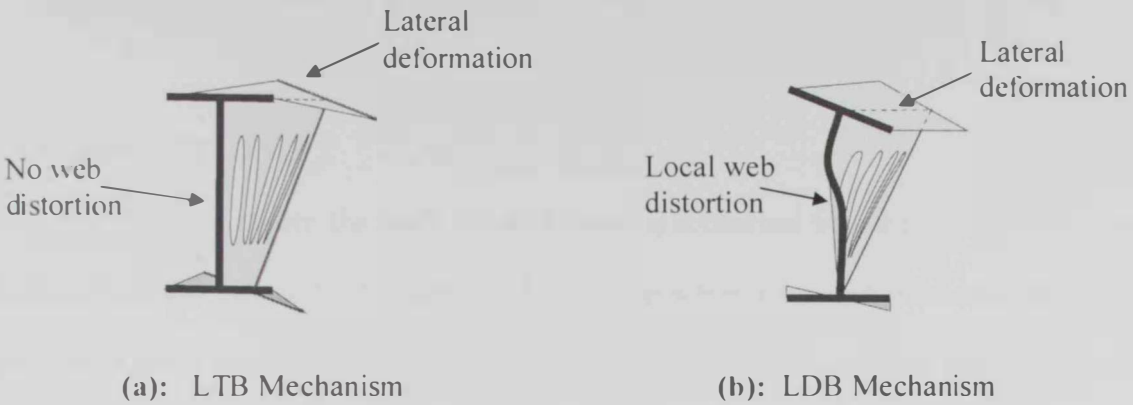

(a): LTB Mechanism **(b):** LDB Mechanism

Figure 2.8: Lateral Torsional Buckling (LTB) and Lateral Distortional Buckling (LDB) Mechanisms in Cellular Beams

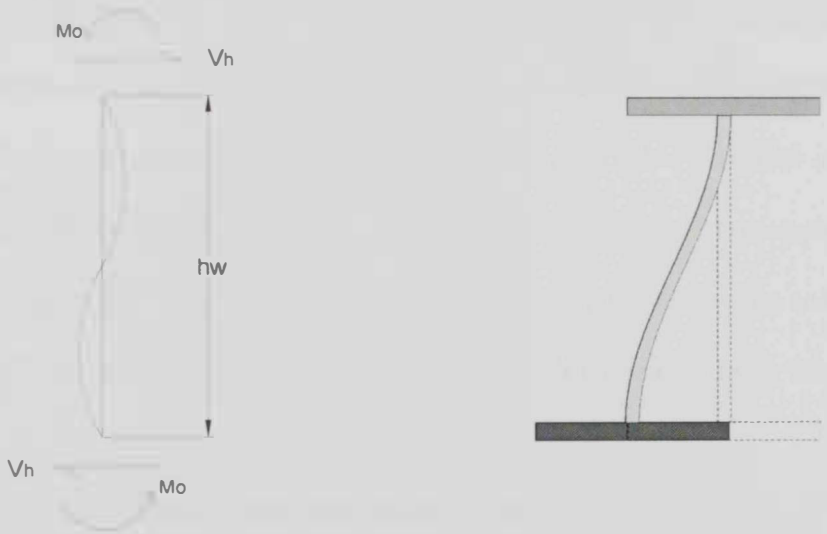

Figure 2.9: Web–Post Shear Buckling Mechanism

CHAPTER 3

FINITE ELEMENT MODELING AND VERIFICATION

3.1 INTRODUCTION

As discussed earlier, the study reported herein is concerned with the assessment of the stability of cellular beams due to lateral buckling when subjected to end–moments, and mid–span concentrated or uniformly distributed loads. To assess the stability of cellular beams, two approaches may be followed. The first is the experimental approach where small–scale or full–scale prototypes of the beams under consideration are built and examined up to failure. Although this approach would result in more realistic representation of the beam behavior, it is very expensive and can only be adopted for few specimens. Therefore, if a parametric study is required to show the effects of the different geometrical or material parameters on the stability of the cellular beam, the experimental approach may not be suitable. Due to the above limitations, numerical simulation presents a more affordable risk–free approach. The Finite Element Method (FEM) is a well–established numerical simulation approach that has been used by many researchers in the area of stress analysis. The following sections explore the usage of the FEM in studying the lateral stability of cellular beams under flexural stresses.

3.2 FINITE ELEMENT METHOD BACKGROUND

The Finite Element Method has been successfully used to study of the elastic and inelastic stability of various structural elements. The method provides an approximate solution to the partial differential equations governing the deformations and stresses of the considered structure. Finite Element method requires discretization of the considered structure or element using a mesh of elements that interconnect together at their corner or mid–side nodes. The deformation field is then approximated by pricewise deformation

functions along each element. Forces and supports are applied at the mesh nodes. The partial differential equations are then approximated by a set of simultaneous linear equations relating the change in nodal forces $\{dF\}$ to the change in nodal displacements $\{du\}$ through the stiffness matrix of the structure $[K]$. This can be written as

$$\{dF\} = [K]\{du\} \tag{3.1}$$

The structural stiffness matrix $[K]$ is dependent on the geometry and stress and strain histories of the elements during incrementing of the load to its final value. If load is applied in increments, Eq. (3.1) can be used to obtain the corresponding increments of deformations. These incremental deformations are used to obtain incremental strains which in turn define the incremental stresses through the proper material constitutive relationships. Total deformations, strains, and stresses may be obtained by summing their incremental counterparts as the loads advance in a predefined loading scenario.

3.3 LINEAR ELASTIC FINITE ELEMENT ANALYSIS

In the special case of small deformations where no significant change occurs in the initial geometry after deformation and linear elastic materials (i.e., stress is proportional to strain with no material yielding or failure), the stiffness matrix $[K]$ becomes constant $[K_E]$ and Eq. (3.1) may be written as

$$\{F\} = [K_E]\{u\} \tag{3.2}$$

In this case, the deformations become proportional to the level of the load. In other words, there is no need to apply the load in increments as the load can be applied with its overall value at which deformations and stresses are required. If strains used in the formulation include both the first and second order terms, the stiffness matrix generated is

composed of the conventional small deformation stiffness matrix, $[K_E]$, and the stress stiffness matrix, $[K_\sigma]$, that accounts for the effect of the existing stresses σ in the element on its stiffness. While the conventional stiffness matrix $[K_E]$ is constant, the stress matrix $[K_\sigma]$ is proportional to the level of the stress developed in the element. Thus, the total stiffness matrix $[K]$ at stress level $\lambda\sigma$ can be written as

$$[K]=[K_E]+\lambda[K_\sigma] \tag{3.3}$$

It is clear that in this case there is no need to apply the load in increments and the analysis can be performed under full load effect. Meanwhile, the total stiffness matrix $[K]$ can be obtained iteratively until the assumed existing stresses converge to the obtained ones. In this case Eq. (3.2) can be expressed as

$$\{F\}=[[K_E]+\lambda[K_\sigma]]\{u\} \tag{3.4}$$

3.3.1 Linear Elastic Stability Analysis

The linear elastic stability analysis of solids/structures is primarily based on Eq. (3.4). For instability, the determinant of the total stiffness matrix $[K]$ should vanish and the solid/structure exhibits increase in its displacements with no corresponding increase in the load. This can be defined in accordance with the following expression

$$|[K_E]+\lambda[K_\sigma]|=0 \tag{3.5}$$

Eq. (3.5) represents an eigenvalue problem which, when solved, provides the lowest eigenvalue, λ_1, that corresponds to the critical stress levels $\sigma_{cr}=\lambda_1\{\sigma\}$ at which instability (or buckling) occurs. In addition, the associated scaled displacement vector $\{u\}$ defines the fundamental mode shape at buckling.

3.4 NO N–LINEAR ELASTO–PLASTIC FINITE ELEMENT ANALYSIS

The current study considers two of the major sources of non–linearity in solids and structures. The first source is the geometrical non–linearity where significant change in geometry of the solid or structure during application of the load increments is experienced. The second source arises from elasto–plastic material non–linearity where stress is non proportional to strain and the material experiences yielding and plastic deformations. In non–linear finite element analysis, the stiffness matrix [K] is no longer constant as it is dependent on both the geometry and the stress level in the solid/structure at the instant of load increment application. Therefore, the total stiffness matrix [K] can be expressed as

$$[K]=[K_E]+[K_G]+[K_\sigma] \tag{3.6}$$

where

$[K_E]$ = constant elastic small–strain stiffness matrix

$[K_G]$ = geometrical stiffness matrix that reflects the contribution of the large deformations to the total stiffness matrix

$[K_\sigma]$ = stress stiffness matrix that reflects the contribution of the stresses to the total stiffness matrix

In this case, Eq. (3.1) can be expressed as

$$\{\mathrm{d}F\} = \left[[K_E]+[K_G]+[K_\sigma]\right]\{\mathrm{d}u\} \tag{3.7}$$

Different procedures that are utilized to solve stress–deformations relations that encounter nonlinearities are discussed in the following subsections.

3.4.1 Newton–Raphson Procedure for Load Application

The Newton–Raphson procedure is often used for the solution of non–linear problems. In this iterative procedure, the load is applied in increments through the application of the following constraint condition to the finite element governing equation

$$\{\mathrm{d}\,F\} = \{F_{n+1}\} - \{F_n\} = \text{Constant} \tag{3.8}$$

where n is the increment index or counter as shown in Fig. 3.1(a). The equilibrium equations are iteratively solved until solution converges.

Fig. 3.1 illustrates the incremental–load and iterative–equilibrium solution. In this solution procedure, the stiffness matrix $[K]$ (called tangent stiffness matrix $[K_T]$) is fully calculated at the start of each iteration and termed $[K_T]_i$ herein, where i is the iteration index. The solution starts with the calculation of the tangent stiffness matrix at the end of the previous load increment (termed $[K_T]_0$). This tangent stiffness matrix along with the load increment $\mathrm{d}\{F\}$ are used to obtain first iterative solution for the deformations $\delta\{u_1\}$ which is followed by obtaining the iterative strains and stresses. The convergence or equilibrium of the first iterative solution is checked by assessing the difference between the integration of the internal stresses over the volume and the external total loads (not incremental ones). This difference is termed residual forces and denoted by $\{R_1\}$ where the subscript refers to the iteration index. The negative values of residual force vector, in turn, are applied to the system again with a new tangent stiffness matrix $[K_T]_1$. The total incremental deformation at the end of iteration i is obtained as

$$\{u_i\} = \{u_n\} + \Delta\{u_i\} = \{u_n\} + \sum_{j=1}^{j=i} \delta\{u_j\} \tag{3.9}$$

The iterative procedure continues until the convergence of the equilibrium condition is achieved (i.e., norm of the residual forces $\|\{R_i\}\|$ approaches a negligible value) which is termed "*Force Convergence Criterion*" expressed as

$$\|\{R_i\}\|/\|d\{F\}\| < Tolerance \tag{3.10}$$

Or, norm of the iterative deformation $\|\delta\{u_i\}\|$ becomes negligible which is termed "*Displacement Convergence Criterion.*" Given by

$$\|\delta\{u_i\}\|/\|\Delta\{u_i\}\| < Tolerance \tag{3.11}$$

where the *Tolerance* is assigned a small value (e.g., 0.001) that is sufficiently near to zero [Gerald et al. (2003), Mathews and Kurtis (2004)].

Despite the rapid quadratic convergence of the Newton–Raphson procedure, it can be time consuming and inconvenient in some particular situations. This is due to the fact that the tangent stiffness matrix has to be calculated and factorized at each iteration. One way to avoid this problem is to formulate the tangent stiffness matrix only at the first iteration (the Modified Newton–Raphson Method) or the first two iterations while it is kept constant over the rest of the iterations. This would save computing time, but will slow down the convergence rate and more iterations may be required. Another draw back of both the Newton–Raphson method and its modified version is that they fail once a behavior exhibiting a peak load is encountered (Fig. 3.1(b)). Thus the peak load is underestimated because a numerical, rather than structural, instability occurs. At this time, it is crucial to resort to an alternative technique that is suitable for peak load cases. The Arc–Length Control Method emerges as a convenient alternative for these cases [Crisfield (1981)].

3.4.2 Arc–Length Control Procedure

As the beam stability problem deals with the evaluation of the critical load, a snap–through behavior for the load–deflection of the beam is expected where sudden instability occurs once the critical load is reached as shown in Fig. 3.1(b). The conventional incremental solution techniques such as Newton–Raphson and modified Newton–Raphson fail to predict the post–peak behavior, and the solution may diverge when the load approaches its critical value. The Arc Length Control Method represents a suitable alternative for this case where neither incremental loads nor incremental displacements are prescribed, but a constraint equation is used instead. The constraint equation may be visualized for a single degree of freedom as an arc of a certain radius which intersects with the load deflection curve at a point that represents the solution for that increment (Fig. 3.2).

In the Arc–Length Control Method, the load increment is not chosen arbitrarily, like in the Newton–Raphson method or its modified version, but adjusted at each iteration under an arc–length constraint equation. Fig. 3.2 shows the details of the iterations applied in an arc–length increment. The load is assumed to be proportional and the load vector is defined by $\lambda\{F\}$ where $\{F\}$ is the nominal load vector and λ is a load multiplier. At the end of the i^{th} iteration, the iterative deformation vector is defined by $\delta\{u_i\}$, the total incremental deformation by $\Delta\{u_i\}$, and the residual force vector by $\{R_i\}$. The residual force vector needs more detailed calculations based on the constraint equation used (shown as arc between points 1', 2', and 3' in Fig. 3.2) [Crisfield (1981), Ritto–Correa and Camotim (2008)]. Similar to the Newton–Raphson method, the Arc–Length iterative procedure continues until the force and/or displacement convergence criteria are achieved as shown in Eqs. (3.10) and (3.11).

3.4.3 Perturbation and Peak–Load

To obtain the buckling load in a non–linear numerical solution scheme, a perturbed geometry of the beam should be implemented. The perturbed geometry is obtained by scaling the geometry of the lateral torsional buckling mode resulting from an elastic eigenvalue analysis as shown in Fig. 3.3. The eigenvalue and its corresponding buckling mode can be obtained by conducting an elastic buckling analysis for each case. The buckled mode is scaled such that the maximum lateral translation at the mid–span is $L/1500$ where L is the span of the beam as shown in Fig. 3.3. This particular value of the initial imperfection amplitude is implemented as it matches the average imperfection adopted by the AISC 360–05 design manual [AISC 360–05 (2005)]. The imperfection introduced into the system triggers the lateral torsional deformation mode during the incremental application of the loads (end moments, uniformly distributed load, or mid–span concentrated load). The peak load (i.e., critical load) is obtained from the load–deformation curve recorded for the applied load increments and the associated lateral displacement of the central node of the top flange.

3.5 F INITE ELEMENT MODEL OF CELLULAR BEAMS

The Finite Element Method is used to model the flexural behavior of cellular beams bending about their axis of major flexural rigidity. As discussed earlier, it is well established that out of plane (i.e., lateral) bending and twisting due to instability will occur when the applied load on the beam reaches its critical value. In this case, the buckling mode is characterized by movement of both of the compression flange and portion of the web, that act as a column, accompanied by twisting of the entire beam cross section as shown in Fig. 3.4. This mode, as will be discussed later, may interact with other buckling modes (e.g., local web buckling mode). In the current study, the general–purpose finite element software, ANSYS (2009), is utilized to determine the elastic and elasto–plastic buckling load of cellular beams.

The strain used in the formulation includes both the first and second order terms with both the elastic and elasto–plastic materials. The nonlinearity considered in the elasto–plastic finite element analysis is due to both geometrical and material nonlinearities.

3.6 DESCRIPTION OF THE FINITE ELEMENT MODEL

A three dimensional (3D) finite element model is developed to simulate the behavior of cellular steel beams having I–shaped cross section. As mentioned earlier, modeling is conducted using the general purpose finite element software package ANSYS (2009). Geometrical details of analyzed beams are simulated using the 4–node shell element (*SHELL181*, as denoted by ANSYS, for both elastic and elasto–plastic analyses). This element has six degrees of freedom at each node, 3 translations and 3 rotations, to allow for explicit simulation of various buckling deformations. Besides, *SHELL181* is suitable for modeling thin to moderately–thick shell structures with both elastic and elasto–plastic material behaviors [ANSYS (2009)]. However, when the level of distortion of this element exceeds a certain limit, warning is provided to the user.

3.6.1 Essential Modeling Considerations

3.6.1.1 *Generation of Geometrical Details*

Fig. 3.4 shows the geometry of the typical I–shaped cellular beam considered in this study. The geometry is defined using a global Cartesian coordinate system with its origin located at the mid–height of the cross section at the mid–span of the beam. As indicated in Fig. 3.5, the depth of the beam is directed along the Y–axis while its longitudinal axis coincides with the Z–axis. The beam geometry is characterized by its span L, flange width b_f, flange thickness t_f, web height h_w, and web thickness t_w. Circular web holes have diameter d_h and are uniformly spaced at distance s along the span. The beam has an even integer–valued

length–to–hole spacing ratio (L/s) which corresponds to having multiple typical panels of width s, each with a single central hole except for the first and last solid panels where considerable shear exists (Fig. 3.5). The beam is pin supported at its left end while roller support is utilized at the right end. Several stiffener plates are used to prevent buckling modes that may interact with the lateral torsional buckling mode. Stiffener plates with thickness twice that of the web are used at both ends of the beam to avoid web crippling associated with localized web yielding due to concentrated reactions. The used thickness of stiffeners is concluded through conducting many FE runs considering many stiffener thicknesses. Extra and similar stiffeners are also used at the point of application of the mid–span concentrated load. An extensive survey has been conducted to identify the commonly used practical dimensions of cellular beams. The specified range is summarized in Table 3.1 for the basic dimensionless parameters defining cellular beam geometry. The justification of expressing the geometry in terms of these dimensionless parameters is discussed in details in Chapters 4 and 5. It should be noted that the exact value of L/h_w ratio is to be calculated such that the ratio $L/s = (L/h_w)\ (s/h_w)$ corresponds to an even integer.

3.6.1.2 *Material Model*

Figs. 3.6(a) and 3.6(b) show the two material models used in the developed finite element model to simulate the elastic and elasto–plastic behavior of the steel material, respectively. For elastic analysis the cellular beam is assumed to have linear elastic material (Fig. 3.6(a)) with Young's modulus E = 210 GPa, and Poisson's ratio ν = 0.3. However, it is important to note that for linear elastic analysis, the results are independent on the selected values of E and ν. Meanwhile, for non–linear elasto–plastic analysis, the beam material is assumed as elasto–plastic with multi–linear isotropic kinematic hardening as shown in Fig. 3.6(b). This multi–linear material model has initial elastic Young's modulus E = 210 GPa,

strain hardening modulus E_t = 6.3 GPa, Poisson's ratio ν = 0.3, yield stress F_y = 250 MPa, and ultimate stress F_u = 400 MPa. These values represent the typical characteristics of Carbon steel as provided by Salmon et al. (2009). However, further study may be done for different types of steel such as A50 steel.

3.6.1.3 *Mesh Development*

Flanges are modelled with twelve elements across the width b_f (i.e., element size in flange = $b_f/12$). Meanwhile, element size in the web is selected to be approximately $h_w/20$ to provide better simulation of the deformations associated with lateral, distortional or local web buckling modes. The size of the elements along the span of the beam is restricted not to exceed $h_w/20$. Several mesh configurations are attempted until the above provided limitations are set after providing convergence of the predicted buckling load within reasonable execution time. A typical mesh configuration is shown in Fig. 3.7 for a cellular beam having b_f= 115 mm, t_f= 11.5 mm, h_w = 200 mm, t_w = 10 mm, d_h = 140 mm and s = 210 mm. It should be noted that although the thickness of the elements does not appear in the figure, it is used internally by ANSYS (2009) to generate the stiffness matrix of the modelled beam.

3.6.2 Boundary Conditions and Load Application

Fig. 3.8 shows the general geometry of the cellular beam with its applied boundary conditions. The beam is pin supported at the left end and supported on a roller at its right end. Accordingly, vertical displacements U_y and out–of–plane displacements U_x are restrained at the central node of the cross section at both ends, while left end only is restrained against longitudinal displacements U_z. Twisting rotations at beam ends are prevented by restraining both the top and bottom flange tip points against out–of–plane displacements U_x as shown in Fig. 3.8. The stiffeners used at both ends of the beam are part of the geometrical model and

mesh as presented in Fig. 3.7. The stiffeners are used to eliminate the warping that may happen to the cross–sections at the beam ends. The remaining nodes are left unrestrained against any kind of deformation.

Beams with various geometrical parameters are analyzed under three different cases of loading to allow for the evaluation of various moment gradient factors C_b. These cases of loading include pure end moments, mid–span concentrated load and uniformly distributed load. As mentioned earlier, finite element models include bearing stiffener plates in the vicinity of concentrated loading and at support reactions to avoid web crippling associated with localized web yielding. In order to avoid any undesirable localized web deformations and stress concentration, the end moment loading is applied in the form of couple forces resulting from uniform loading applied at top and bottom flanges of the beam end sections. In this loading scheme, the top flange is subjected to compressive longitudinal forces, while the bottom flange is subjected to tensile forces opposing the compressive ones as presented in Fig. 3.9(a).

An idealized effect of transverse loading requires application of these loads at the shear center of the section to avoid destabilizing or stabilizing effects of loading applied above or below shear center, respectively. However, the presence of web perforations does not allow for direct application of transverse loads at shear center. A typical solution to overcome such a problem is adopted by applying half the load at the top flange and the other half at the bottom flange with both portions acting along the same direction as shown in Figs. 3.9(b) and 3.9(c) for uniformly distributed and mid–span concentrated loads, respectively. As a result, torques produced by both load portions, when acting on the deformed geometry of the beam, will counteract each other. This eliminates any stabilizing/destabilizing effects on

the beam and consequently leads to an overall response that simulates that of loading applied at the shear center of the beam. A detailed discussion on this effect is presented in Chapter 4.

3.7 VERIFICA TION OF THE FINITE ELEMENT MODEL

To verify the performance of the developed three dimensional finite element model described in the previous section, the model is employed to identify the elastic and elasto–plastic buckling loads of various beams with solid and perforated webs. The obtained critical loads are compared to theoretical, experimental findings and numerical outcomes that are reported in the literature to validate the accuracy of the proposed model. As previously mentioned, no experimental or numerical results related to lateral torsional buckling of cellular beams are available in the literature. Therefore, the verification with perforated–web beams will be limited only to those with castellated webs.

3.7.1 Lateral Torsional Buckling of I–Beams with Solid Web

The verification phase starts with evaluating the critical elastic buckling moment of solid web beams having different geometrical dimensions and subjected to uniform end moments. Selected beam sections are assumed to have a web height to thickness ratio (h_w/t_w) of 45 and flange width–to–thickness ratio (b_f/t_f) of 12, 16 and 20 (as shown in Table 3.2). Each beam is analyzed twice considering span to depth ratio (L/h_w) of 20 and 30. Finite element predictions are then compared to the analytical solution of the critical buckling moment M_{o-cr} given by [Timoshenko and Gere (1961)]:

$$M_{o-cr} = \frac{\pi}{L}\sqrt{EI_y GJ + \left(\frac{\pi E}{L}\right)^2 I_y C_w} \tag{3.12}$$

where L is the unbraced span of the beam and I_y is the minor–axis moment of inertia of the cross section, G is the shear modulus of elasticity, J is the torsional constant of the cross

section, E is Young's modulus of elasticity and C_w is the warping torsional constant of the cross section. Comparison between analytical solutions and elastic finite element predictions (eigenvalue problem) are presented in Table 3.2 indicating an excellent match with absolute maximum relative error of 0.47%.

3.7.2 Experimental Lateral Torsional Buckling of Castellated I–Beams by Nethercot and Kerdal (1982)

Nethercot and Kerdal (1982) have reported experimental values of critical lateral buckling loads of simply supported castellated beams subjected to two point loads. Experimental results reported for specimen (M5–1, 534 x 127 x 39) are used for the validation of the developed finite element model. Fig. 3.10 shows the geometry and cross–section properties of the tested beam M5–1 while the location of the two point loads and lateral supports at top and bottom flanges are shown in Fig. 3.11. Vertical supports are provided at the bottom flanges of the beams' ends. The elasto–plastic multi–linear material model used in the verification process is shown in Fig. 3.12. A yield stress F_y = 280 MPa was used, which represents an average value for the measured yield stresses reported by Nethercot and Kerdal (1982). Meanwhile, the ordinates of points (2) and (3) on the material properties curve are assumed based on the typical characteristics of carbon steel [Salmon et al. (2009)].

The proposed finite element model is used to perform elasto–plastic buckling analysis of the tested beam. Lateral imperfection amplitude of $L/1500$, as described earlier, is used to trigger the lateral buckling mode of the analyzed beam. The Arc–Length control method and both force and displacement convergence criteria with *Tolerance* = 0.001 is implemented in the adopted model. Nethercot and Kerdal (1982) reported an experimental critical moment of 205 kN.m. The finite element critical moment associated with the critical point load is

estimated to be 202 kN.m (1.46% difference from the experimental values). This indicates excellent agreement exists between the finite element predictions and the experimental results reported by Nethercot and Kerdal (1982).

3.7.3 Numerical Lateral Torsional Buckling of Castellated I–Beams by Mohebkhah (2004)

Mohebkhah (2004) reported several elasto–plastic numerical predictions of critical buckling loads of simply supported castellated beams subjected to uniform bending moments, M, mid–span concentrated load, P, and uniformly distributed load, W. Accordingly, the critical buckling loads for these cases are defined by M_{cr}, P_{cr}, and W_{cr}. In addition, Mohebkhah (2004) reported also the C_b values for the two cases of concentrated and uniformly distributed loads. Reported results are related to castellated beams with full lateral supports of both flanges at supports locations only. Stiffeners are used at locations of applied concentrated loads and at the support locations. A multi–linear elasto–plastic material model is utilized in the finite element model as shown in Fig. 3.13. In this figure, the ordinates of points (1) and (2) as well as the values of the elastic modulus and strain hardening modulus are based on the tri–linear material model indicated by Mohebkhah (2004). Meanwhile, the ordinates of point (3) are assumed to follow those for typical carbon steel [Salmon et al. (2009)]. It should be noted that no information was provided for the theoretical boundary conditions and the type and size of the geometrical imperfection used in the modeling and analyses of these beams [Mohebkhah (2004)].

The proposed finite element model, developed in the current study for cellular beams, is modified for CPE140 castellated beam section with span lengths and web castellation details as provided by Mohebkhah (2004). As shown in Fig. 3.14, particular cross section

dimensions of the castellated section are b_f = 73 mm, t_f = 6.9 mm, h_w = 196.2 mm and t_w = 4.7 mm. The beam is analyzed using the developed model for different span lengths of 1.26, 1.68, 2.10, 2.52, 2.94, 3.36, and 4.20 m. Lateral imperfection with maximum amplitude of $L/1500$ is used to trigger the lateral buckling mode of the analyzed beams. The proposed finite element model is used to perform elasto–plastic buckling analyses of Mohebkhah beams using the Arc–Length control method and both force and displacement convergence criteria with *Tolerance*=0.001.

A summary of obtained results, under various cases of loading, along with a comparison between the results (M_{cr}, P_{cr}, and W_{cr}) of the proposed finite element model and values reported by Mohebkhah (2004) is presented in Table 3.3. Tabulated results reveal very good agreement between both sets of results for the cases of long beams with spans L = 2.94, 3.36, and 4.20 m, where lateral buckling mode is dominant, with absolute maximum relative error of 4.1%. Other sets of shorter beams, L = 1.26, 1.68, 2.10, and 2.52 m, show less agreement with maximum relative error of 17.2%. This is attributed to the fact that Mohebkhah (2004) did not provide any details about the imperfection profile used and amplitude in addition to using a course mesh, Fig. 3.15(a), relative to the mesh of the proposed model in this study depicted by Fig. 3.15(b). Comparison between estimated C_b values summarized in Table 3.4 reveals excellent agreement with maximum absolute relative difference of 4.17%. This improved agreement is primarily due to the fact that the C_b value represents a ratio between the critical moment due to a particular case of loading (P or W) relative to the pure bending moment case M which reduces the effect of the mesh size leading to better agreement between the obtained finite element results and those reported by Mohebkhah (2004).

3.7.4 Experimental Lateral Torsional Buckling of Castellated Beams after Zirakian (2008) and Zirakian and Showkati (2006)

Experimental investigations on the distortional buckling of six (6) simply supported castellated beams under mid–span concentrated loads have been conducted by Zirakian (2008) and Zirakian and Showkati (2006). The general geometry of the tested beams is shown in Fig. 3.16 while detailed geometrical properties are summarized in Table 3.5. Vertical supports are provided at beneath the bottom flanges of the beams' ends. The top flanges of the beams are laterally supported at a distance of 165 mm from the supported edge as described by Zirakian (2008) and Zirakian and Showkati (2006). Although tested beams have 150 mm overhangs that extend beyond vertically supported locations of the beams, they are ignored in the numerical analysis reported herein. Two stiffeners are used at the support locations. Lateral support for the compression flange is imposed at the point of load application (i.e., at mid span).

The multi–linear elasto–plastic material models used in the verification with Zirakian (2008) and Zirakian and Showkati (2006) experimental buckling loads are shown in Fig. 3.17(a) and Fig. 3.17(b) for the two beam profiles, IPE 12 and IPE 14, respectively. It is worth mentioning that the shown values for the yield and ultimate stresses correspond to the least experimentally measured values by Zirakian (2008) and Zirakian and Showkati (2006) of both the flanges and the web of each profile. Meanwhile, the ordinates of points (2) and (3) are assumed based on typical profile provided by Salmon et al. (2009).

A lateral initial imperfection of size $L/1500$, is used to trigger the lateral buckling mode of the beam. Elasto–plastic buckling analyses have been performed using the Arc–Length control method and both force and displacement convergence criteria with *Tolerance*

= 0.001. Table 3.6 shows a comparison between the experimental values of the critical mid–span concentrated load and the corresponding finite element predictions. The results of the two beams, C180–5200 and C210–4400, are reported by Zirakian (2008) and Zirakian and Showkati (2006) to be in error because of due to the reasons reported in Table 3.6. Aside from these two particular cases, the tabulated comparison shows an absolute difference in the range of 2.4% and 13.7%. This reflects the very good agreement between the finite element results and the experimental outcomes. This confirms the validity and accuracy of the developed finite element model.

3.8 CONCLUSION OF THE VALIDATION PROCESS

The previous section reports the finite element predictions for several critical buckling loads of solid beams and perforated beams. These predictions are compared to their theoretical counterparts and to experimental findings and numerical outcomes that are reported in the literature. All performed comparisons show very good to excellent agreements with the results evaluated using the three dimensional finite element model. This conclusion validates the accuracy of the developed finite element model and confirms its reliability to be used in performing the elastic and elasto–plastic stability analyses reported in Chapters 4 and 5, respectively.

Table 3.1: Geometrical Parameters of the Cellular Beams

Geometrical Parameter		
Parameter	**Minimum**	**Maximum**
h_w / t_w	20	80
b_f / t_f	10	20
L / h_w	About 10	About 38
s / h_w	1.05	2.1
d_h / h_w	0.5	0.8

Table 3.2: Finite Element and Theoretical Buckling Moments for Plain–Webbed Beams

b_f (mm)	t_f (mm)	h_w (mm)	t_w (mm)	L (m)	M_{FE} (kN.m)	M_{o-cr} (kN.m) [Timoshenko and Gere (1961)]	% Error
200	10	450	10	13.5	65.29	65.05	0.37%
200	10	450	10	9.0	112.70	112.18	0.47%
160	10	450	10	13.5	41.94	41.82	0.27%
160	10	450	10	9.0	69.10	68.83	0.40%
120	10	450	10	13.5	24.72	24.68	0.17%
120	10	450	10	9.0	39.01	38.90	0.29%

Table 3.3: Comparison between the Finite Element Predictions and Mohebkhah's Numerical Results for Castellated Beams

L (m)	$^{(1)}M_{cr}$ (kN.m)	$^{(2)}M_{cr}$ (kN.m)	$^{(3)}$%Diff	$^{(1)}P_{cr}$ (kN)	$^{(2)}P_{cr}$ (kN)	$^{(3)}$%Diff	$^{(1)}W_{cr}$ (kN/m)	$^{(2)}W_{cr}$ (kN/m)	$^{(3)}$%Diff
1.26	28.00	30.80	10.0	74.7	82.5	10.4	129.68	147.00	13.4
1.68	26.42	29.64	12.2	59.0	66.4	12.5	74.53	83.80	12.4
2.10	24.27	28.44	17.2	47.1	54.0	14.6	46.33	52.19	12.6
2.52	20.95	22.56	7.7	38.6	43.3	12.2	28.55	31.00	8.6
2.94	18.70	18.32	-2.0	34.2	32.8	-4.1	19.37	19.00	-1.9
3.36	15.52	15.40	-0.8	24.9	24.6	-1.2	12.33	12.40	0.6
4.20	11.53	11.60	0.6	14.8	14.9	0.7	5.87	6.00	2.2

(1) Results from this study
(2) Results after Mohebkhah (2004)
(3) %Difference = [(2) – (1)] / (1) * 100 %

Table 3.4: Comparison between C_b Values from the Developed Finite Element Model and Mohebkhah's Results

L (m)	(1) $(P_{cr}L)/(4M_{cr})$	(2) $(P_{cr}L)/(4M_{cr})$	(3)%Diff.	(1) $(W_{cr}L^2)/(8M_{cr})$	(2) $(W_{cr}L^2)/(8M_{cr})$	(3)%Diff.
1.26	0.84	0.84	0.40	0.92	0.95	3.05
1.68	0.94	0.94	0.32	1.00	1.00	0.22
2.10	1.02	1.00	-2.16	1.05	1.01	-3.87
2.52	1.16	1.21	4.17	1.08	1.09	0.83
2.94	1.34	1.32	-2.10	1.12	1.12	0.12
3.36	1.35	1.34	-0.43	1.12	1.14	1.35
4.20	1.35	1.35	0.07	1.12	1.14	1.60

(1) Results from this study
(2) Results after Mohebkhah (2004)
(3) %Difference = [(2) – (1)] / (1) * 100 %

Table 3.5: Geometrical Properties of Tested Beams after Zirakian and Showkati (2006)

Profile	Label	h (mm)	b_f (mm)	t_f (mm)	t_w (mm)	L (mm)	x_e (mm)
IPE 12	C180–5200	176.67	64	6.3	4.4	5200	215
IPE 12	C180–4400	176.33	64	6.3	4.4	4400	172
IPE 12	C180–3600	176.33	64	6.3	4.4	3600	125
IPE 14	C210–5200	211.67	73	6.9	4.7	5200	166
IPE 14	C210–4400	210.25	73	6.9	4.7	4400	203
IPE 14	C210–3600	206.50	73	6.9	4.7	3600	251

Table 3.6: Comparison between the Experimental Values of the Critical Mid–Span Concentrated Load and the Corresponding Finite Element Predictions

Profile	Label	(1) P_{exp} (kN)	(2) P_{FEM} (kN)	(2) / (1)	Notes
IPE 12	C180–5200	25.92	13.78	0.532	Interaction between the two halves of the tested beam led to higher experimental load P_{exp}
IPE 12	C180–4400	15.63	17.76	1.137	
IPE 12	C180–3600	21.58	22.10	1.024	
IPE 14	C210–5200	24.90	22.99	0.923	
IPE 14	C210–4400	39.94	31.23	0.782	Considerable friction between the loading point and the beam led to higher experimental load P_{exp}
IPE 14	C210–3600	37.22	38.28	1.028	

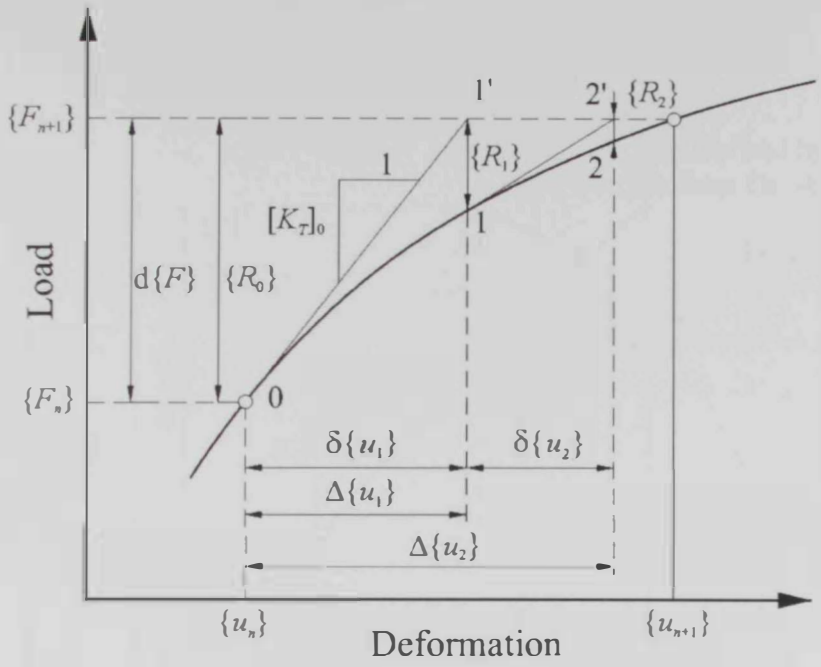

(a): Load and Deformations Increments

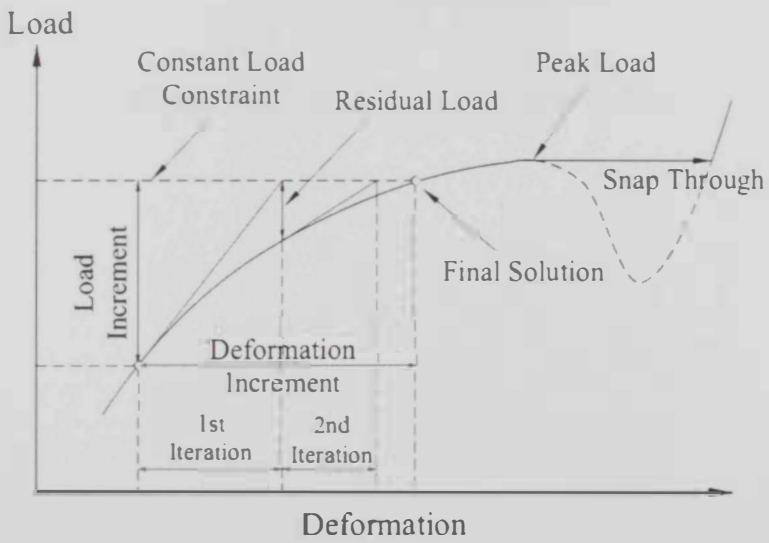

(b): Failure to Obtain Peak Critical Load with Newton–Raphson Method

Figure 3.1: Newton–Raphson Iterative Procedure

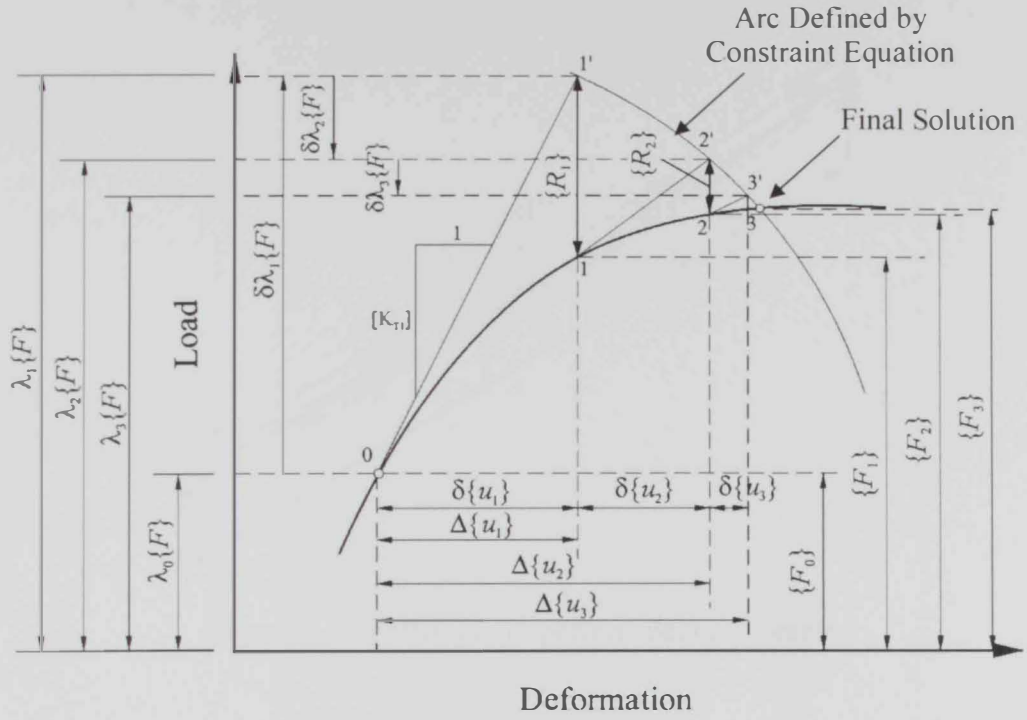

Figure 3.2: Arc–Length Control Procedure

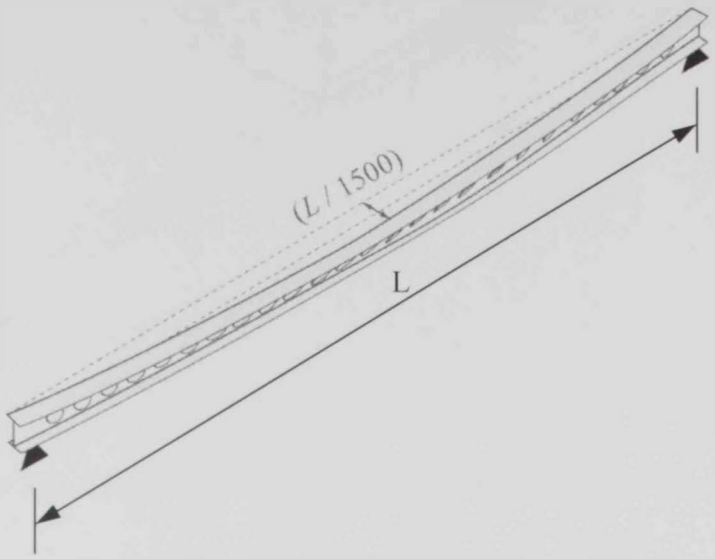

Figure 3.3: Perturbed (Imperfect) Beam Geometry

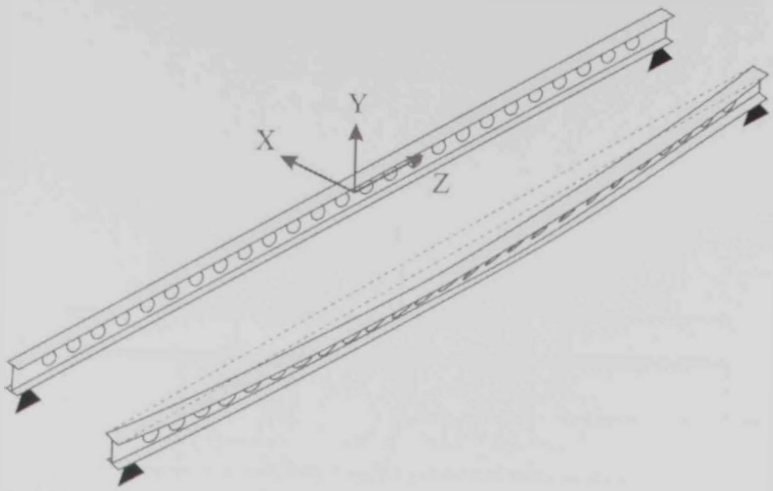

Figure 3.4: Typical Lateral Torsional Buckling Mode of Cellular Beams

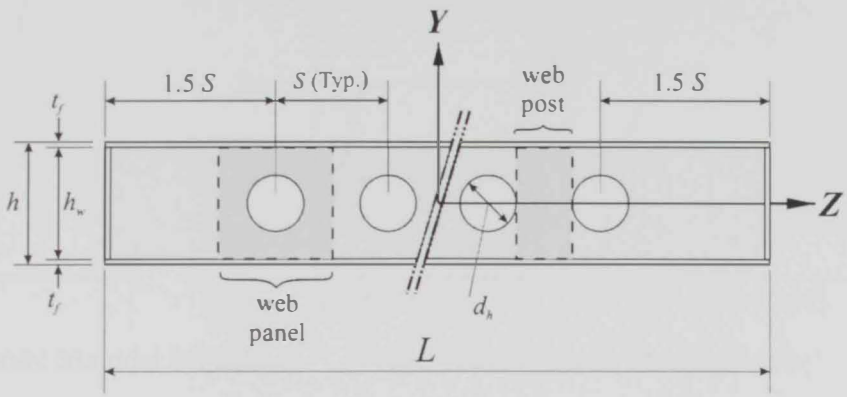

Figure 3.5: Geometry of a Typical Cellular Beam

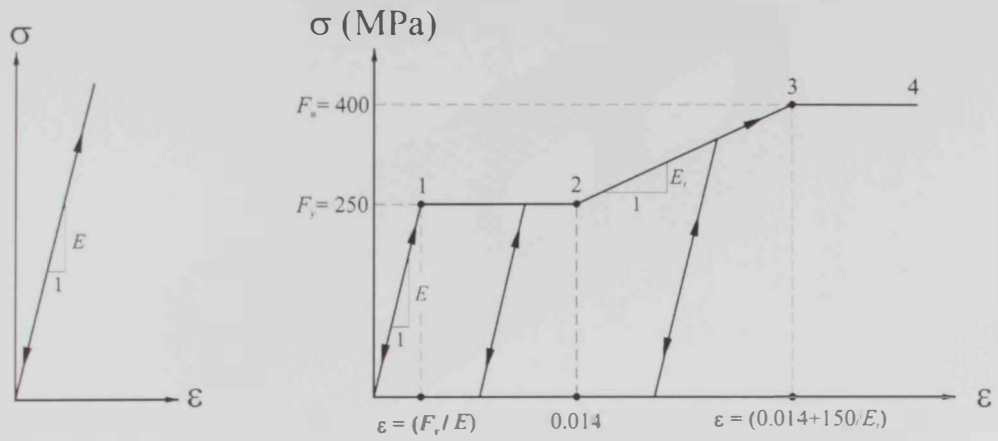

(a): Elastic Material Model **(b):** Elasto–Plastic Material Model

Figure 3.6: Material Models for Elastic and Elasto–Plastic Analyses

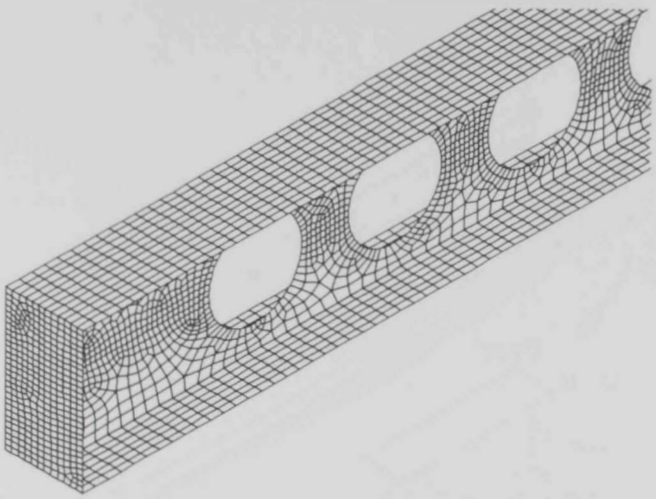

Figure 3.7: Sample Finite Element Mesh for Cellular Beam

(b_f= 115 mm, t_f= 11.5 mm, h_w = 200 mm, t_w = 10 mm, d_h = 140 mm, and s = 210 mm)

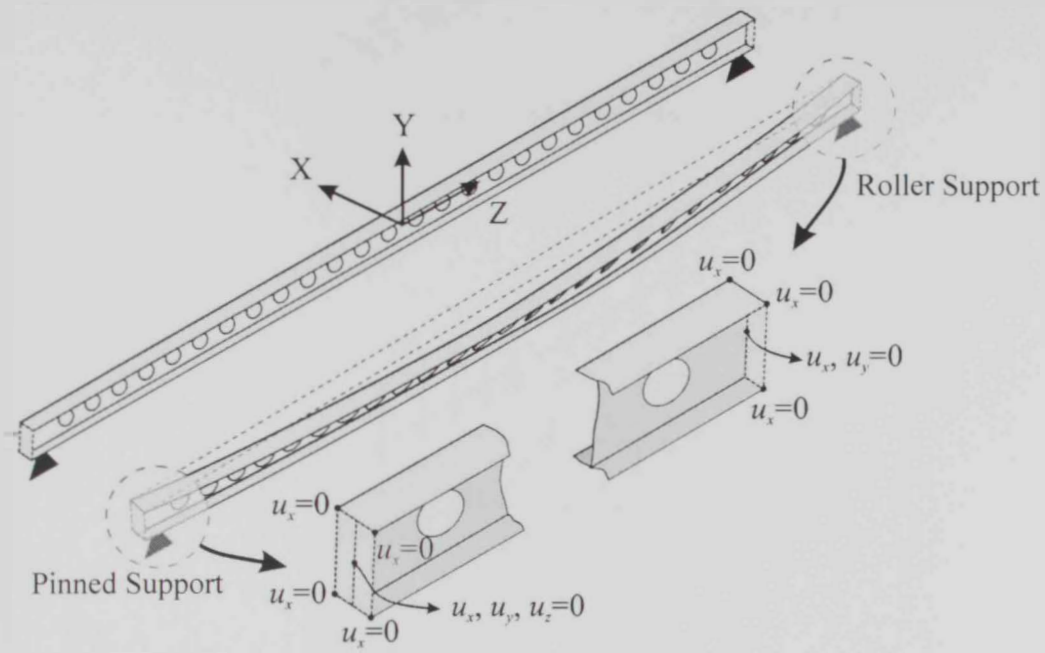

Figure 3.8: Boundary Conditions for the Cellular Beam Model

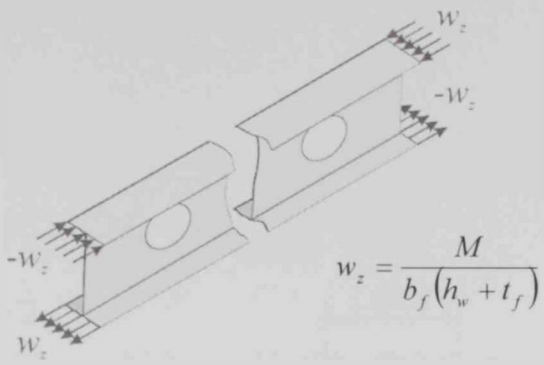

(a): End Moments

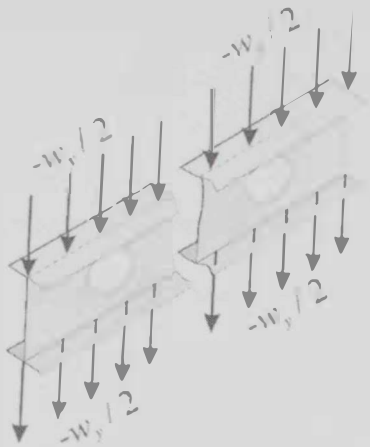

(b): Uniformly Distributed Load

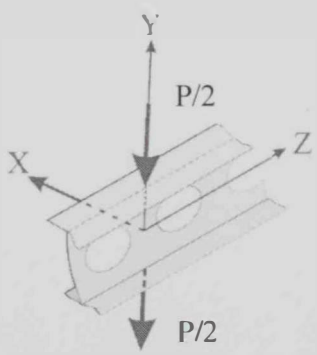

(c): Mid–Span Concentrated Load

Figure 3.9: Idealized Loads on Cellular Beam

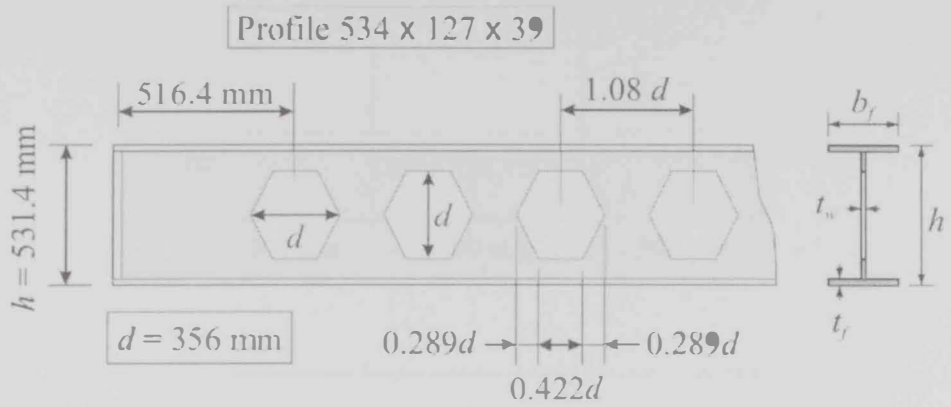

Figure 3.10: Dimensions of Castellated Beam (M5–1, 534 x 127 x 39)

after Nethercot and Kerdal (1982)

(L = 6800 mm, h = 1.5 d = 531.4 mm, b_f = 126.0 mm, t_f = 10.7 mm, and t_w = 6.6 mm)

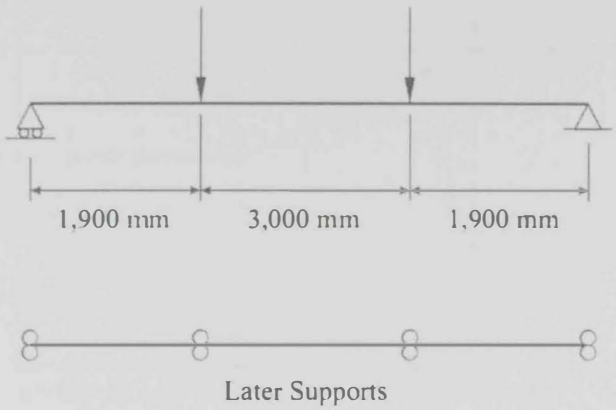

Figure 3.11: Castellated Beam M5–1 after Nethercot and Kerdal (1982)

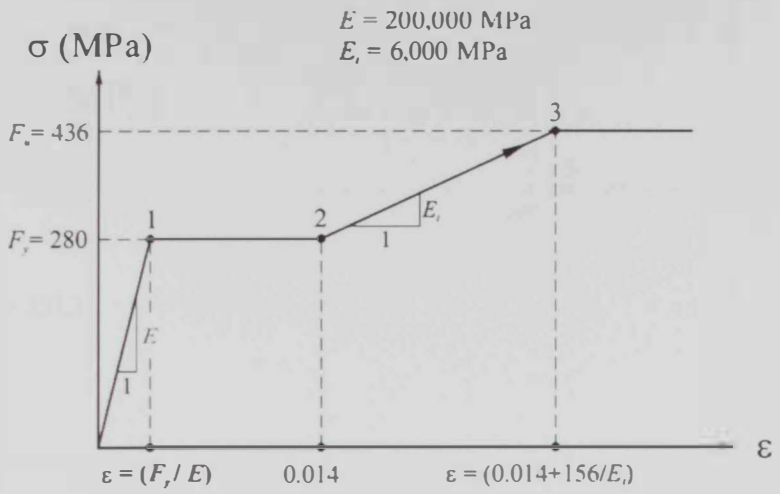

Figure 3.12: Elasto–Plastic Material Model for Comparison with Nethercot and Kerdal (1982)

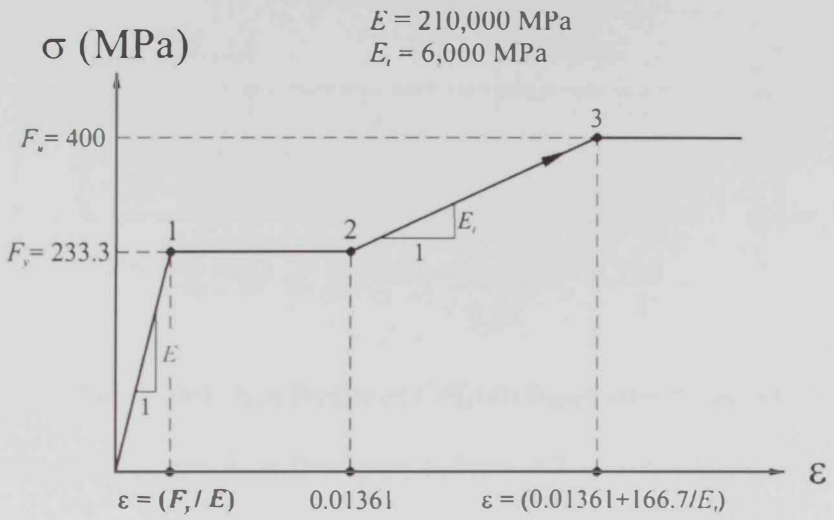

Figure 3.13: Elasto–Plastic Material Model for Comparison with Mohebkhah (2004)

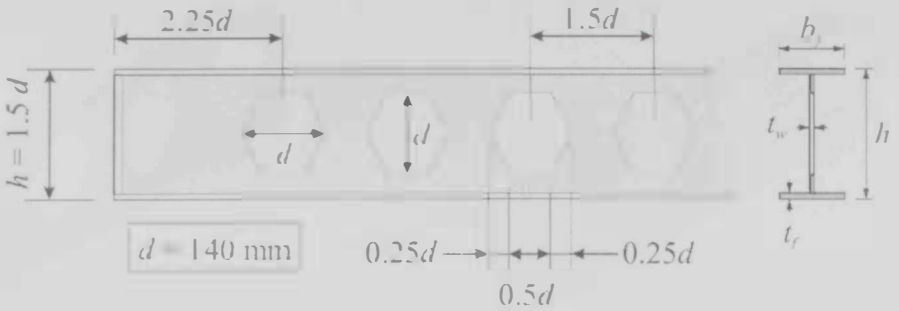

Figure 3.14: Castellation Profile of CPE140 Beam after Mohebkhah (2004)

(b_f = 73 mm, t_f = 6.9 mm, h_w = 196.2 mm and t_w = 4.7 mm, h = 210 mm, d = 140 mm)

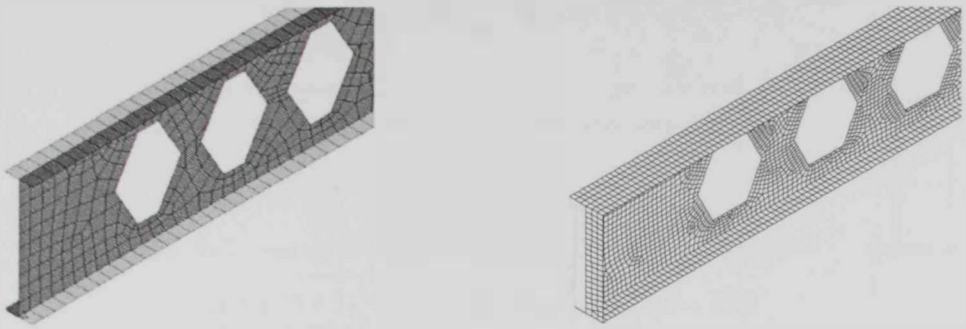

(a): Mesh after Mohebkhah (2004) **(b):** Mesh Used in the Current Study

Figure 3.15: Mesh Used in the Analysis of Mohebkhah (2004) Castellated Beams

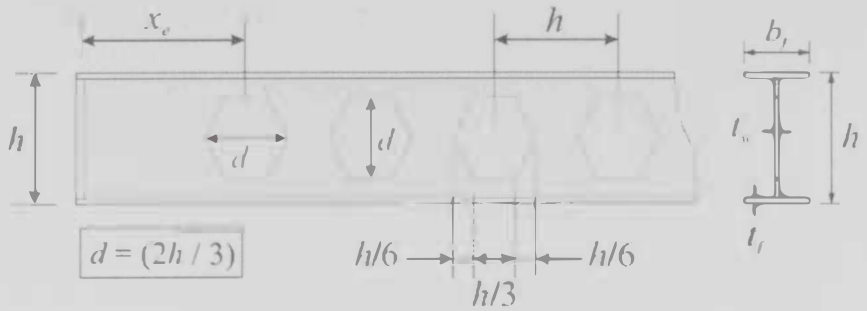

Figure 3.16: Geometrical Properties of the Tested Castellated Beams after Zirakian and Showkati (2006)

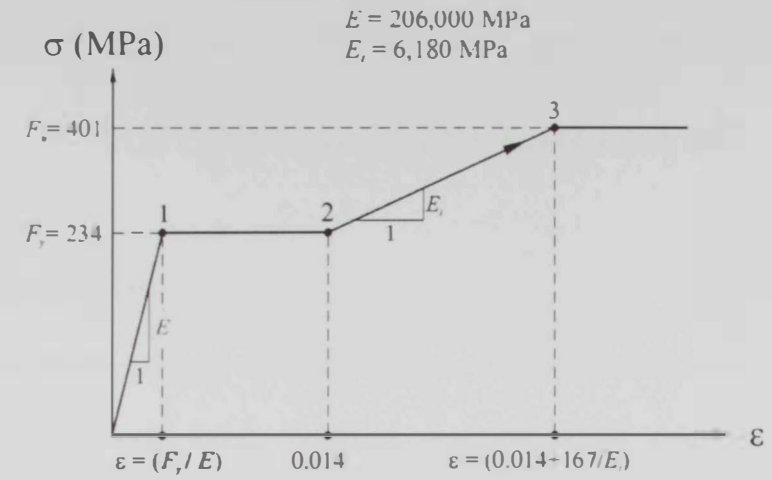

(a): Finite Element Material Model for IPE 12

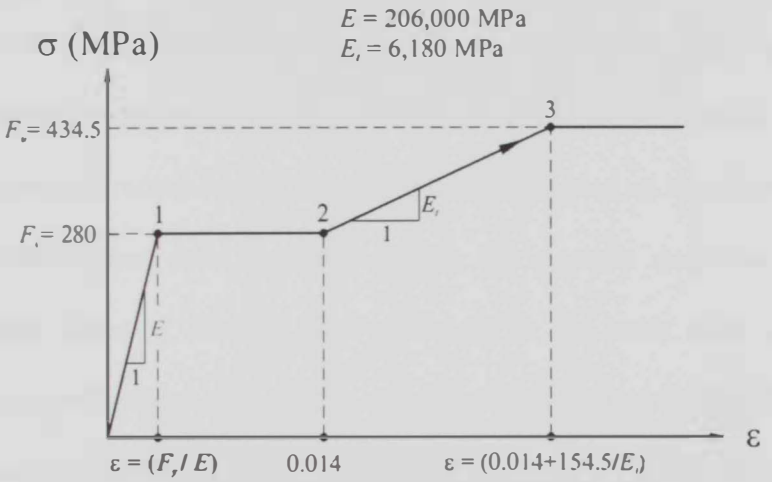

(b): Finite Element Material Model for IPE 14

Figure 3.17: Elasto–Plastic Material Model for Comparison with Zirakian and Showkati (2006)

CHAPTER 4

ELASTIC LATERAL TORSIONAL BUCKING OF SIMPLY SUPPORTED CELLULAR BEAMS

4.1 INTRODUCTION

Cellular beams are now broadly used as main structural elements in a wide variety of structures including multi–storey buildings, commercial and industrial buildings, airport terminals, exhibition halls, parking garages and stadiums. In addition to the weight reduction that is achieved by using such beams, web perforations allow for easy installation of piping, electrical and mechanical ductworks without increasing the floor–to–floor height as shown in Fig. 4.1(a). Furthermore, the appealing aesthetical appearance of cellular beams makes them essential elements in construction of exposed structures as presented in Fig. 4.1(b). Structural designs are always attracted by the fact that the augmentation of the cellular section height, compared to its original solid section, enhances its in–plane structural characteristics. It should be noted, however, that the non–uniformity in the beam cross section due to the presence of web perforations may have an adverse effect on the in–plane flexural capacity of cellular beams in case of instability failure before reaching their full flexural capacity. Similar to castellated beams, it is expected that instability failure of cellular beams may be controlled by any one/combination of the following modes [Kerdal and Nethercot (1984), Chung et al. (2000), Mohebkhah (2004), Zirakian and Showkati (2006)]:

1. Lateral torsional buckling
2. Lateral distortional buckling
3. Shear buckling of the web post
4. Compression buckling of the web post

The elastic stability of beams is typically a concern during the construction stage when lateral bracing elements are not yet installed. As such, the unbraced length of the cellular beam is sufficiently long for elastic instability to occur. Furthermore, the increase in the flexure capacity of cellular beams may result in structural designs of beams with longer spans which are more susceptible to elastic instability.

This chapter is motivated by the lack of information related to elastic lateral torsional buckling of cellular steel beams. The material presented in the chapter represents an extension to the recent work on the stability of cellular steel beams by Sweedan (2011) that focused on the elastic lateral stability of cellular beams under transverse loads acting at the shear centre of the beam section. In the current chapter, the influence of location of load application is studied numerically using three–dimensional finite element modeling. Extensive parametric analyses are performed to evaluate the impact of variation of cross section dimensions, beam slenderness, and web openings size and spacing on the load carrying capacity of cellular steel beams.

4.2 GEOMETRICAL PARAMETERS FOR ELASTIC ANALYSIS

The finite element elastic model developed in Chapter 3 is utilized to investigate the influence of beam geometry and web perforation on elastic stability of cellular beams. A wide range of cross section dimensions is considered in the analysis to cover the common range of practical dimensions of steel beams. To facilitate application of the study outcomes, controlling parameters are presented in a general non–dimensional form. Performed analysis considers cross sections with web slenderness h_w/t_w that ranges between 20 and 80 with an increment of 10. Flange aspect ratio b_f/t_f equals 10, 15 and 20. Circular web openings are expressed through a hole diameter to web height ratio d_h/h_w that varies between 0.5 and 0.8

with an increment of 0.1. Holes are uniformly spaced with a spacing to web height ratio s/h_w of 1.05 to 2.1 which corresponds to a spacing to diameter ratio s/d_h that extends from 1.3 to 4.2. Moreover, a wide spectrum of beam span values is taken into consideration as expressed by span to web height ratio L/h_w. Such ratio varies between 10.50 and 37.8 for the case of s/h_w equals 1.05. For higher s/h_w values the L/h_w ratio is increased accordingly to maintain the same number of web perforations for each particular cross section. This allows the influence of change in hole spacing on the buckling behavior, excluding any impact from variation in the number of holes, to be investigated. As a result, L/h_w ranges from 15.75 to 56.70 for s/h_w of 1.575 and from 21.0 to 75.60 for s/h_w of 2.10. Each beam is analyzed under three different load cases including uniform moment due to pure end moments, mid–span concentrated load, and uniformly distributed load. Results are used to calculate the moment gradient factor, C_b, for the two basic cases of loading of mid–span concentrated load and uniformly distributed load.

4.3 JUSTIFICATION OF USING DIMENSIONLESS PARAMETER k_e

As mentioned earlier, each of the beams described in the previous section is analyzed under three different loading cases; uniform moment, mid–span concentrated load, and uniformly distributed load. For each beam, buckling moment values at the mid–span obtained from both cases of concentrated and uniform loading are used to calculate the moment gradient factor, C_b, through their normalization with respect to the corresponding critical moment at mid–span that results from the uniform moment case of loading:

$$C_b = \frac{M_{FE-P}}{M_{FE-M}} \qquad \text{for the concentrated load case} \qquad (4.1(a))$$

$$C_b = \frac{M_{FE-W}}{M_{FE-M}} \qquad \text{for the uniformly distributed load case} \qquad (4.1(b))$$

where

M_{FE-M} is the buckling moment at mid–span due to uniform moment distribution,

M_{FE-P} is the buckling moment at mid–span due to concentrated mid–span load, and

M_{FE-W} is the buckling moment at mid–span due to uniformly distributed load.

For all analyzed cases, the variation of obtained C_b factor is presented with respect to a non–dimensional factor k_e that accounts for the major characteristics of the beam including, the beam length L, the torsional rigidity of the beam GJ, and the warping rigidity EC_w [Sweedan (2011)]:

$$k_e = \frac{\pi}{L}\sqrt{\frac{EC_w}{GJ}} \tag{4.2}$$

where

E is Young's modulus of elasticity,

C_w is the warping torsional constant of the cross section,

G is the shear modulus of elasticity, and

J is the torsional constant of the cross section.

For a solid web I–section, the torsional constant J and the warping torsional constant C_w can be approximated by [Timoshenko and Gere (1961), Salmon et al. (2009)]:

$$J = \sum \frac{bt^3}{3} \tag{4.3}$$

$$C_w = \frac{t_f b_f^3 h_o^2}{24} \tag{4.4}$$

where

b is the width of each element of the I–shaped cross–section,

t is the thickness of each element of the I–shaped cross–section,

b_f is the width of the flange,

t_f is the thickness of the flange, and

h_o is the height between centers of both flange plates (i.e.; $h_o = h_w + t_f$).

A careful investigation of Eq. (4.2) shows that as h_w/t_w and b_f/t_f increase (i.e., when the cross–sectional elements become more slender) the value of k_e increases. On the contrary, as the length of the beam increases, the value of k_e decreases. It is therefore important to note that low values of k_e correspond to long beams with thick cross–sectional elements (referred to as slender beams) where the beams become more susceptible to lateral torsional buckling. Meanwhile, large values of k_e correspond to short beams with slender elements in their cross–sections leading to beams that can resist lateral torsional buckling allowing for other buckling modes to develop.

For the particular case of cellular beams, the dimensions of the net section at the center of the web hole are utilized in the calculation of the cross section properties. As such the J_{net} parameter is obtained in accordance with the following expression:

$$J_{net} = \frac{2}{3} b_f t_f^3 + \frac{1}{3}\left(h_w t_w^3 - d_h t_w^3\right) \tag{4.5}$$

Throughout the subsequent calculations included in this thesis, the same approach is followed whenever other cross sectional properties (such as area or inertia) are calculated. The only exception for this approach applies to the warping torsional constant C_w which is negligibly affected by the web openings [Kohnehpooshi and Showkati (2009)] and, therefore, is calculated for cellular beams using the same expression presented by Eq. (4.4).

An essential characteristic that justifies using the k_e factor is that different cellular beams with the same k_e value and the same perforation configuration (d_h/h_w) and (s/h_w) have

the same C_b factor under a particular case of loading [Sweedan (2011)]. The sample results presented in Table 4.1 confirms this characteristic where it can be observed that although the first three beams are different in cross section dimensions and span, they have equal C_b factors under the same case of loading. As indicated by these tabulated values, different beams with equal (b_f/t_f), (h_w/t_w), (A_f/A_w), (d_h/h_w), (s/h_w), and (L/h_w) ratios have equal k_e value and consequently the same C_b factor. On the contrary, once any of the above mentioned ratios varies, the k_e and C_b factors are no longer equal. Examples of such rule are given in rows 4 and 5 of Table 4.1 where different (b_f/t_f) and (h_w/t_w) ratios, respectively, result in change in the k_e and C_b factors relative to those obtained in the first three rows.

4.4 FINITE ELEMENT RESULTS AND DISCUSSION

Elastic lateral stability of cellular beams under idealized application of transverse loading has been studied by Sweedan (2011). In that study load effects simulated the idealized case of load application at the shear center of the beam cross section to preclude any destabilizing or stabilizing effects of loading applied above or below shear center, respectively. Simulations are performed by applying half the load at the top flange and the other half at the bottom flange with both portions acting along the same direction as shown in Fig. 4.2(a) [Sweedan (2011)]. Under these idealized loading conditions, a series of elastic buckling analyses was carried out to identify the critical buckling moment of cellular beams along with the corresponding fundamental buckling mode. The variation of the moment gradient factor C_b with cellular beam geometry and perforation configurations was also assessed. Outcomes of the study [Sweedan (2011)] revealed that elastic buckling of long span cellular beams is dominated by pure elastic lateral torsional buckling mode (LTB) as shown in Fig. 4.3(a). For such long beams, C_b values are slightly higher or lower than recommended code values for solid beams (±5% of code C_b values). Sweedan (2011) also showed that the

elastic buckling of intermediate span cellular beams is controlled by lateral distortional buckling mode (LDB) where web distortion (deviation from its initial planar shape) is coupled with lateral deformations as shown in Fig. 4.3(b). In addition, the study showed that short span cellular beams exhibit a buckling mode that is dominated by a high level of web distortion associated with the high shear stresses induced in the web plates. This case of short beams buckling is dominated by local web deformations while no lateral buckling (LTB or LDB) takes place as presented in Fig. 4.3(c). This response is associated with low C_b values of less than 1.1 and 1.0 for beams subjected to mid–span concentrated load and uniformly distributed load, respectively [Sweedan (2011)]. The transition stage between lateral buckling response (LTB and LDB) and local web buckling response (WLB) is controlled by an interaction between LDB and WLB modes as presented in Fig. 4.3(d). It has been also shown that cellular beams with slender web plates (i.e.; having higher h_w/t_w values), cellular beams with big hole size (d_h/h_w), and cellular beams with closely spaced holes (small s/h_w values) are more prone to shear deformations and, therefore, are mostly governed by local web buckling. Such beams are less likely to experience lateral buckling modes (LTB or LDB) unless they have significantly long spans. The results have also revealed that cellular beams with relatively wide flanges show more torsional stability which, consequently, reduces the encountered reduction in the C_b factor due to the web perforations.

Detailed discussions on the behavior of cellular beams subjected to transverse loads applied at different levels along with in depth comparison to that related to loads applied at shear center of the cross section are presented in the next section.

4.4.1 Effect of Load Application Level on the Elastic Stability of Cellular Beams

This section discusses the buckling moment results and the associated buckling behavior of cellular steel beams subjected to uniform bending moment, mid–span concentrated load and uniformly distributed load. Investigations include a wide spectrum of geometrical and perforation configurations as outlined in Section 4.2. In addition to the conventional load application scheme in which transverse loads act at the shear center of the cross section that was studied by Sweedan (2011), two other practical schemes of loads applied at the top flange or the bottom flange of the beam are considered. Results of these two loading schemes require performing a total of 11,340 finite element analyses. Outcomes of such analyses are utilized to obtain the moment gradient factor C_b in accordance with Eqs. (4.1(a)) and (4.1(b)). The variation of the C_b factor is presented with respect to the dimensionless factor k_e presented by Eq. (4.2) and calculated using the net torsional constant J_{net}.

Figures 4.4 and 4.5 present sample results to demonstrate the variation of the C_b factor with respect to the K_e factor for simply supported beams subjected to mid–span concentrated load and uniformly distributed load, respectively. Results presented in these figures correspond to the particular case of cellular beams with $(b_f/t_f) = 15$, $(d_h/h_w) = 0.6$, and $(s/h_w) = 1.05$. Meanwhile, three representative (h_w/t_w) values of 30, 50 and 70 are considered in these figures for illustrative purposes. Figs. 4.4(a), 4.4(b) and 4.4(c) correspond to mid–span concentrated load that is applied at top flange, shear center, and bottom flange of the cellular cross section, respectively. Similarly, Figs. 4.5(a), 4.5(b) and 4.5(c) present the results of uniform distributed loading acting at top flange, shear center and bottom flange of the cross section, respectively. All these figures indicate a general behavior of cellular beams that is similar to that of solid beams where beams subjected to mid–span concentrated load can

sustain higher moments (i.e., have higher C_b values) than those supporting uniformly distributed load. This is attributed to the fact that in the former case of loading the high flange compression is localized around the mid–span, whereas in the latter case relatively high moment values are affecting longer portion of the beam's span. For both cases of loading, the stabilizing/ destabilizing effect of loads applied below/above the shear center can be observed. This is reflected in the increase in the moment carrying capacity, and consequently, in the C_b value for a certain beam as the load application level is lowered from being above the shear center (e.g. at top flange as shown in Figs. 4.4(a) and 4.5(a)), to the shear center (Figs. 4.4(b) and 4.5(b)), and finally below the shear center (Figs. 4.4(c) and 4.5(c)). The decreasing stability of beams loaded above their shear center results from the fact that vertical loads, when acting on the laterally deformed beam, exert an additional destabilizing torque about the shear center, which results in additional twisting of the beam (Fig. 4.6(a)) leading to earlier instability failure of the beam. On the contrary, loads applied below the shear center of a deformed beam result in a stabilizing twist about the shear center that counteracts the original lateral deformation of the beam (Fig. 4.6(b)). As such, buckling failure of this beam occurs at a higher load value than the one required to buckle the same beam when loaded above its shear center.

For both cases of loading, and irrespective of the level of application of the vertical load, a general trend of variation in the C_b factor indicates higher C_b values for slender beams (i.e., with high L/h_w and lower k_e values). A reduction in the C_b value is demonstrated for shorter beams (i.e., with low L/h_w and high k_e values). This observation can be explained in view of the buckling modes influencing the response of beams with various slenderness values and subjected to loads at different levels of application.

Starting with the conventional case of a cellular beam subjected to a concentrated load at the shear center as depicted in Fig. 4.4(b), it can be seen that slender beams (i.e., with lower k_e values) and/or beams with large k_e and small h_w/t_w possess C_b values that are very close to the value 1.32 that is recommended by AISC 360–05 (2005) for solid beams. Finite element results reveal that the response of beams having these characteristics is dominated by pure elastic lateral torsional buckling mode (LTB) as shown in Fig. 4.3(a). For beams with higher h_w/t_w values, and as the beam slenderness decreases (i.e., k_e value increases) the level of web distortion during lateral buckling increases. This leads to the formation of lateral distortional buckling mode (LDB) where local web distortion and lateral buckling occur simultaneously as shown in Fig. 4.3(b). Such beams encounter a reduction in their moment carrying capacity as indicated by the associated lower C_b values as represented by points (A) and (B) in Fig. 4.4(b). Moreover, with further increase in the k_e value, a significant reduction in the C_b factor is observed where C_b values less than unity are obtained for points (C) and (D) in Fig. 4.4(b). Finite element results indicate that this significant reduction in the C_b value is associated with the local web buckling mode as shown in Fig. 4.3(c) where shear deformations are dominant and lateral deformations are insignificant. Similar behavior is observed for cellular beams subjected to uniformly distributed load at their shear center as shown in Fig. 4.5(b). This figure demonstrates that slender beams and/or shorter beams with small h_w/t_w buckle by pure elastic lateral torsional buckling (LTB) where their C_b values are very close to 1.14 as recommended by AISC 360–05 (2005) for solid beams. Points (A) and (B) are characterized by lateral distortional buckling mode (LDB) and points (D), (E) and (F) represent beams failing by local web buckling. Point (C) represents the transition stage between lateral buckling modes (LTB and LDB) and local buckling. Along this transition stage, lateral deformations decrease while localized deformations are progressively introduced. Such a stage is controlled by interaction between these two types of modes as

shown in Fig. 4.3(d). Along this transition stage, lateral deformations gradually decrease with progressive introduction of localized deformations until the overall buckling mode is governed by local non–lateral deformations. For cellular beams subjected to mid–span concentrated load at their shear center, C_b values that are equal to or less than 1.1 are associated with such non–lateral buckling modes. Meanwhile, for beams subjected to uniformly distributed load at the shear center level, formation of local non–lateral buckling modes is expected at C_b values less than 1.0 as reported by Sweedan (2011).

The behavior of cellular beam subjected to concentrated and uniformly distributed loads at the top flange is shown in Figs. 4.4(a) and 4.5(a), respectively. These figures indicate that for both loading cases all C_b values are significantly less than AISC 360–05 (2005) recommended values for solid beams. This observation confirms the destabilizing effect of transverse loads applied above the shear center. Similar to the case of loads applied at the shear center, identified buckling modes reveal that slender beams (lower k_e values) and/or shorter beams with small h_w/t_w values buckle by pure elastic lateral torsional buckling (LTB). The only exception for this behavior in beams subjected to a concentrated load is denoted by points (A) and (B) in Fig. 4.4(a) where failure of short beams with h_w/t_w = 70 occurs by lateral–local buckling interaction and pure local web buckling modes, respectively. For the case of uniformly distributed load (Fig. 4.5(a)) points (A) through (E) represent beams failing by lateral distortional buckling (LDB). Meanwhile, points (F) and (G) correspond to failure by local web buckling. For cellular beams loaded at the top flange level, C_b values of 0.8 and 0.7 may conservatively represent the limiting values below which the response is controlled by non–lateral buckling modes for mid–span concentrated loading and uniformly distributed loading, respectively. Although these limits reasonably apply to all studied beams when

loaded at the top flange level, they are based on the strict results pertaining to cellular beams with closely–spaced web perforations (s/h_w = 1.05).

The variation of the C_b values of cellular beam subjected to concentrated and uniformly distributed loads at the bottom flange is shown in Figs. 4.4(c) and 4.5(c), respectively. As indicated by these figures, t he majority of the obtained C_b values are significantly higher than the AISC 360–05 (2005) values for solid beams. As reported for other beams loaded at and above their shear center, slender beams (lower k_e values) and/or shorter beams with small h_w/t_w experience pure elastic lateral torsional buckling failure (LTB). On the contrary, beams represented by points (A) through (F) in Fig. 4.4(c) and points (A) through (E) in Fig. 4.5(c) for beams subjected to concentrated load and uniformly distributed load, respectively, experience local web buckling with no associated lateral deformations. These points correspond to intermediate and short span cellular beams with slender webs (high h_w/t_w values). It should be noted that for all cellular beams failing by lateral buckling modes in Figs. 4.4(c) and 4.5(c), the corresponding C_b values are significantly higher than the values for the same beams when subjected to loads at or above the shear center. This emphasizes the stabilizing influence of transverse loads applied below the shear center of cellular beams. In general, cellular beams loaded at the bottom flange level, C_b values of 1.6 and 1.3 may conservatively represent the limiting values below which the response is controlled by non–lateral buckling modes for mid–span concentrated loading and uniformly distributed loading, respectively. As was mentioned earlier, these limits are applicable to all beams considered in this study when loaded at the bottom flange level. However, they are based on the strict results corresponding to cellular beams with closely–spaced web perforations (s/h_w = 1.05).

4.4.2 Effect of Beam Geometry on the Moment Gradient Factor C_b

Following the explanation of the general behavior of cellular beams that was presented in the previous section for a sample set of finite element results, a more general discussion for the variation in C_b factor related to a broader spectrum of geometrical parameters is presented in the following sub–sections.

4.4.2.1 Effect of Web Slenderness h_w/t_w

All cellular beams considered in this section have a b_f/t_f value of 15. Web openings are uniformly spaced at constant intervals with s/h_w = 1.05. Figs. 4.7(a), (b), (c) and (d) show the variation in the C_b factor for cellular beams having web holes defined by d_h/h_w = 0.5, 0.6, 0.7 and 0.8, respectively. All beams are subjected to mid–span concentrated load at top flange level. Each of these figures includes seven plots that correspond to various web slenderness values h_w/t_w that vary from 20 to 80 with an increment of 10. These figures reveal that, for a particular hole size, beams with different h_w/t_w values have very close C_b value for failure cases dominated by lateral torsional buckling (LTB). Meanwhile, beams with slender web plates (i.e., high h_w/t_w values) experience shear deformations in their web plates and, therefore, are controlled by combined lateral–local buckling or pure local buckling modes at higher k_e values. Similar behavior is also observed for the same set of beams when subjected to mid–span concentrated load at bottom flange level as shown in Figs. 4.8(a), (b), (c) and (d) for cellular beams with d_h/h_w = 0.5, 0.6, 0.7 and 0.8, respectively. Comparison between Figs. 4.7 and 4.8 reveal that the influence of localized web distortions occurs at lower k_e values for a particular beam loaded at its bottom flange compared to its counter part with load application at the top flange level. This observation is attributed to the fact that loads applied below the shear center resist the formation of lateral torsional buckling mode. Thus, other failure modes that are dominated by localized web deformations are introduced to the

response earlier than what typically occurs in beams loaded above their shear center level where LTB is triggered by extra load–position–related torque. Similar behavior is demonstrated for the same beams when subjected to uniformly distributed load at top and bottom flange levels as depicted by Figs. 4.9(a) through (d)) and Figs. 4.10(a) through (d), respectively.

4.4.2.2 Effect of Web Hole Size d_h/h_w

It can be also observed from Figs. 4.7(a), (b), (c) and (d) that beams with the same web slenderness h_w/t_w experience slight decrease in the C_b value as a result of increasing the web hole size d_h/h_w. This observation applies only to slender beams and/or beams with small h_w/t_w values that fail by lateral torsional buckling (LTB). On the contrary, increasing the web hole size in shorter beams with more slender web plates leads to the development of higher shear deformations in these web plates. Thus, response of these beams is primarily dominated by combined lateral–local buckling or pure local buckling modes rather than LTB mode. This change in failure mode is associated with a significant reduction in the C_b value, which becomes more apparent with bigger hole sizes. The same observation applies to cellular beams loaded with a concentrated load at bottom flange level as shown in Figs. 4.8(a), (b), (c) and (d) for web hole sizes d_h/h_w = 0.5, 0.6, 0.7 and 0.8, respectively. Similar behavior is also shown for cellular beams subjected to uniformly distributed load at top or bottom flange levels as presented in Figs. 4.9(a) through (d) and Figs. 4.10(a) through (d), respectively.

4.4.2.3 Effect of Hole Spacing s/h_w

Figs. 4.7, 4.11 and 4.12 correspond to cellular beams with b_f/t_f = 15 subjected to mid–span concentrated load at the top flange with web holes spaced at s/h_w = 1.05, 1.575 and 2.1, respectively. Comparison between these figures reveals that cellular beams with widely

spaced web holes (i.e.; high s/h_w values) provide higher shear stiffness. As such, less shear deformation is introduced in the web and the buckling response is controlled by lateral buckling modes (LTB and/or LDB). This is evident by the elimination of the combined lateral–local buckling and pure local buckling modes (occurring in Fig. 4.7 for s/h_w = 1.05) once s/h_w increases to 1.575 and 2.1 (Figs. 4.11 and 4.12, respectively). The performance of cellular beams with b_f/t_f = 15 subjected to a concentrated load at the bottom flange with web holes spaced at s/h_w = 1.05, 1.575 and 2.1 is shown in Figs. 4.8, 4.13 and 4.14, respectively. Based on these figures, by increasing s/h_w to a value of 1.575 all the beams fail by lateral torsional buckling (LTB) with the exception of a few short beams (high k_e value) and beams with slender web values (h_w/t_w = 70 and 80) that experience combined lateral–local buckling or pure local buckling (Figs. 4.13(a) through (d)). With a further increase of s/h_w to a value of 2.1, the response becomes fully governed by lateral torsional buckling modes (LTB) as depicted by Figs. 4.14(a) through (d).

Beams subjected to uniformly distributed loads at the top or bottom flange show similar response to that of corresponding beams under concentrated load as shown in Figs. 4.9, 4.15 and 4.16 for top flange loading and Figs. 4.10, 4.17 and 4.18 for bottom flange loading with web holes spaced at s/h_w = 1.05, 1.575 and 2.1, respectively.

4.4.2.4 Effect of Flange Dimensions b_f/t_f

This section reports on the influence of the flange aspect ratio on the moment gradient factor C_b for representative cases of cellular beams with closely–spaced web perforations (s/h_w = 1.05). The variation of the moment gradient factor C_b is presented with respect to the non–dimensional factor k_e based on the results of two extreme cases of flange aspect ratio where b_f/t_f = 10 and 20. Presented results herein correspond to various web slenderness values

h_w/t_w that vary from 20 to 80 with an increment of 10. In addition, hole size effect is taken into account by considering various hole diameters represented by d_h/h_w = 0.5, 0.6, 0.7 and 0.8. Figs. 4.19 and 4.20 summarize the results for cellular beams subjected to mid–span concentrated load at the top flange having b_f/t_f = 10 and 20, respectively. Comparison between these two sets of figures reveals, irrespective of doubling the flange aspect ratio, insignificant change is observed in the C_b factor for cellular beams having equal k_e values. As was discussed before, Fig. 4.19 indicates a clear reduction in the C_b factor for short cellular beams (at high k_e values) as a result of the web distortions that develop in beams with shorter spans.

It should be noted that such a reduction is more pronounced in beams with flanges of smaller aspect ratio (b_f/t_f = 10) relative to those with higher flange aspect ratio (b_f/t_f = 20) as indicated by Figs. 4.19 and 4.20, respectively. This observation may be attributed to the fact that larger flange plates provide more effective torsional restrains for the perforated webs. As a result, the encountered reduction in the C_b factor with (b_f/t_f = 20) appears in beams that are relatively shorter than those experiencing similar reduction while having b_f/t_f = 10. The same effect is observed for performance of cellular beams subjected to mid–span concentrated load at bottom flange level as shown in Figs. 4.21(a) through (d) and Figs. 4.22(a) through (d) for flanges having b_f/t_f = 10 and 20, respectively.

Furthermore, cellular beams subjected to uniformly distributed load have also shown similar performance to those subjected to a concentrated load as depicted by Figs. 4.23(a) through (d)) and Figs. 4.24(a) through (d) for loaded top flange with b_f/t_f = 10 and 20, respectively, and Figs. 4.25(a) through (d)) and Figs. 4.26(a) through (d) for loaded bottom flange with b_f/t_f = 10 and 20, respectively.

4.5 SUMMARY AND CONCLUSIONS

This chapter investigates the influence of load application location on the elastic lateral torsional buckling of I–shaped cellular beams under various loading conditions. A three–dimensional finite element model is developed to identify the critical buckling load and the associated buckling modes of analyzed beams. A comprehensive parametric analysis is conducted to evaluate the impact of various cross section dimensions, beam slenderness, and web openings size and spacing on the buckling capacity and associated modes of cellular steel beams. Results of conducted analyses are utilized to evaluate the variation of the moment gradient factor C_b relative to a non–dimensional factor k_e that relates the warping rigidity to the torsional rigidity of cellular beams. Results are analyzed and discussed for loads applied at the top flange level and the bottom flange level. Discussions include comparison to the results of the conventional case of loading whereby loads are applied at the shear center reported in the literature. The finite element analyses conducted for 11,340 cellular beams during this study resulted in the following conclusions:

- Loads applied at the top flange level of cellular beams result in destabilizing effect on the response of cellular beams. This effect results from the additional torque exerted by applied loads which produces additional twisting of the beam leading to earlier instability failure of the beam.
- On the contrary, loads applied at the bottom flange level enhance the lateral stability of cellular beams. This is attributed to the load–related torque that counteracts the original lateral deformation of the beam. As a result, buckling failure of the beam occurs at higher load value than the one needed to buckle the same beam when loaded at levels higher than its shear center.
- In general, long span cellular beams are shown to buckle elastically with pure lateral torsional buckling mode (LTB). Meanwhile, buckling of intermediate span beams is

controlled by lateral distortional buckling mode (LDB) where web distortion o ccurs simultaneously with lateral deformations. Buckling of short span beams is highly dominated by the high level of web distortion associated with the high shear stresses induced in the web. For these beams, no lateral buckling occurs and significant reduction in C_b values occurs.

- Non–lateral buckling failure of cellular beams loaded at the top flange level is associated with C_b values that are less than 0.8 and 0.7 for mid–span concentrated loading and uniformly distributed loading, respectively. Meanwhile, C_b values of 1.6 and 1.3 provide limits for non–lateral buckling failure of cellular beams loaded at their bottom flange level.
- Obtained results indicate that cellular beams with slender web plates (i.e.; high h_w/t_w values) and cellular beams with closely–spaced big holes (i.e.; low s/h_w and high d_h/h_w values) are more sensitive to shear deformations and, therefore, are mostly governed by local web buckling. Such beams are less likely to experience lateral buckling modes (LTB or LDB) unless having significantly long spans.
- Cellular beams with relatively small b_f/t_f experience more reduction in the moment gradient factor C_b than those with higher b_f/t_f values. Higher values of b_f/t_f provide more effective torsional restrains of the perforated webs which, consequently, minimizes the encountered reduction in the C_b factor.

Table 4.1: Correlation between the Moment Gradient Factor C_b and the Non–Dimensional Factor k_e for Beams with ($d_h/h_w = 0.7$) and ($s/h_w = 1.05$).

Beam Properties								k_e	C_b (Concentrated Load)	C_b (Uniform Load)
b_f (mm)	t_f (mm)	h_w (mm)	t_w (mm)	b_f/t_f	h_w/t_w	A_f/A_w	L (m)			
140	14	350	7	10	50	0.8	7.35	0.613	1.340	1.114
170	17	425	8.5	10	50	0.8	8.93	0.613	1.341	1.115
200	20	500	10	10	50	0.8	10.50	0.613	1.341	1.115
120	8	250	5	15	50	0.768	5.25	0.900	1.332	1.108
220	10	450	5	22	90	0.978	9.45	1.332	1.308	1.085

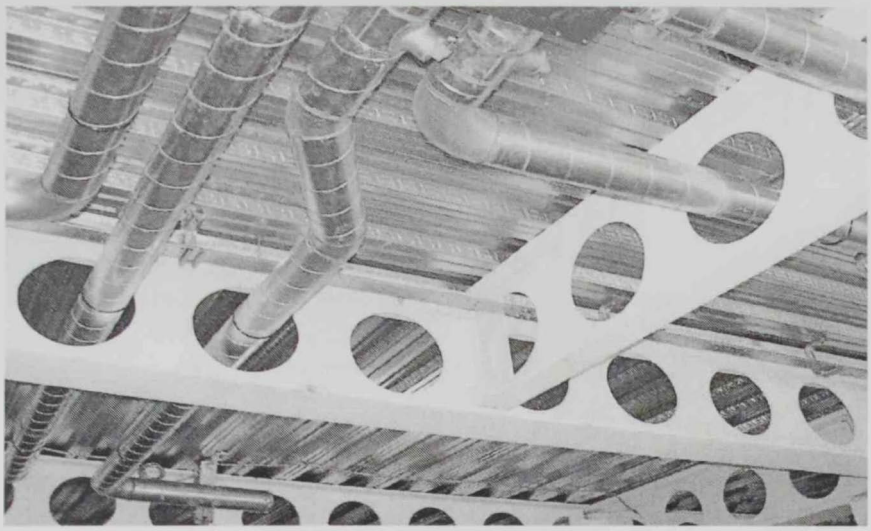

(a): Passage of Mechanical Ducts through Web Perforations

(b): Cellular Beams as Structurally Exposed Elements

Figure 4.1: Applications of Cellular Beams

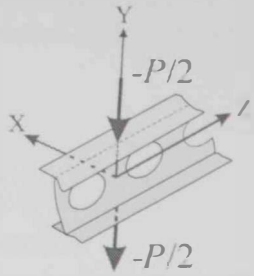

Concentrated Load (P)

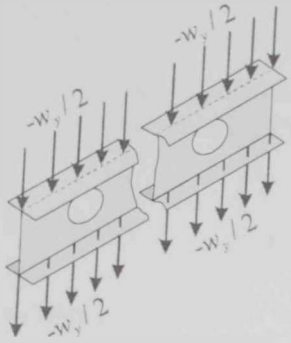

Uniform Load (w_y)

(a): Transverse Load Effects at Shear Center

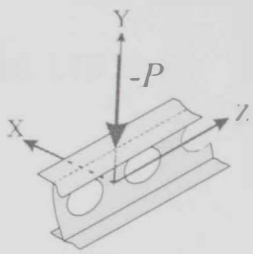

Concentrated Load (P)

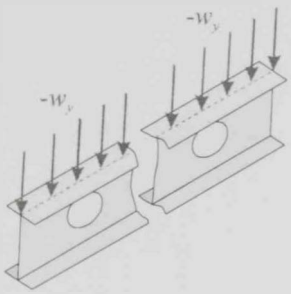

Uniform Load (w_y)

(b): Transverse Loads Applied at Top Flange

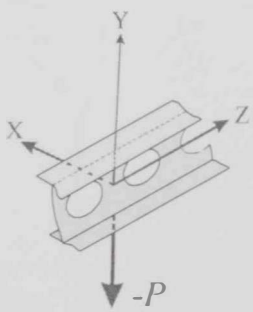

Concentrated Load (P)

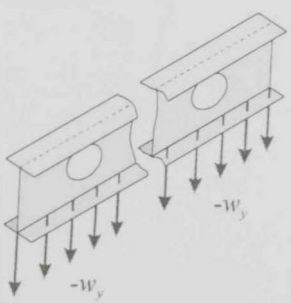

Uniform Load (w_y)

(c): Transverse Loads Applied at Bottom Flange

Figure 4.2: Transverse Loads Application Location

(a): LTB Mode

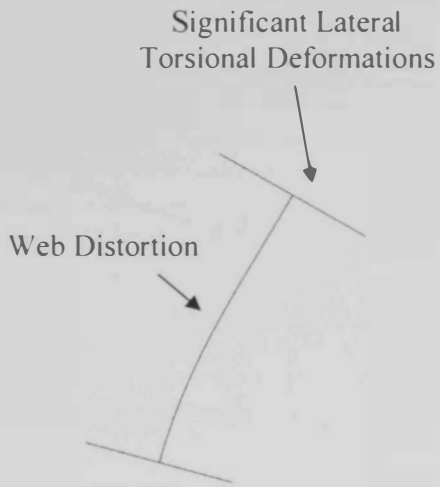

(b): LDB Mode

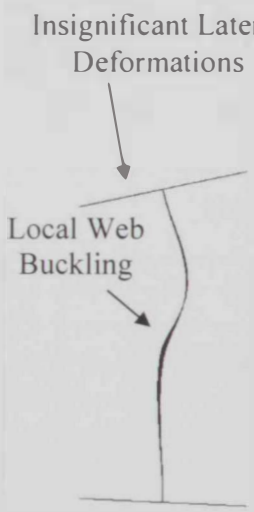

4.3(c): WLB Mode

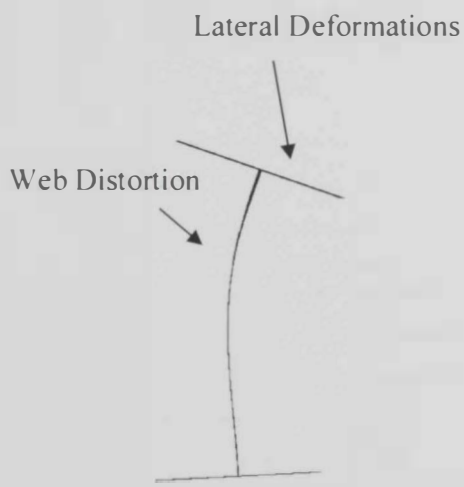

(d): LDB–WLB Mode

Figure 4.3: Various Elastic Buckling Modes of Cellular Beams

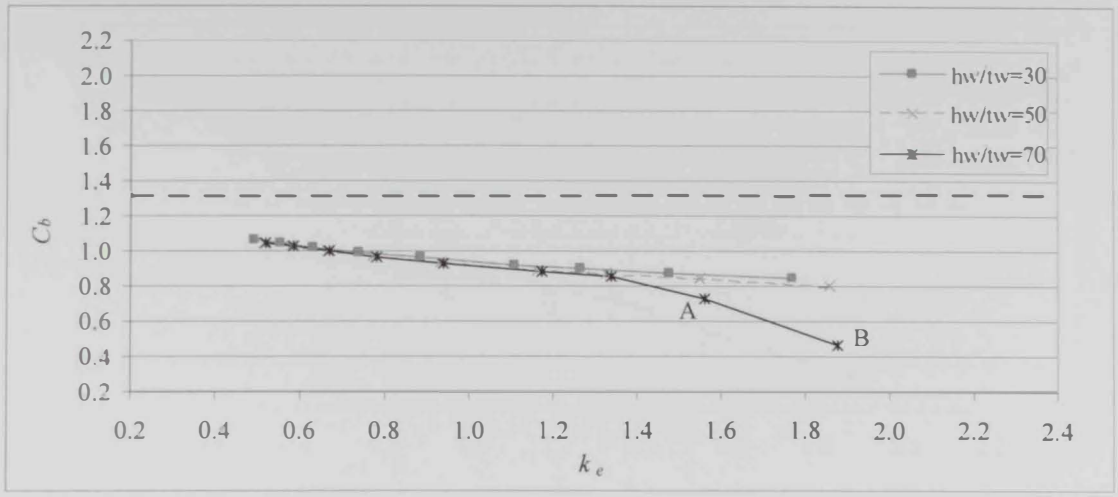

(a): Concentrated Load Applied at Top Flange

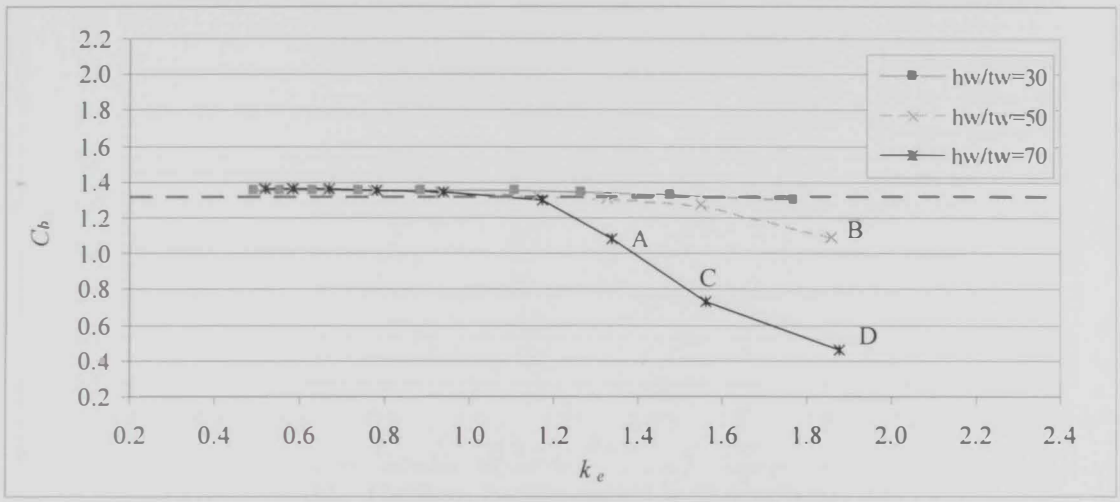

(b): Concentrated Load Applied at Shear Center

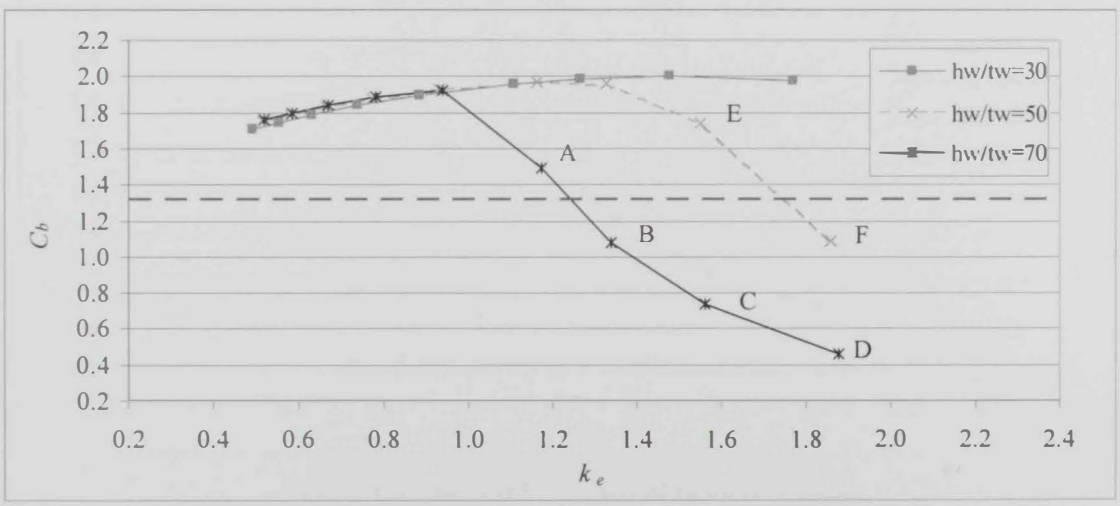

(c): Concentrated Load Applied at Bottom Flange

Figure 4.4: Moment Gradient Factor for (b_f/t_f = 15, d_h/h_w = 0.6 and s/h_w = 1.05)

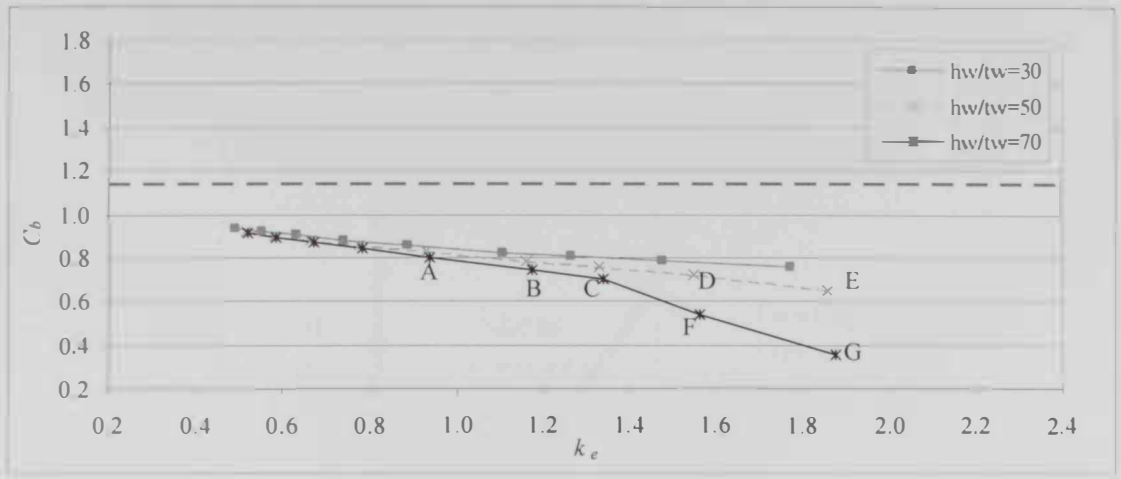

(a): Uniform Load Applied at Top Flange

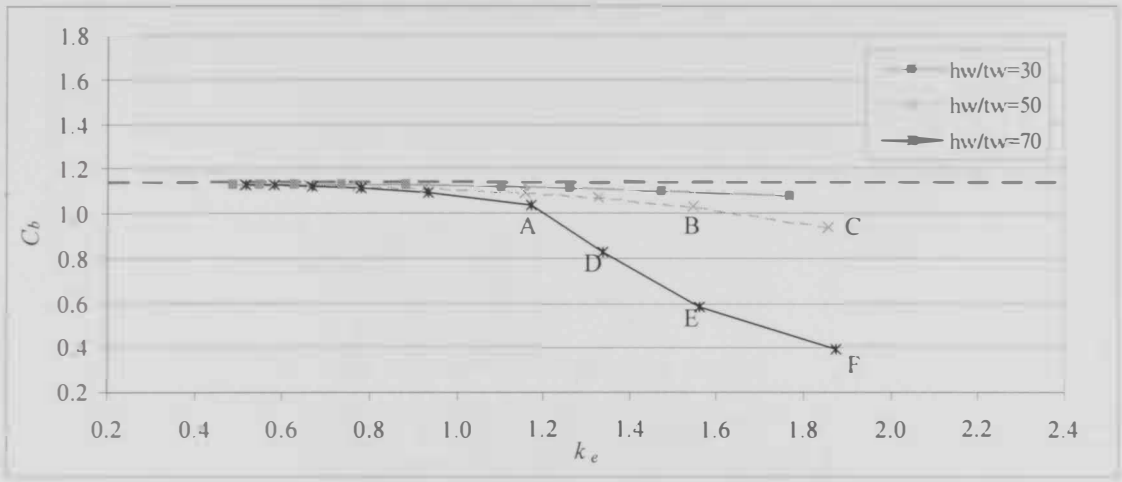

(b): Uniform Load Applied at Shear Center

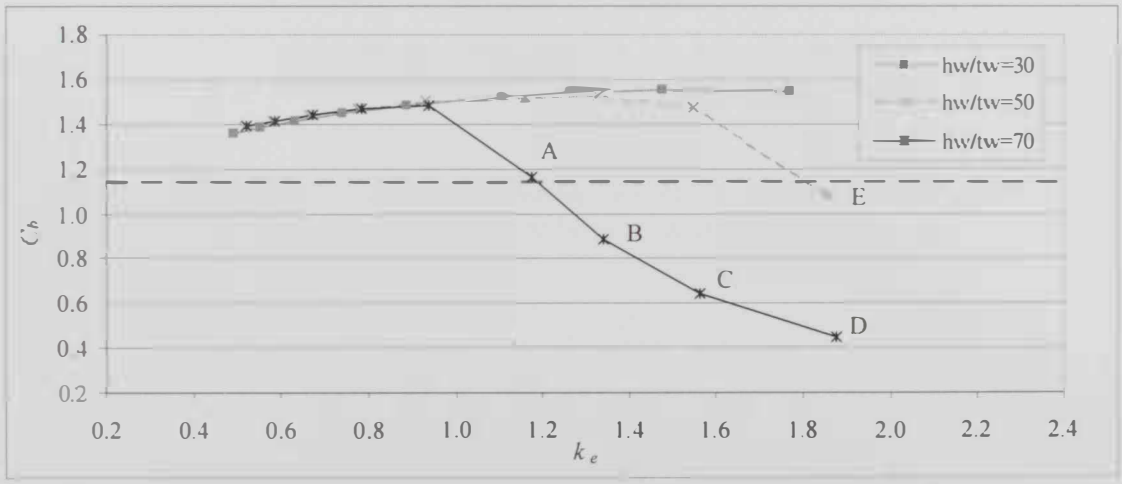

(c): Uniform Load Applied at Bottom Flange

Figure 4.5: Moment Gradient Factor for (b_f/t_f = 15, d_h/h_w = 0.6 and s/h_w = 1.05)

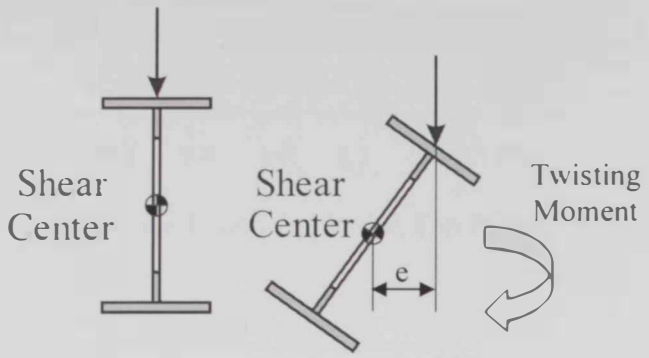

(a): Destabilizing Moment for Loading above Shear Center

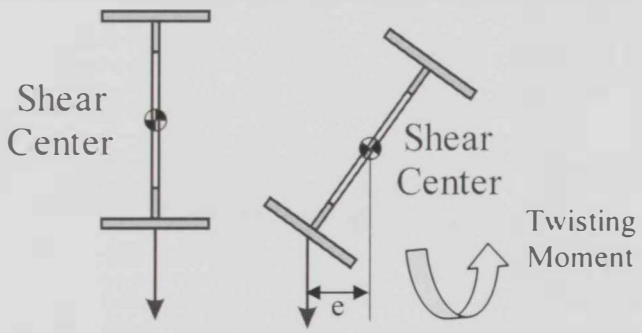

(b): Stabilizing Moment for Loading below Shear Center

Figure 4.6: Stabilizing/Destabilizing Twisting Moment According to Location of Loading Relative to Shear Center

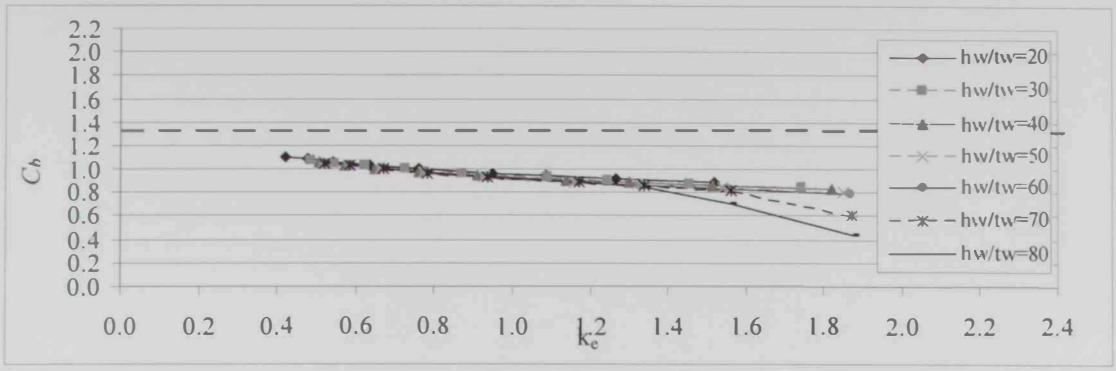

(a): Concentrated Load Applied at Top Flange (d_h/h_w = 0.5)

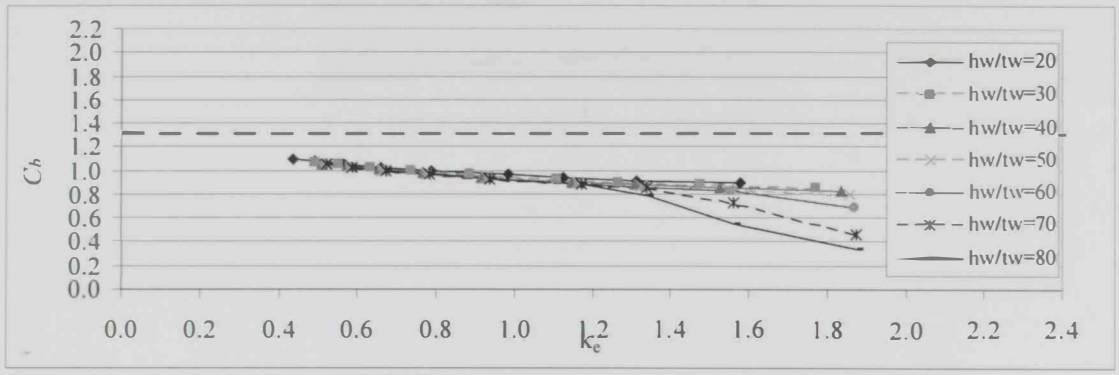

(b): Concentrated Load Applied at Top Flange (d_h/h_w = 0.6)

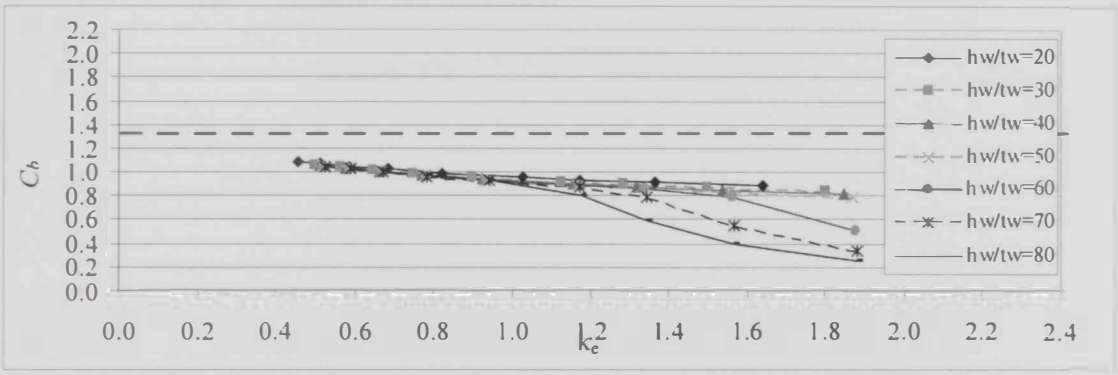

(c): Concentrated Load Applied at Top Flange (d_h/h_w = 0.7)

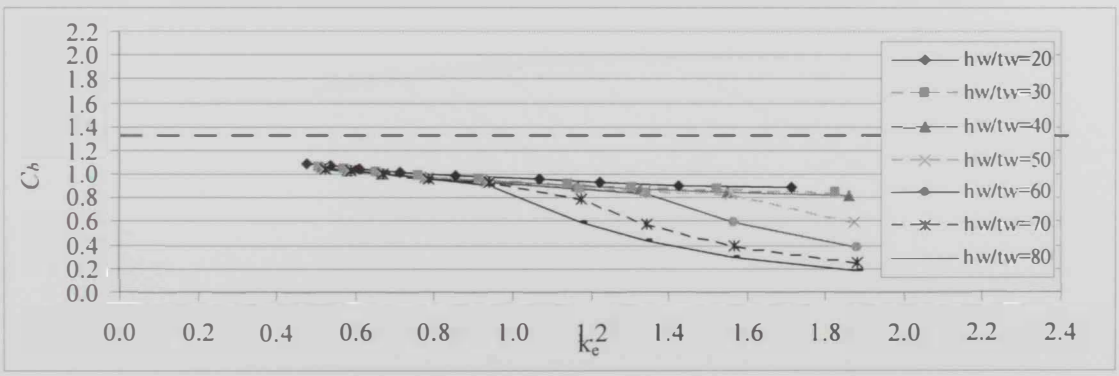

(d): Concentrated Load Applied at Top Flange (d_h/h_w = 0.8)

Figure 4.7: Moment Gradient Factor for (b_f/t_f = 15 and s/h_w = 1.05)

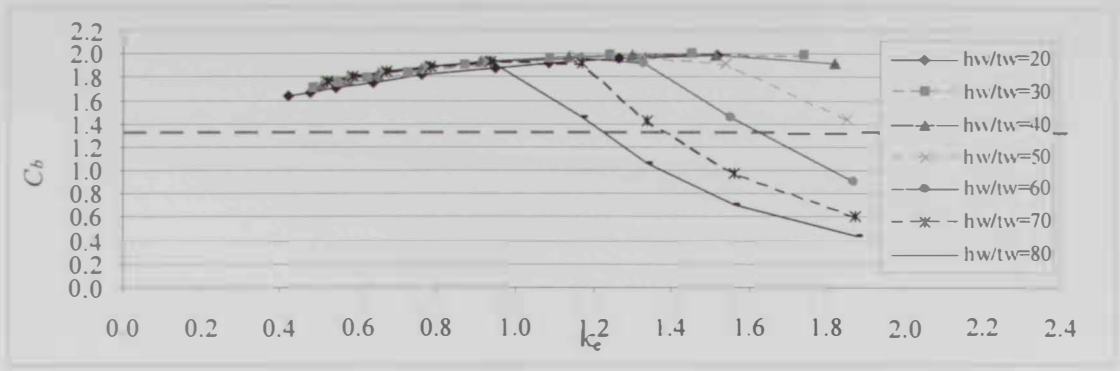

(a): Concentrated Load Applied at Bottom Flange (d_h/h_w = 0.5)

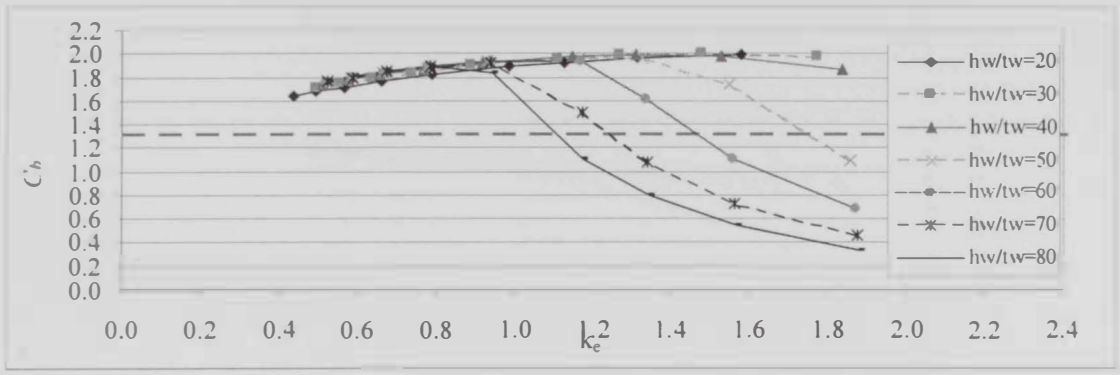

(b): Concentrated Load Applied at Bottom Flange (d_h/h_w = 0.6)

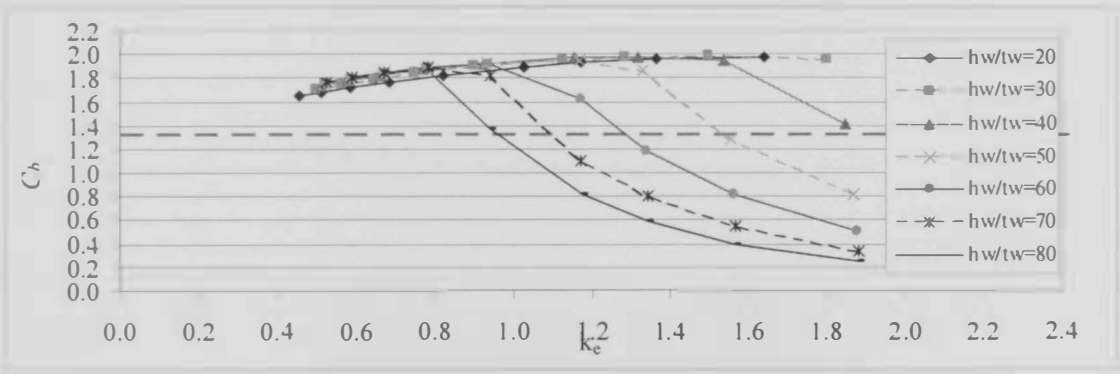

(c): Concentrated Load Applied at Bottom Flange (d_h/h_w = 0.7)

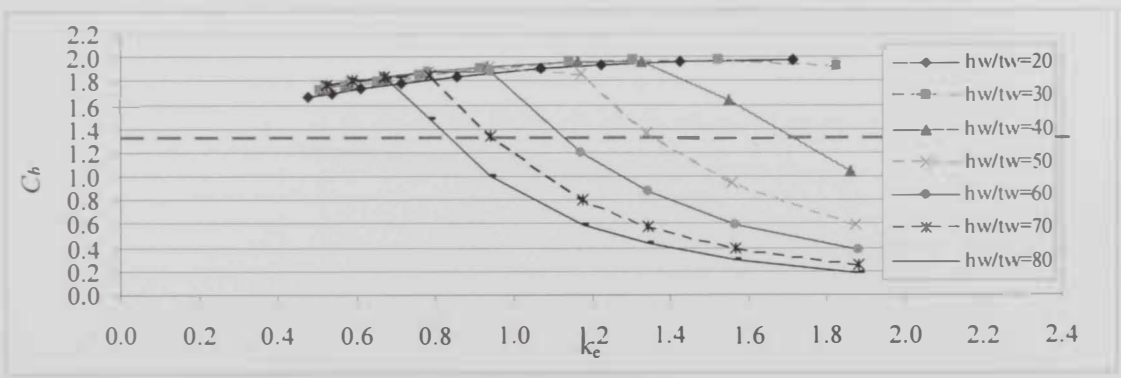

(d): Concentrated Load Applied at Bottom Flange (d_h/h_w = 0.8)

Figure 4.8: Moment Gradient Factor for (b_f/t_f = 15 and s/h_w = 1.05)

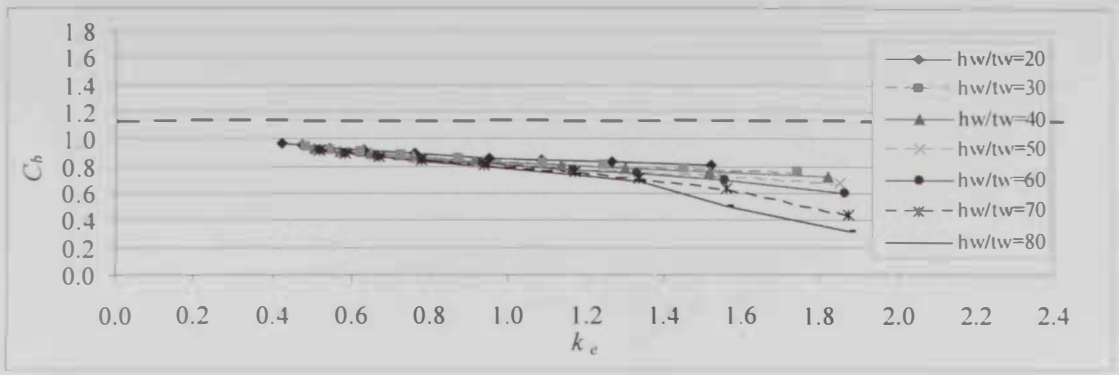

(a): Uniform Load Applied at Top Flange (d_h/h_w = 0.5)

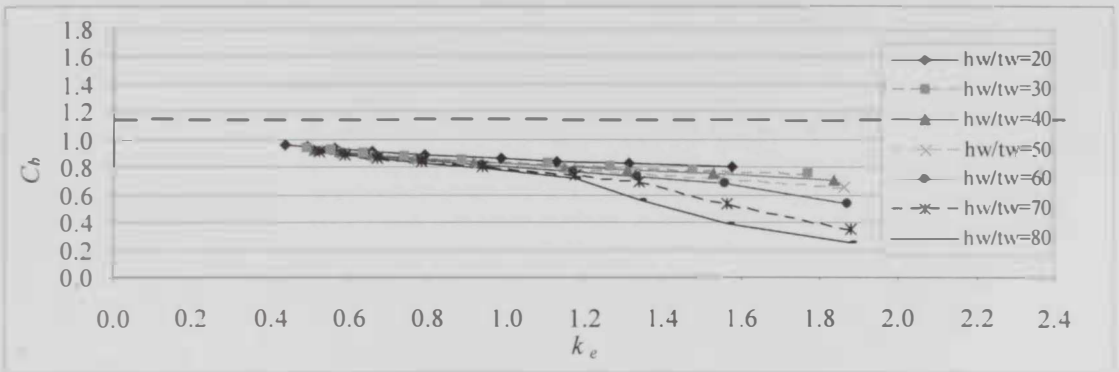

(b): Uniform Load Applied at Top Flange (d_h/h_w = 0.6)

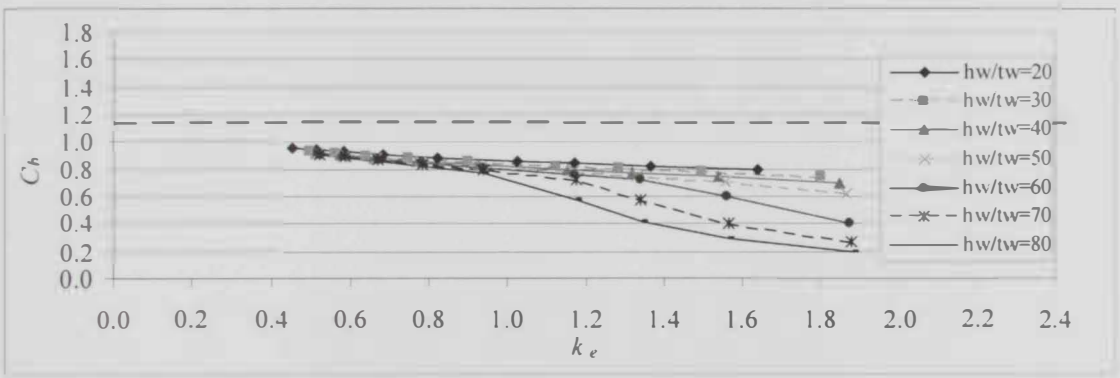

(c): Uniform Load Applied at Top Flange (d_h/h_w = 0.7)

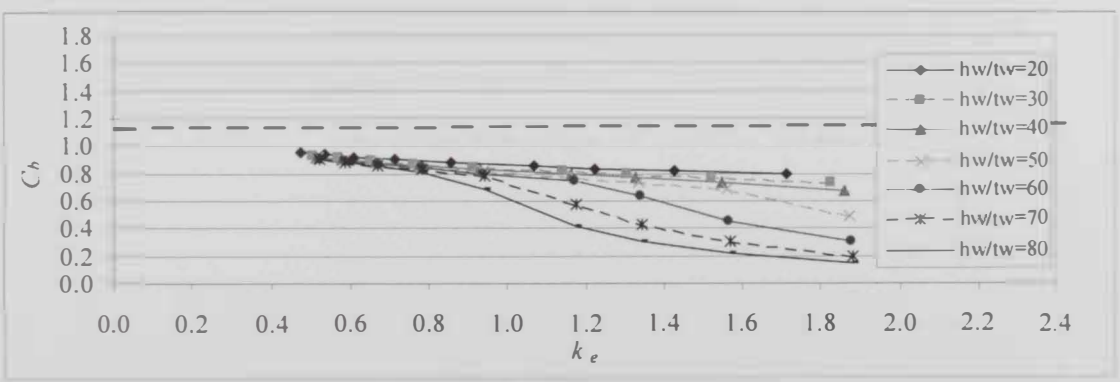

(d): Uniform Load Applied at Top Flange (d_h/h_w = 0.8)

Figure 4.9: Moment Gradient Factor for (b_f/t_f = 15 and s/h_w = 1.05)

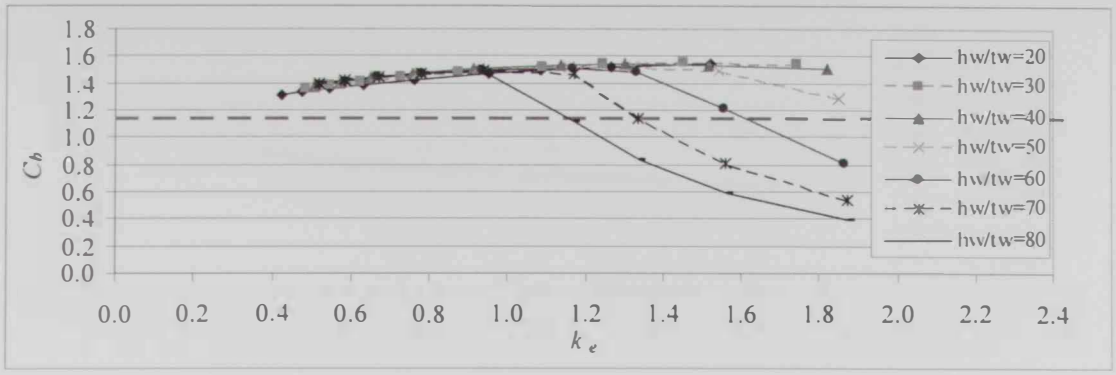

(a): Uniform Load Applied at Bottom Flange (d_h/h_w = 0.5)

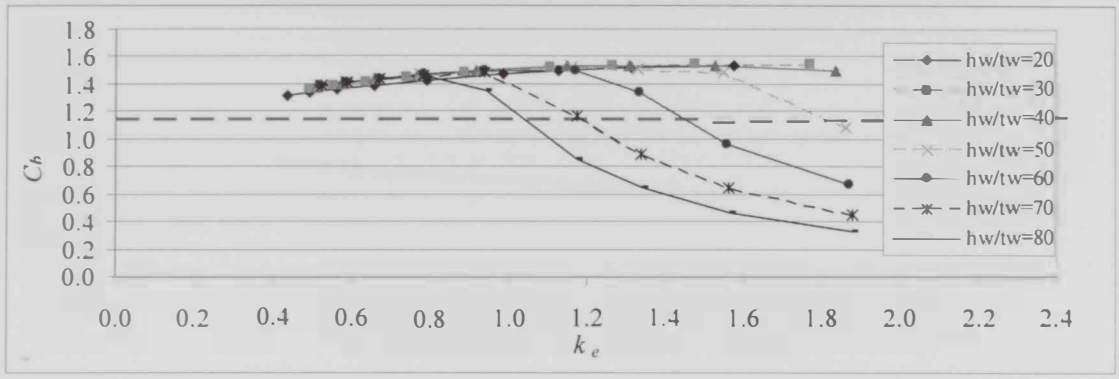

(b): Uniform Load Applied at Bottom Flange (d_h/h_w = 0.6)

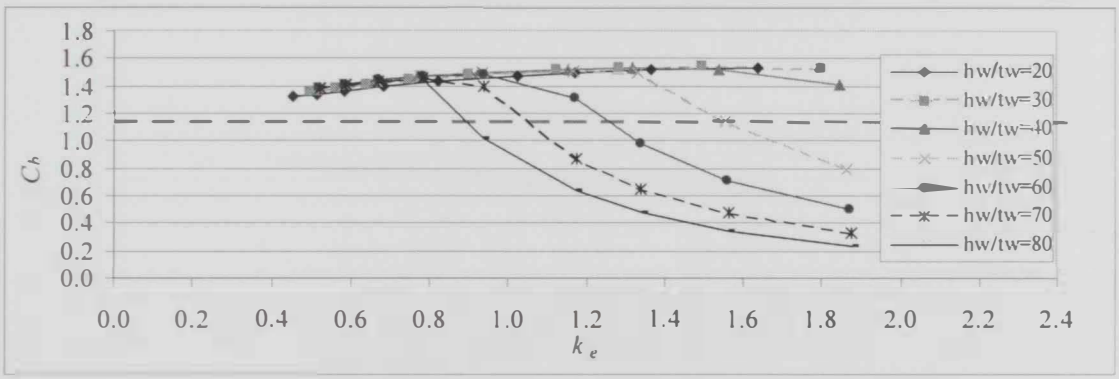

(c): Uniform Load Applied at Bottom Flange (d_h/h_w = 0.7)

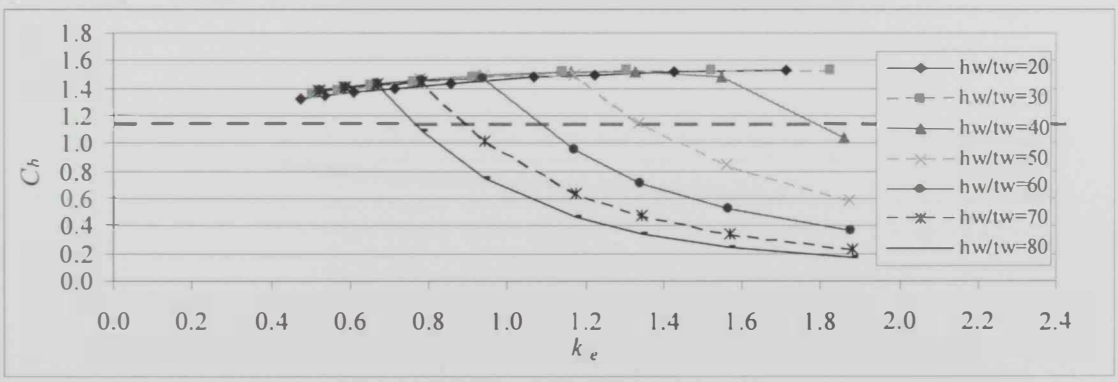

(d): Uniform Load Applied at Bottom Flange (d_h/h_w = 0.8)

Figure 4.10: Moment Gradient Factor for (b_f/t_f = 15 and s/h_w = 1.05)

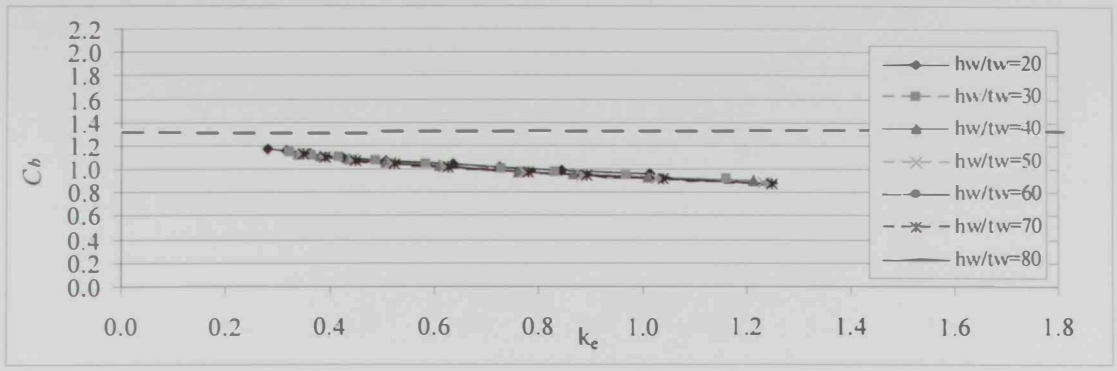

(a): Concentrated Load Applied at Top Flange (d_h/h_w = 0.5)

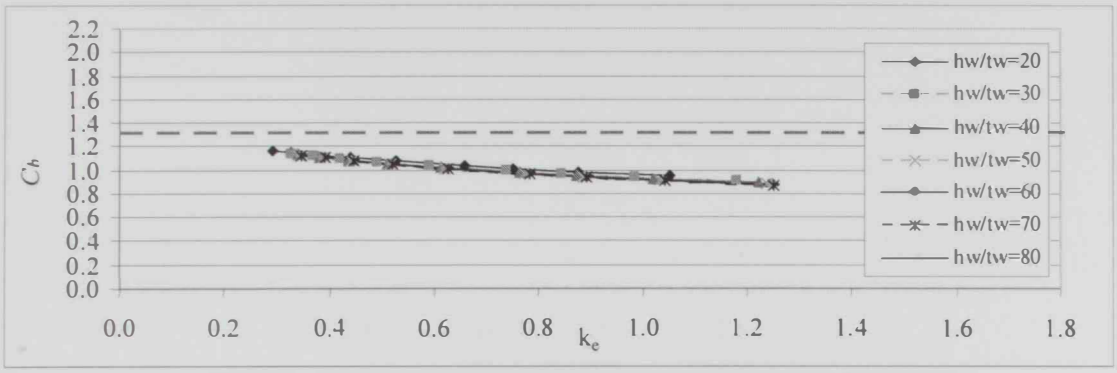

(b): Concentrated Load Applied at Top Flange (d_h/h_w = 0.6)

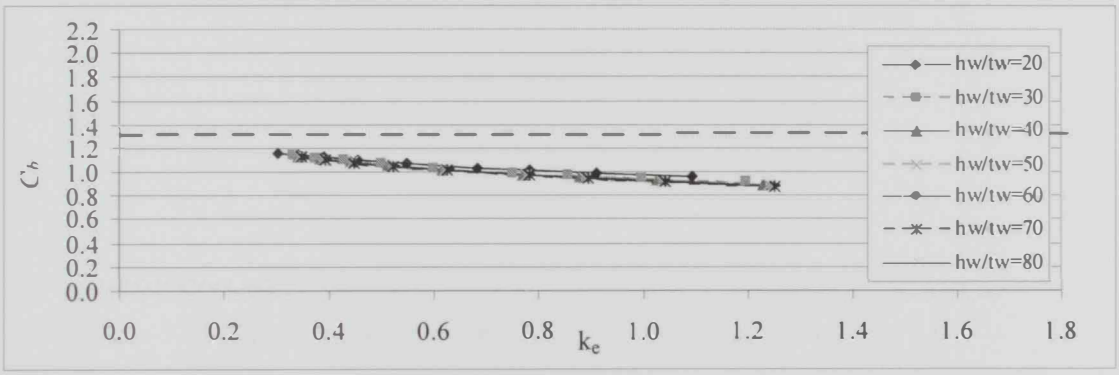

(c): Concentrated Load Applied at Top Flange (d_h/h_w = 0.7)

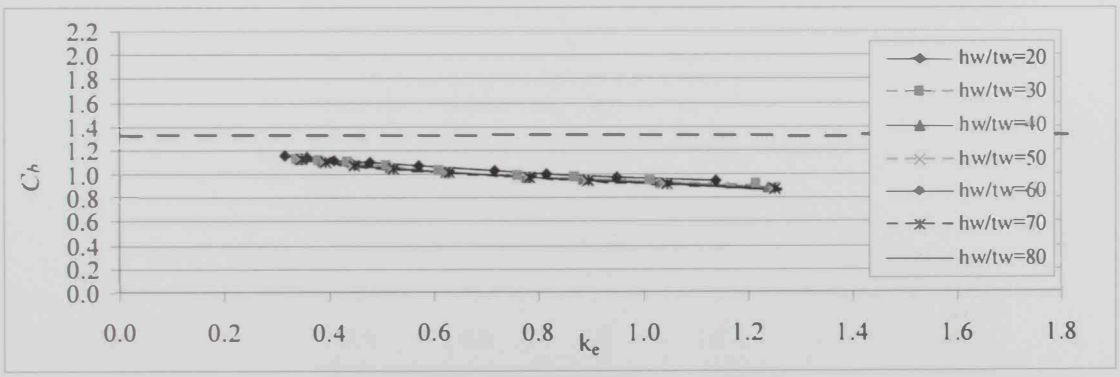

(d): Concentrated Load Applied at Top Flange (d_h/h_w = 0.8)

Figure 4.11: Moment Gradient Factor for (b_f/t_f = 15 and s/h_w = 1.575)

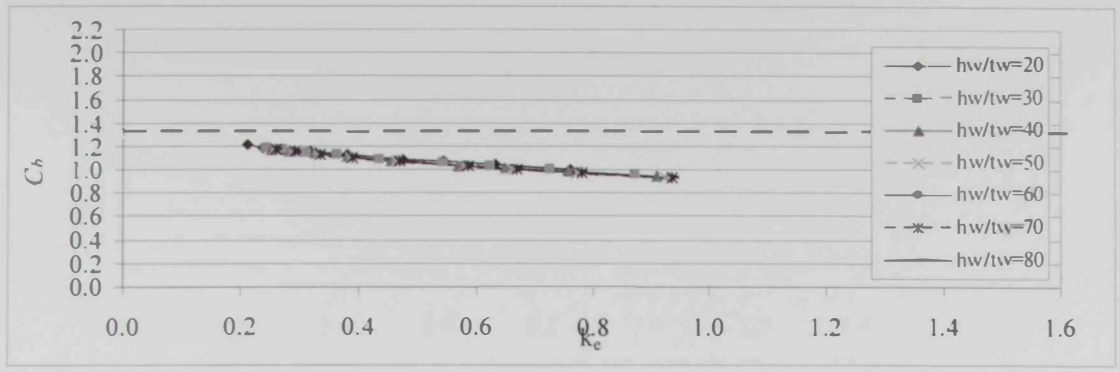

(a): Concentrated Load Applied at Top Flange (d_h/h_w = 0.5)

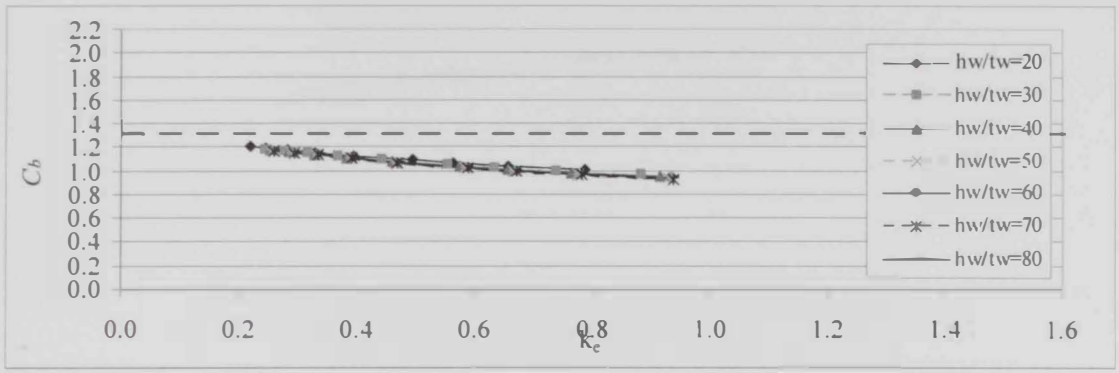

(b): Concentrated Load Applied at Top Flange (d_h/h_w = 0.6)

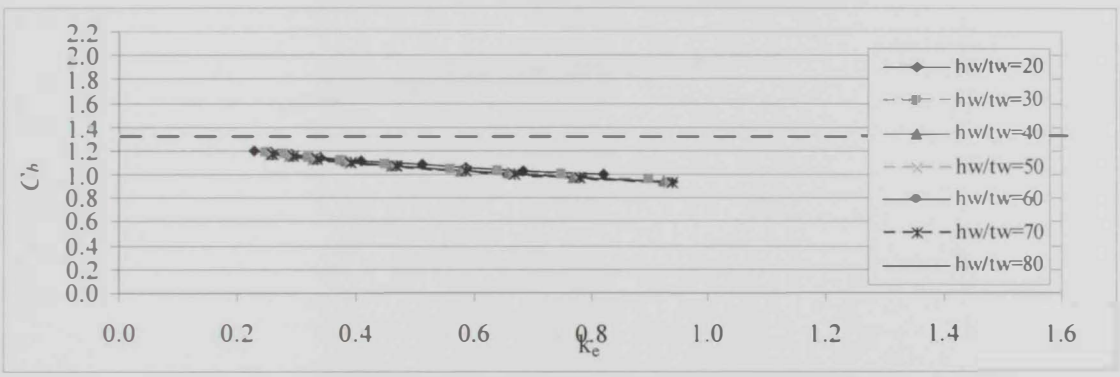

(c): Concentrated Load Applied at Top Flange (d_h/h_w = 0.7)

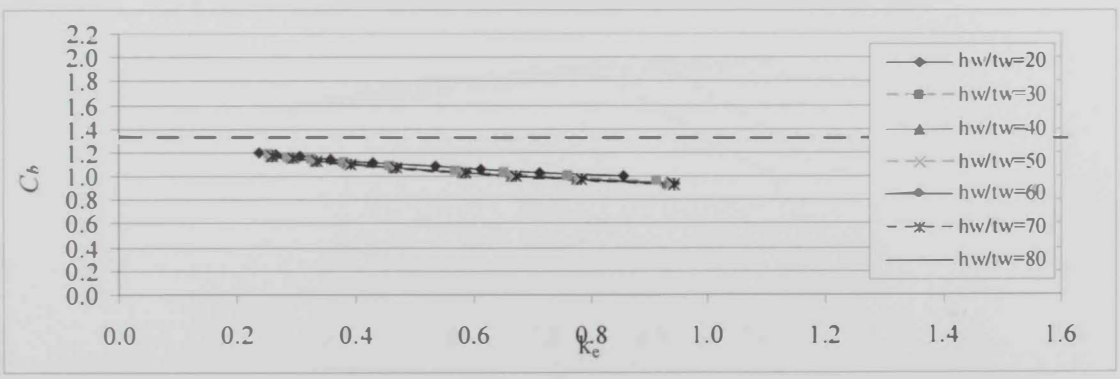

(d): Concentrated Load Applied at Top Flange (d_h/h_w = 0.8)

Figure 4.12: Moment Gradient Factor for (b_f/t_f = 15 and s/h_w = 2.1)

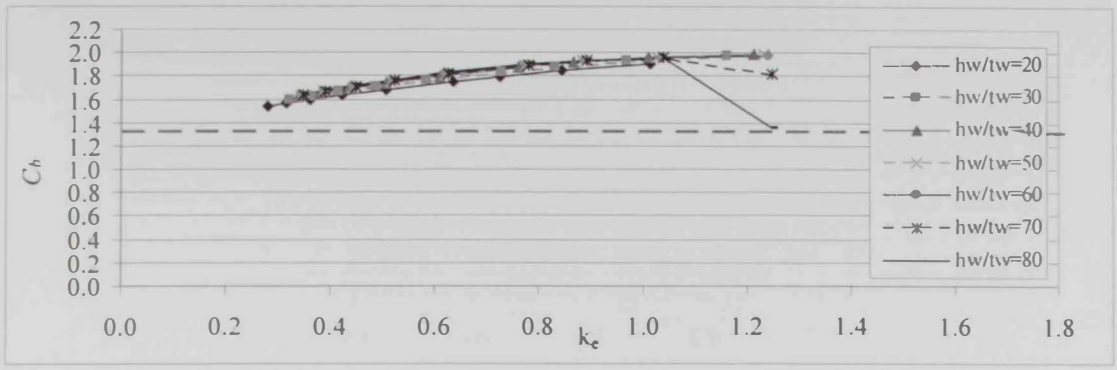

(a): Concentrated Load Applied at Bottom Flange (d_h/h_w = 0.5)

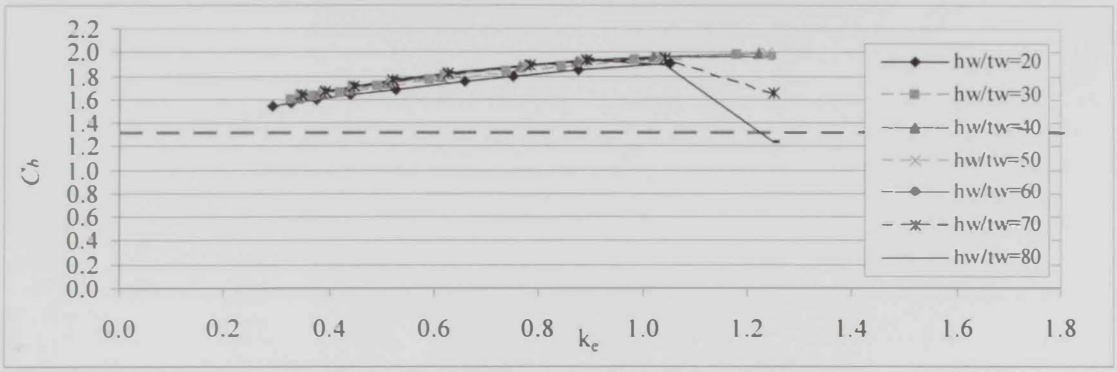

(b): Concentrated Load Applied at Bottom Flange (d_h/h_w = 0.6)

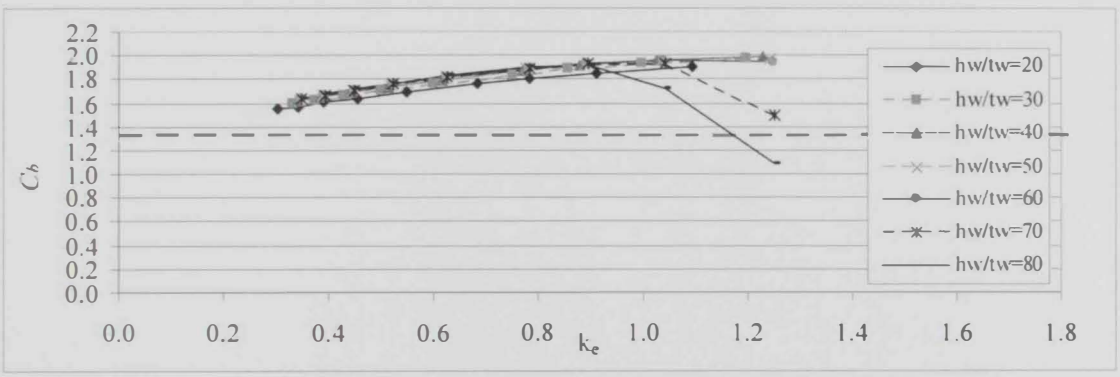

(c): Concentrated Load Applied at Bottom Flange (d_h/h_w = 0.7)

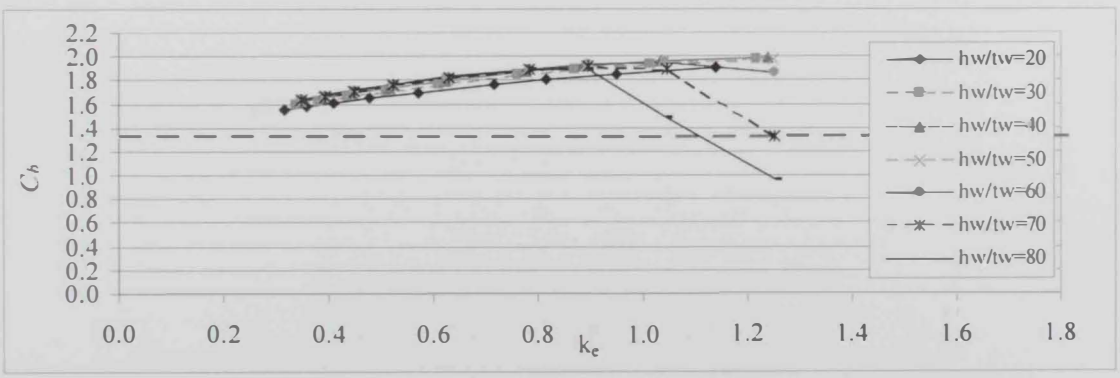

(d): Concentrated Load Applied at Bottom Flange (d_h/h_w = 0.8)

Figure 4.13: Moment Gradient Factor for (b_f/t_f = 15 and s/h_w = 1.575)

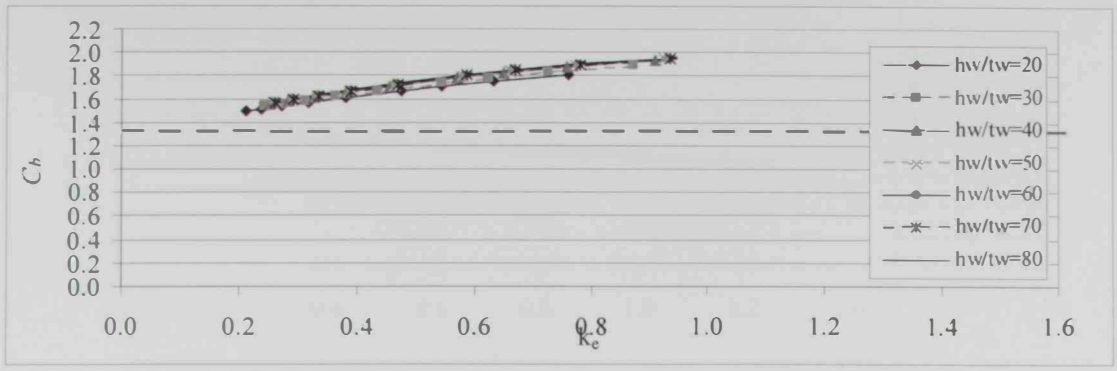

(a): Concentrated Load Applied at Bottom Flange (d_h/h_w = 0.5)

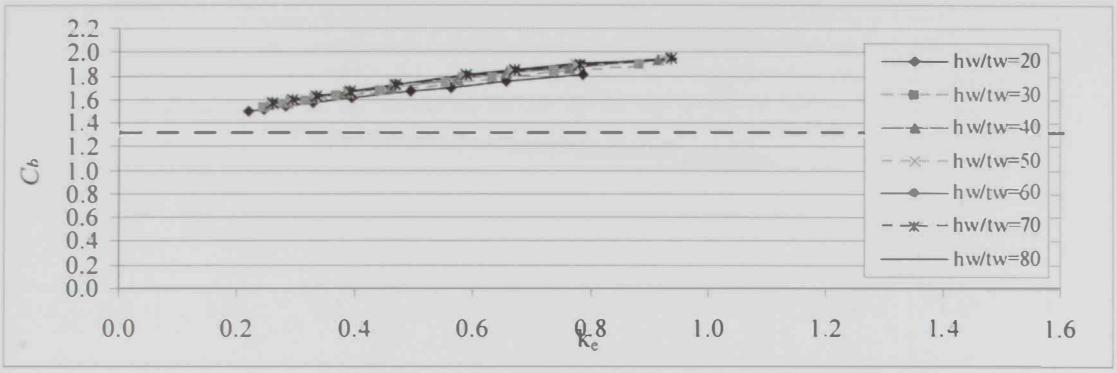

(b): Concentrated Load Applied at Bottom Flange (d_h/h_w = 0.6)

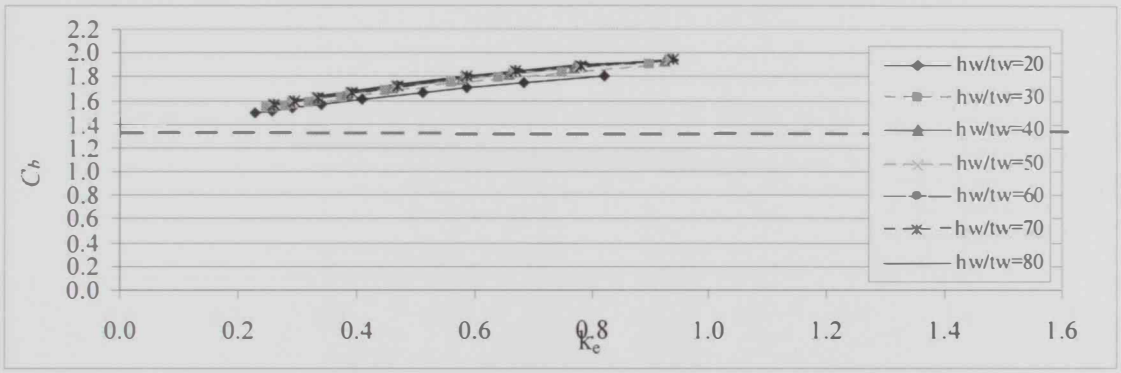

(c): Concentrated Load Applied at Bottom Flange (d_h/h_w = 0.7)

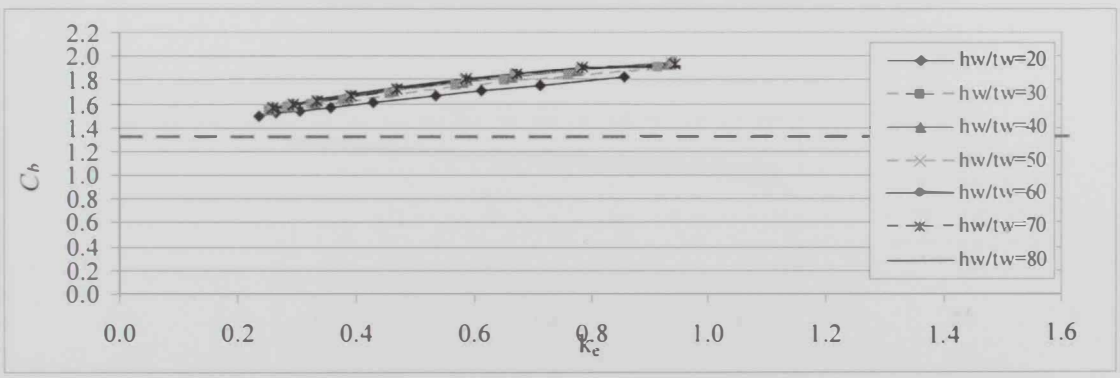

(d): Concentrated Load Applied at Bottom Flange (d_h/h_w = 0.8)

Figure 4.14: Moment Gradient Factor for (b_f/t_f = 15 and s/h_w = 2.1)

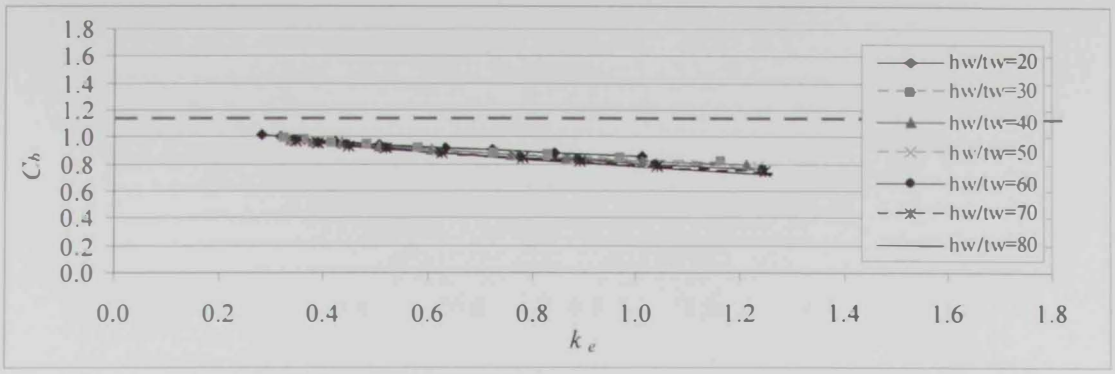

(a): Uniform Load Applied at Top Flange (d_h/h_w = 0.5)

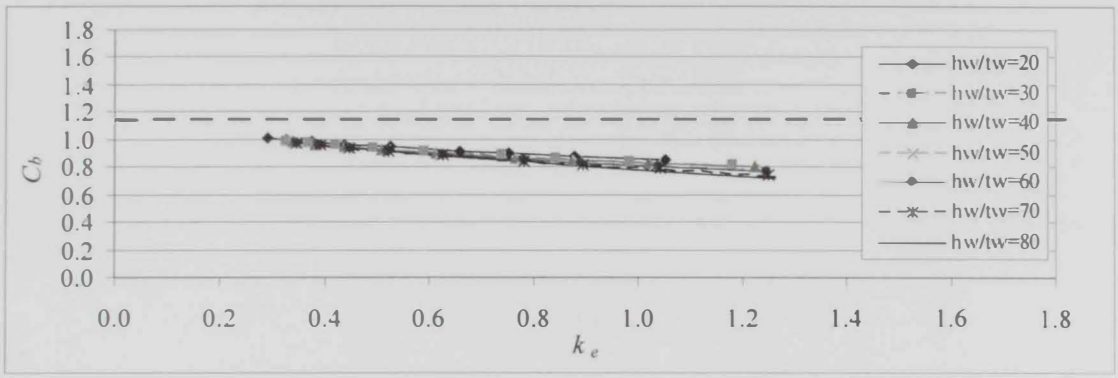

(b): Uniform Load Applied at Top Flange (d_h/h_w = 0.6)

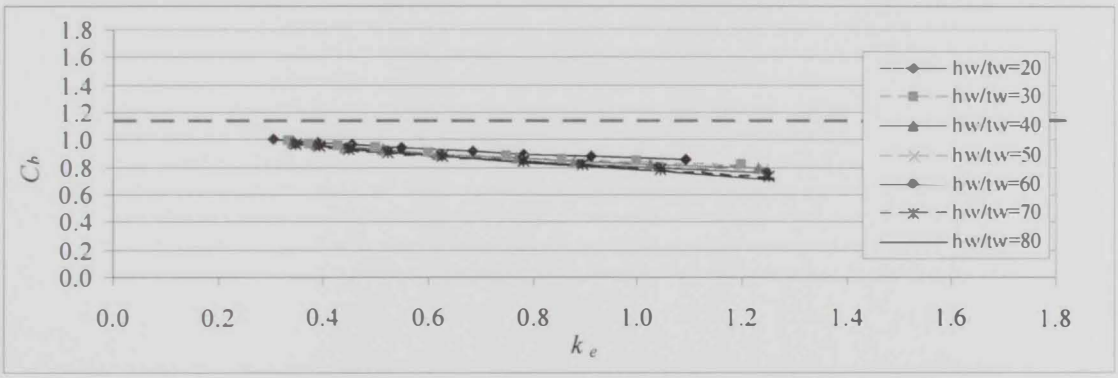

(c): Uniform Load Applied at Top Flange (d_h/h_w = 0.7)

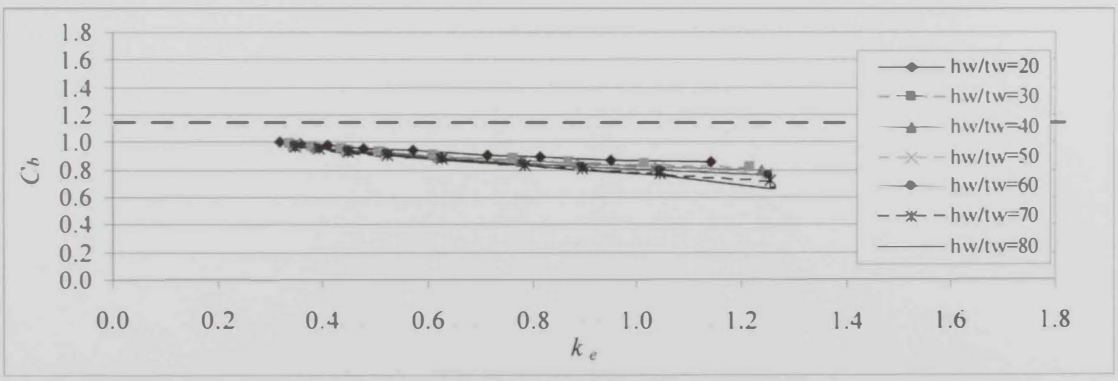

(d): Uniform Load Applied at Top Flange (d_h/h_w = 0.8)

Figure 4.15: Moment Gradient Factor for (b_f/t_f = 15 and s/h_w = 1.575)

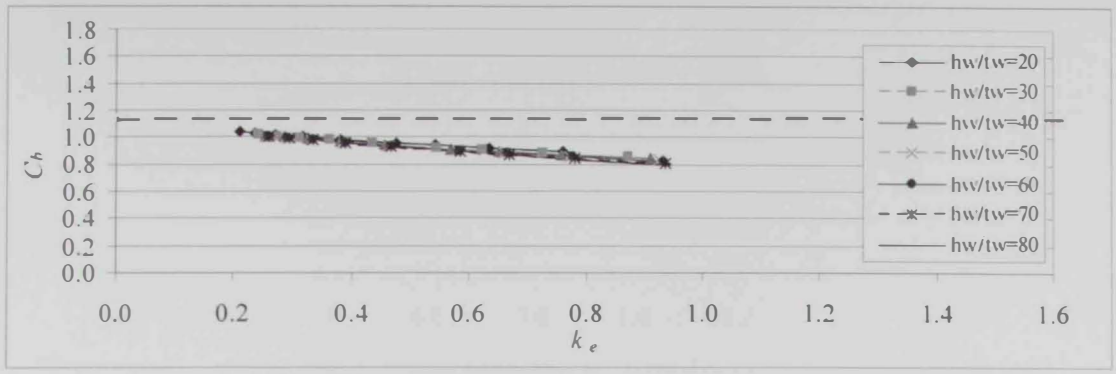

(a): Uniform Load Applied at Top Flange ($d_h/h_w = 0.5$)

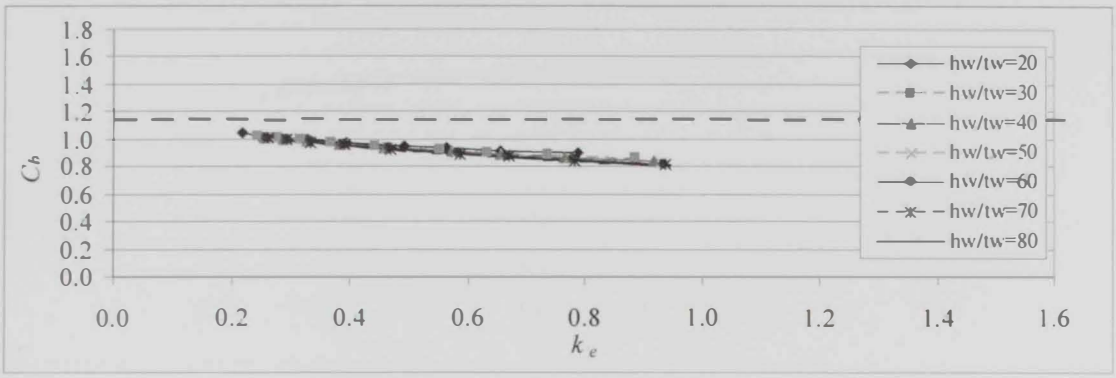

(b): Uniform Load Applied at Top Flange ($d_h/h_w = 0.6$)

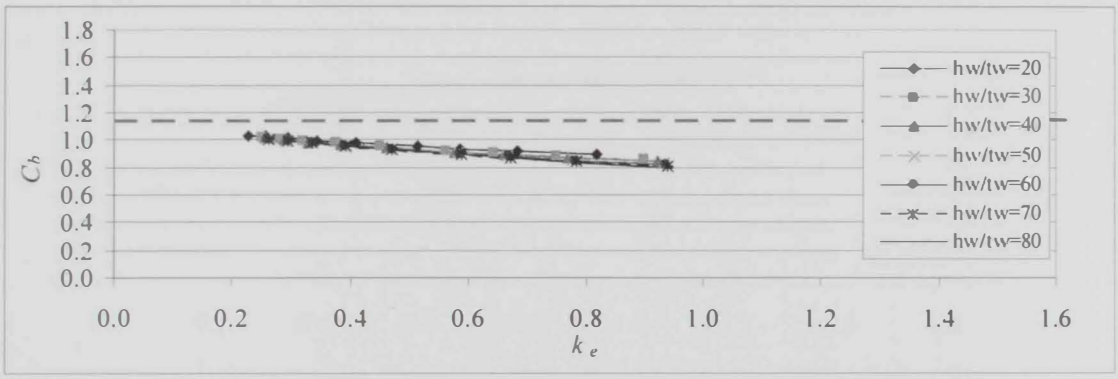

(c): Uniform Load Applied at Top Flange ($d_h/h_w = 0.7$)

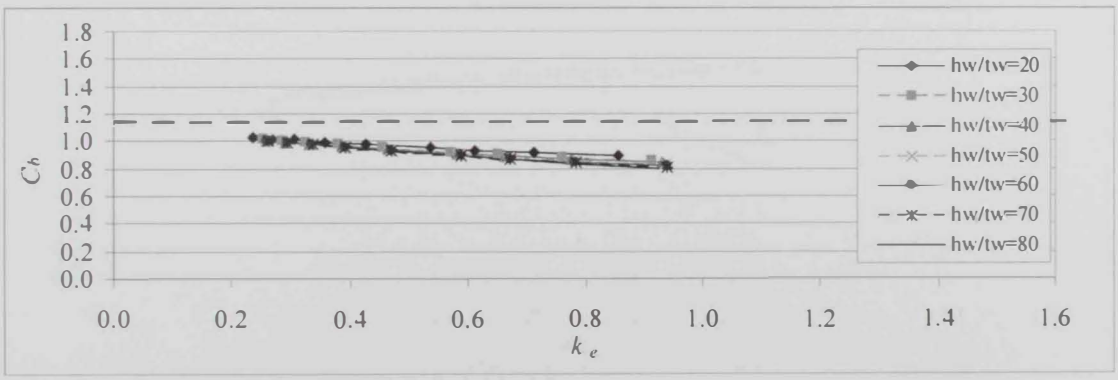

(d): Uniform Load Applied at Top Flange ($d_h/h_w = 0.8$)

Figure 4.16: Moment Gradient Factor for ($b_f/t_f = 15$ and $s/h_w = 2.1$)

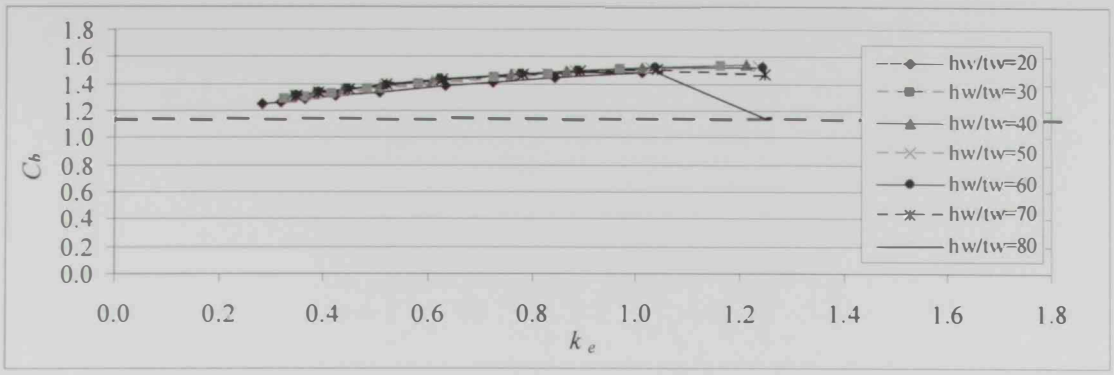

(a): Uniform Load Applied at Bottom Flange (d_h/h_w = 0.5)

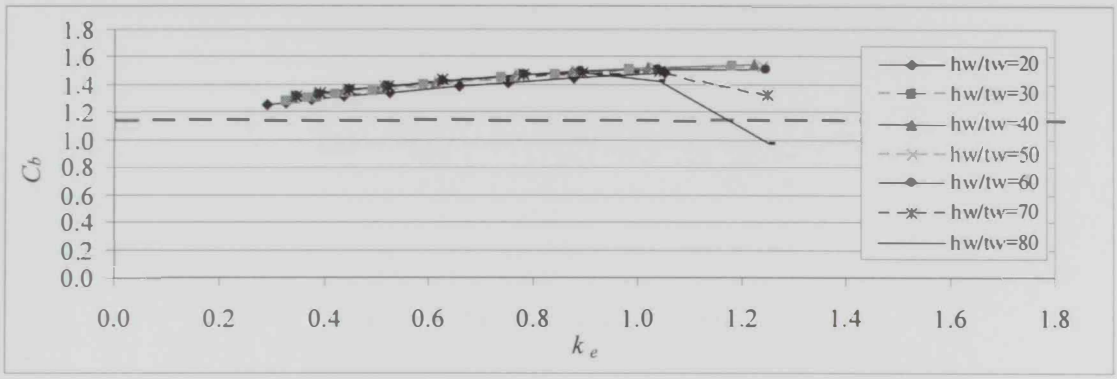

(b): Uniform Load Applied at Bottom Flange (d_h/h_w = 0.6)

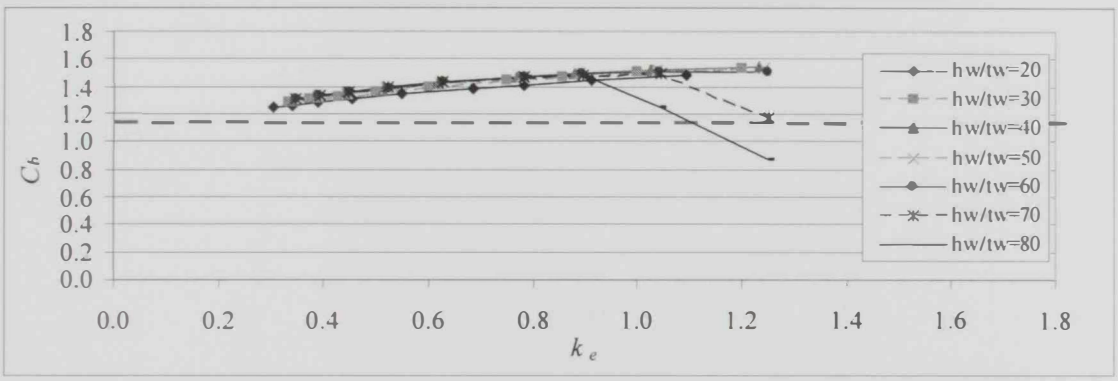

(c): Uniform Load Applied at Bottom Flange (d_h/h_w = 0.7)

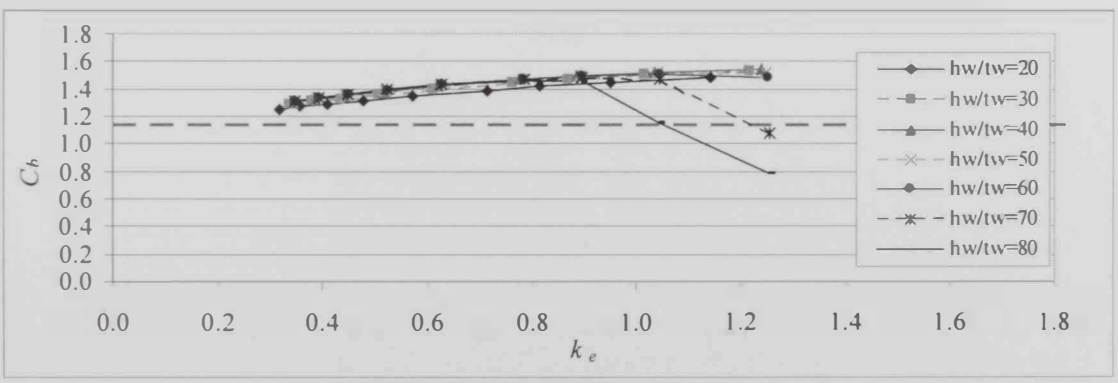

(d): Uniform Load Applied at Bottom Flange (d_h/h_w = 0.8)

Figure 4.17: Moment Gradient Factor for (b_f/t_f = 15 and s/h_w = 1.575)

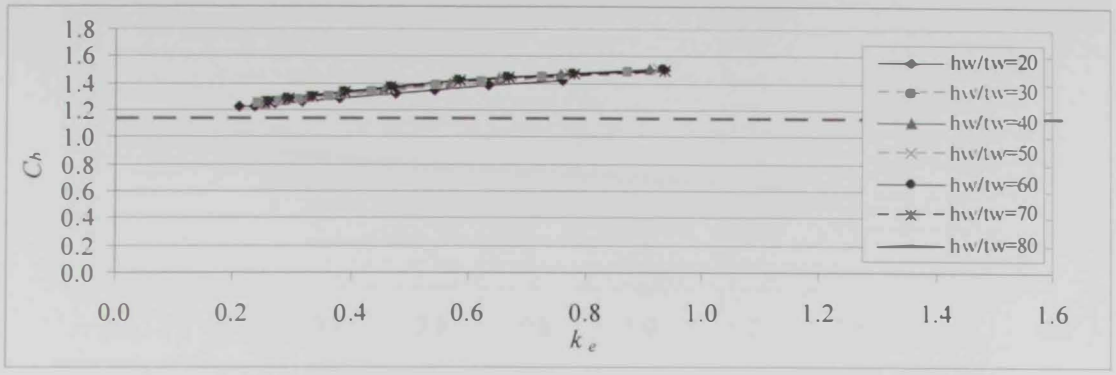

(a): Uniform Load Applied at Bottom Flange (d_h/h_w = 0.5)

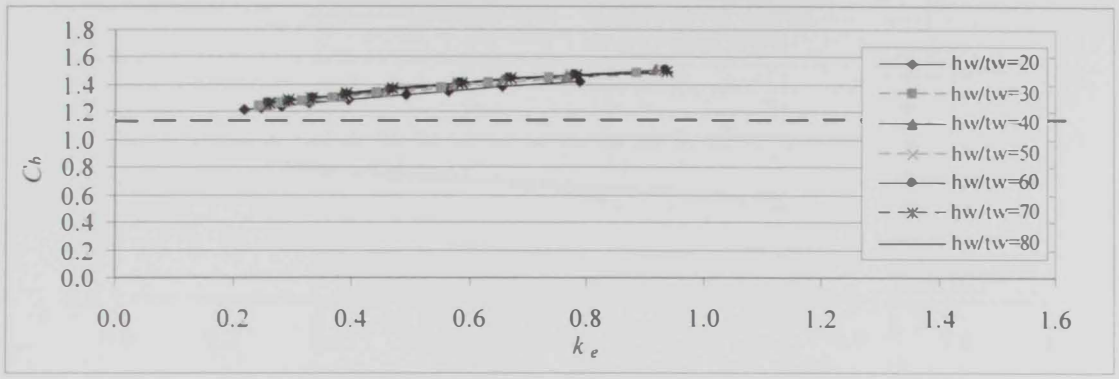

(b): Uniform Load Applied at Bottom Flange (d_h/h_w = 0.6)

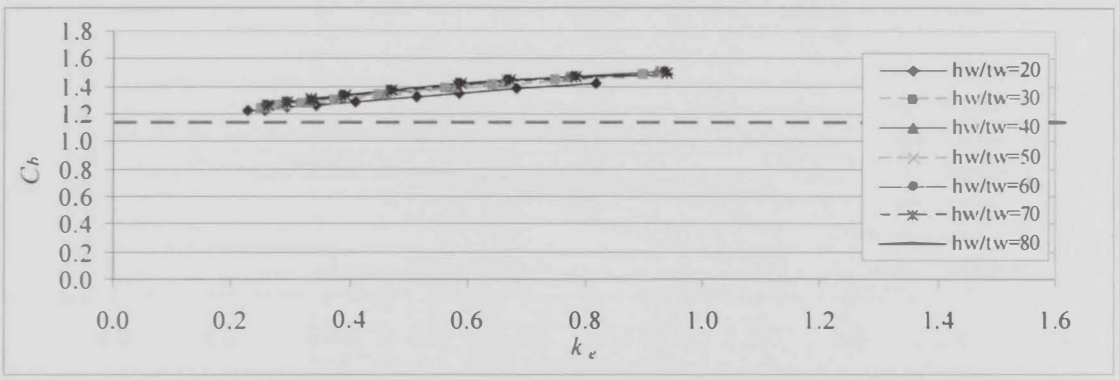

(c): Uniform Load Applied at Bottom Flange (d_h/h_w = 0.7)

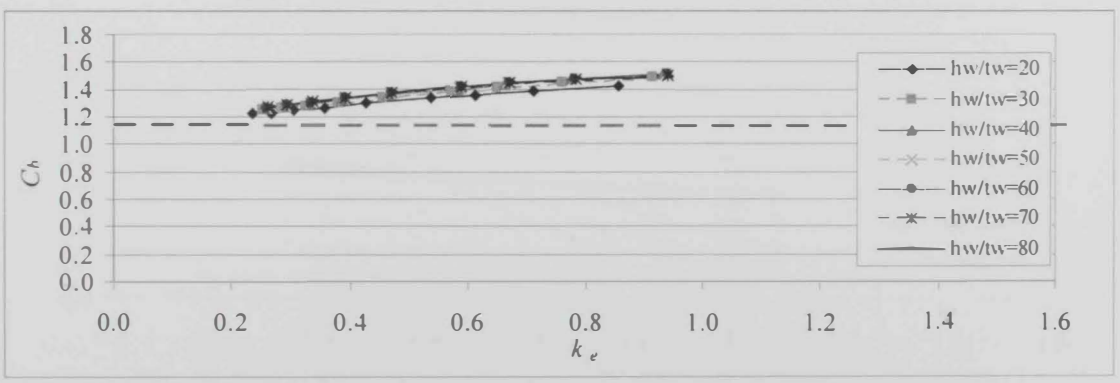

(d): Uniform Load Applied at Bottom Flange (d_h/h_w = 0.8)

Figure 4.18: Moment Gradient Factor for (b_f/t_f = 15 and s/h_w = 2.1)

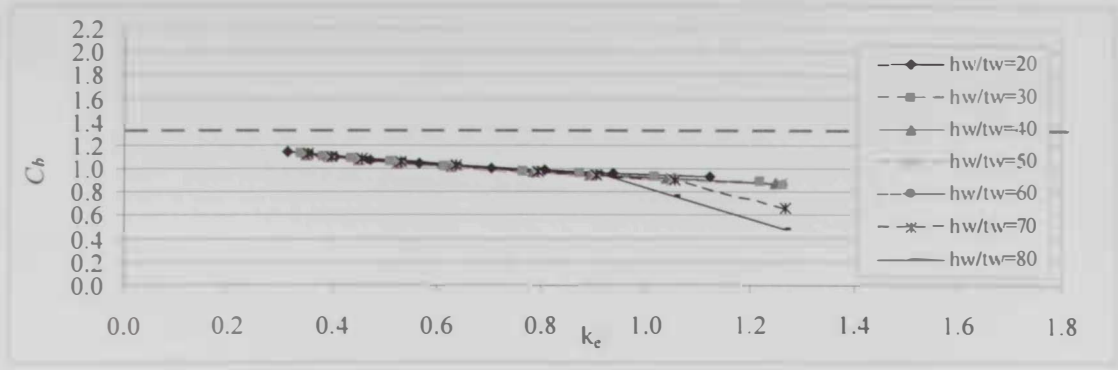

(a): Concentrated Load Applied at Top Flange (d_h/h_w = 0.5)

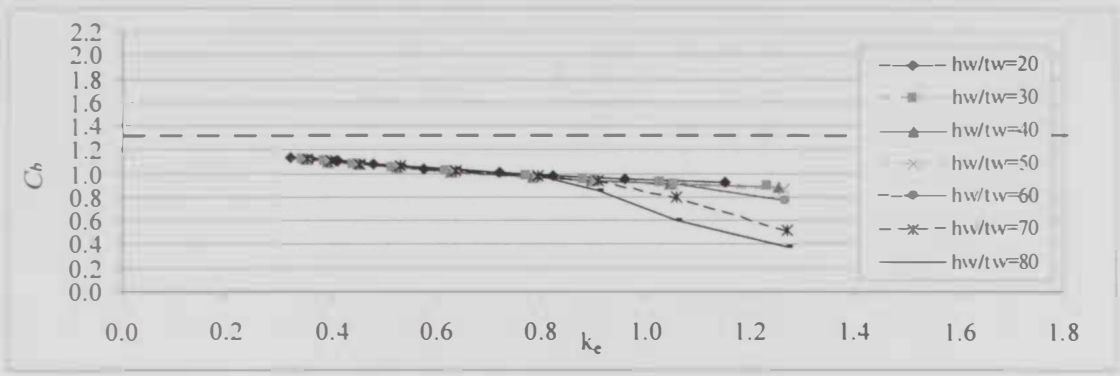

(b): Concentrated Load Applied at Top Flange (d_h/h_w = 0.6)

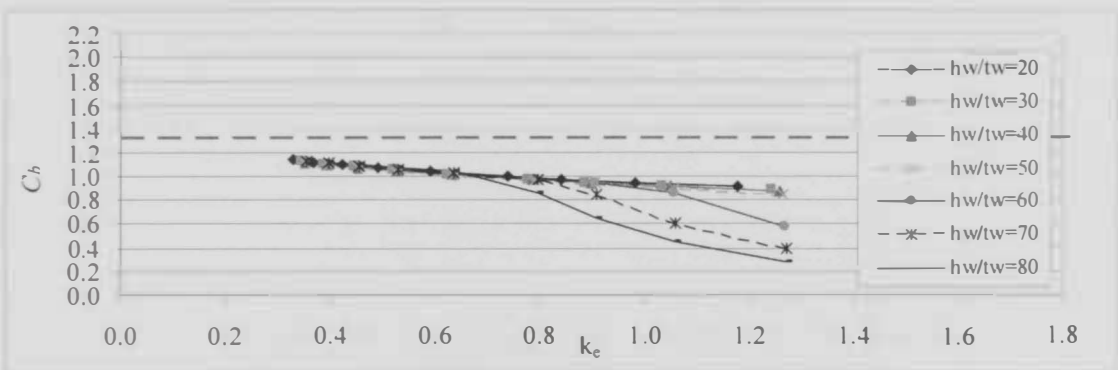

(c): Concentrated Load Applied at Top Flange (d_h/h_w = 0.7)

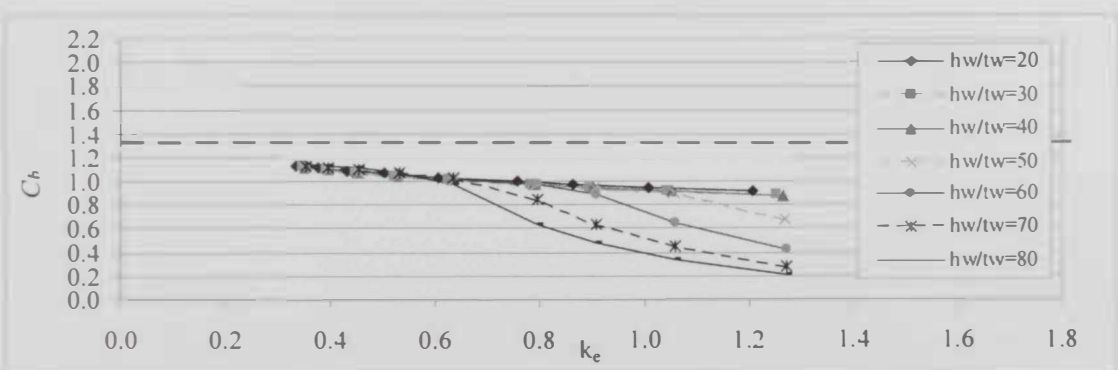

(d): Concentrated Load Applied at Top Flange (d_h/h_w = 0.8)

Figure 4.19: Moment Gradient Factor for (b_f/t_f = 10 and s/h_w = 1.05)

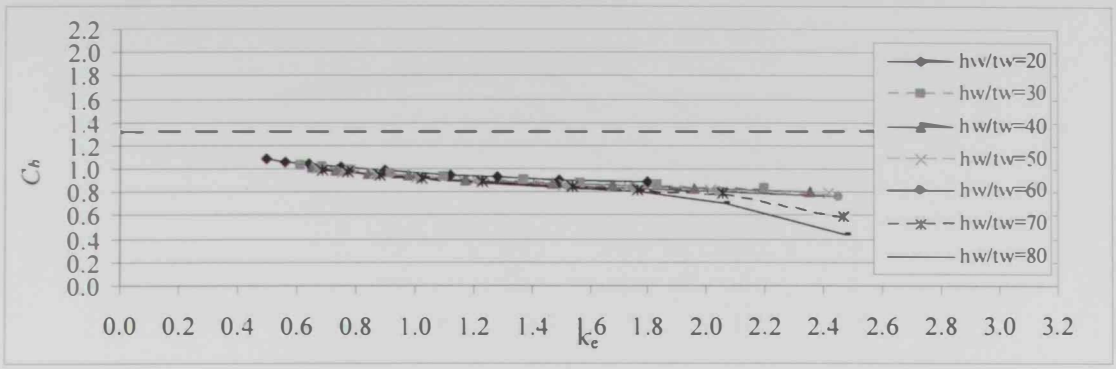

(a): Concentrated Load Applied at Top Flange (d_h/h_w = 0.5)

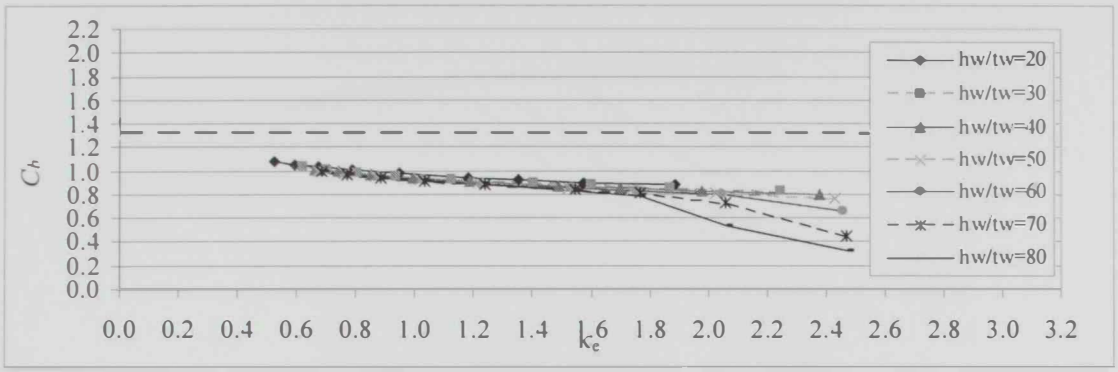

(b): Concentrated Load Applied at Top Flange (d_h/h_w = 0.6)

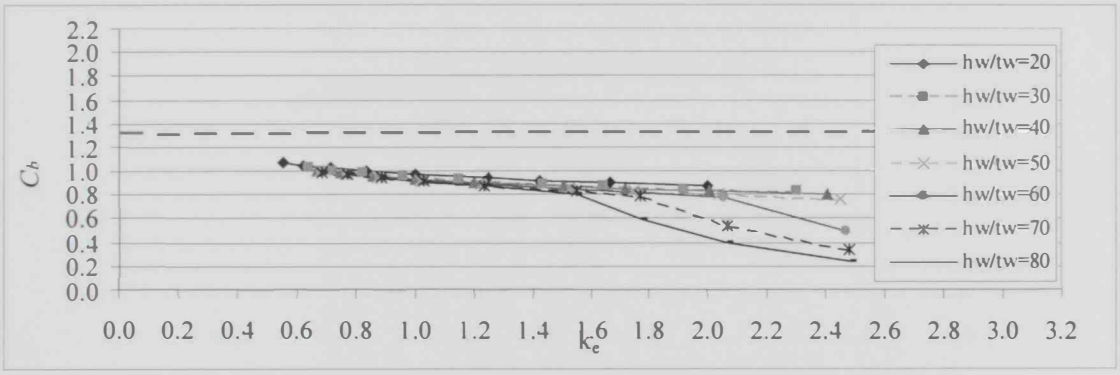

(c): Concentrated Load Applied at Top Flange (d_h/h_w = 0.7)

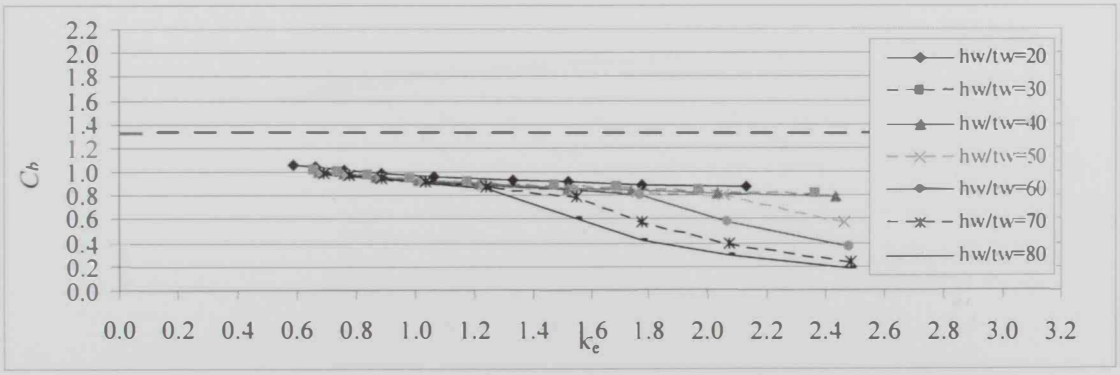

(d): Concentrated Load Applied at Top Flange (d_h/h_w = 0.8)

Figure 4.20: Moment Gradient Factor for (b_f/t_f = 20 and s/h_w = 1.05)

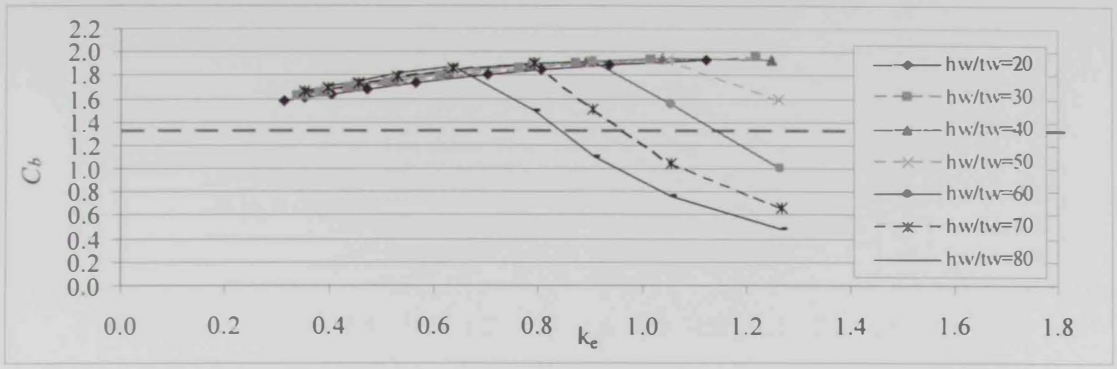

(a): Concentrated Load Applied at Bottom Flange (d_h/h_w = 0.5)

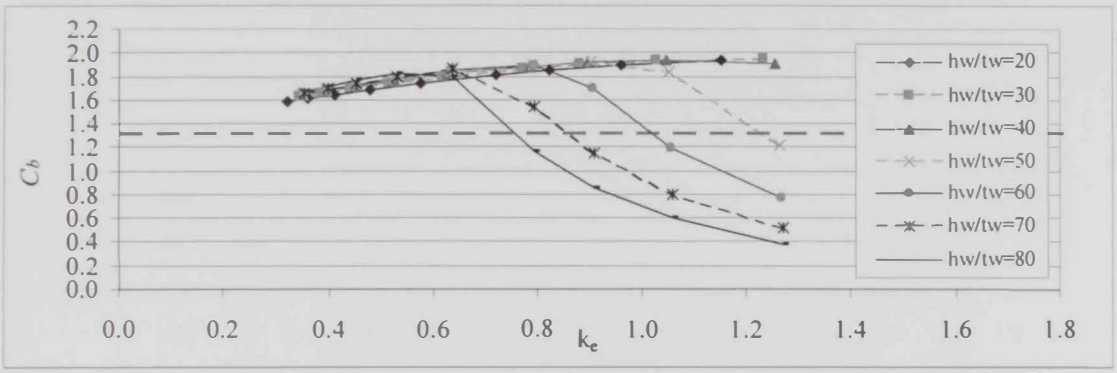

(b): Concentrated Load Applied at Bottom Flange (d_h/h_w = 0.6)

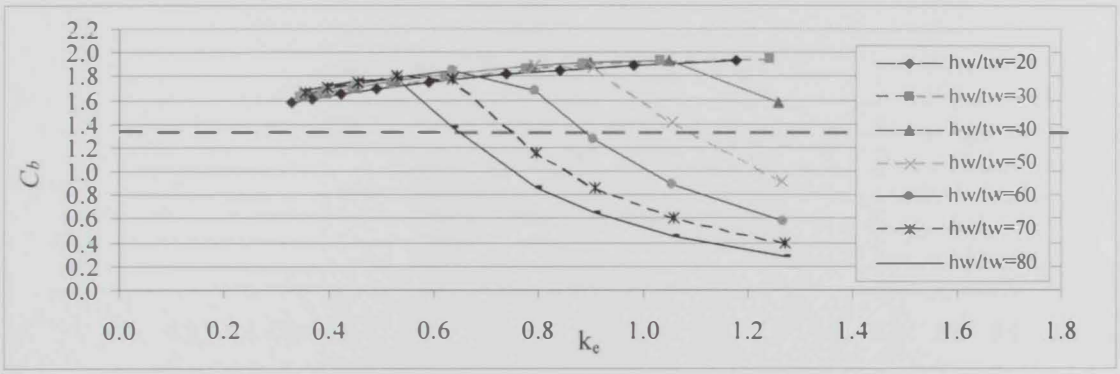

(c): Concentrated Load Applied at Bottom Flange (d_h/h_w = 0.7)

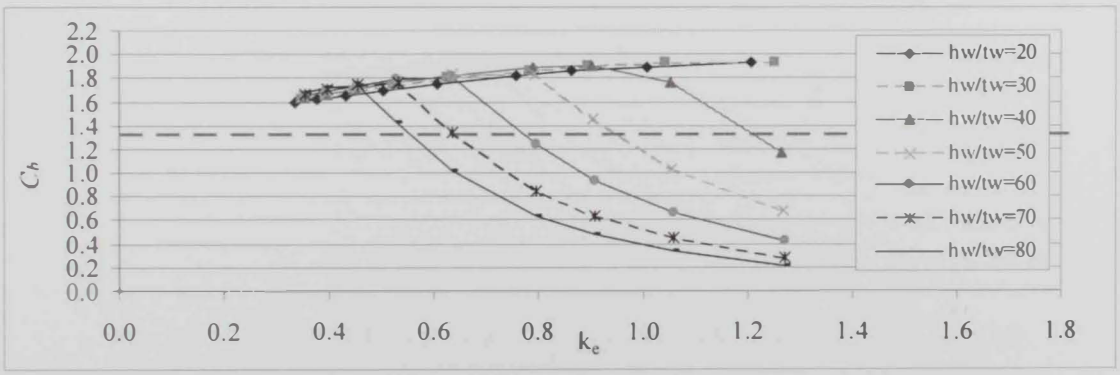

(d): Concentrated Load Applied at Bottom Flange (d_h/h_w = 0.8)

Figure 4.21: Moment Gradient Factor for (b_f/t_f = 10 and s/h_w = 1.05)

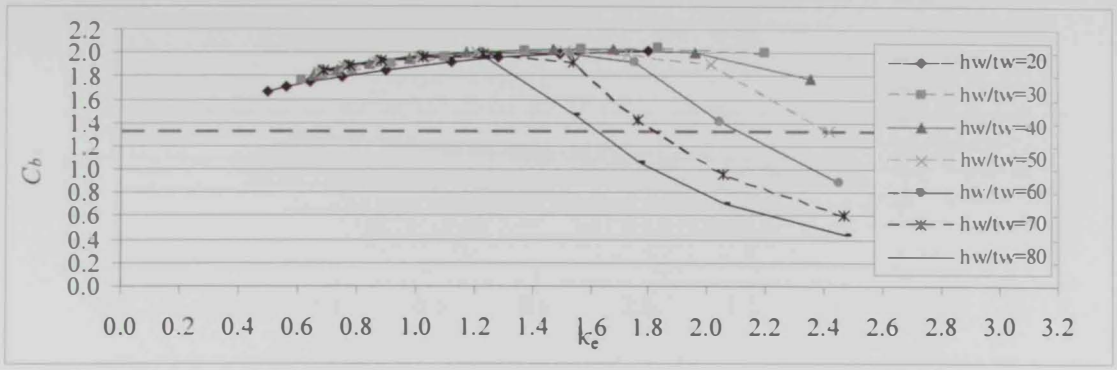

(a): Concentrated Load Applied at Bottom Flange (d_h/h_w = 0.5)

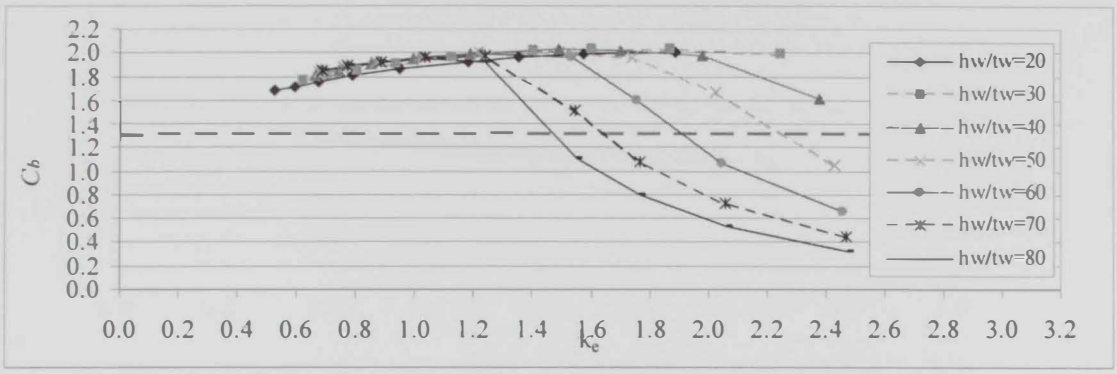

(b): Concentrated Load Applied at Bottom Flange (d_h/h_w = 0.6)

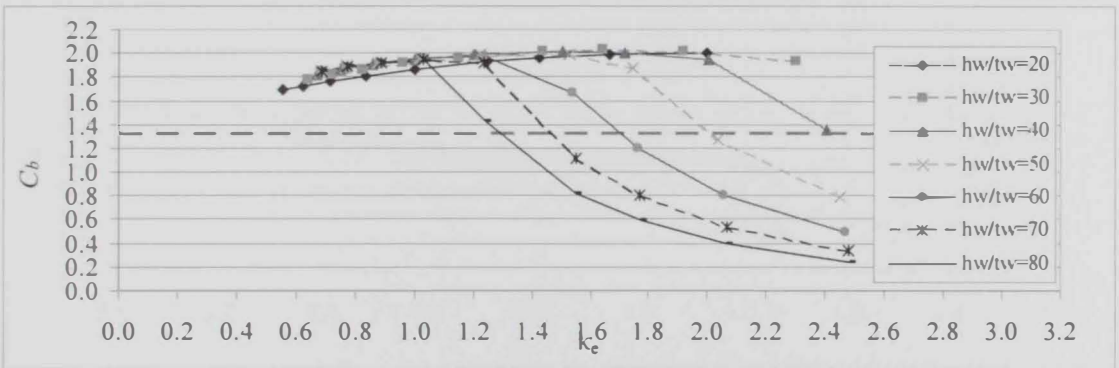

(c): Concentrated Load Applied at Bottom Flange (d_h/h_w = 0.7)

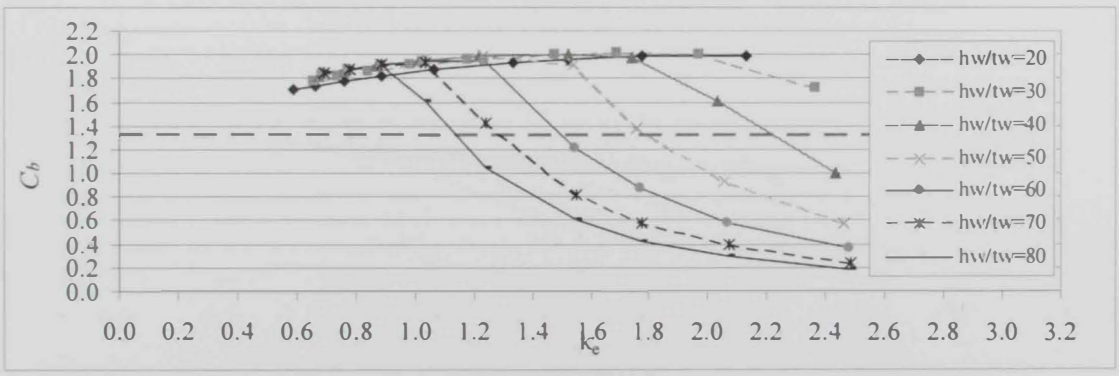

(d): Concentrated Load Applied at Bottom Flange (d_h/h_w = 0.8)

Figure 4.22: Moment Gradient Factor for (b_f/t_f = 20 and s/h_w = 1.05)

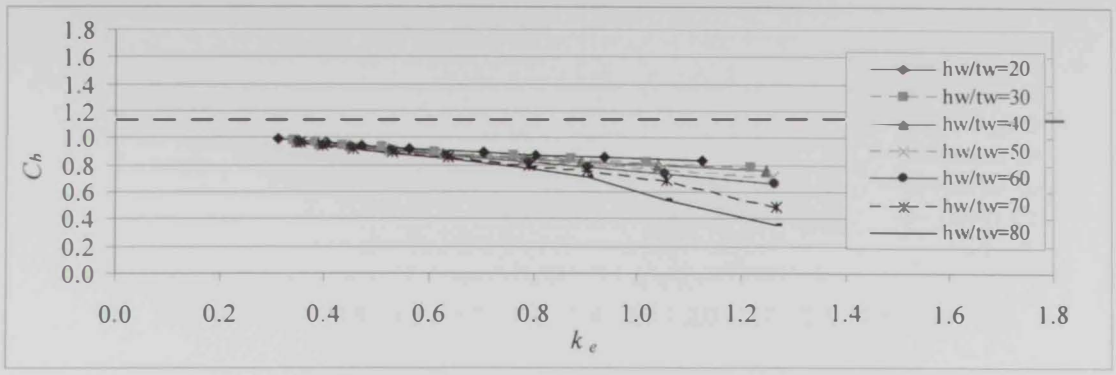

(a): Uniform Load Applied at Top Flange ($d_h/h_w = 0.5$)

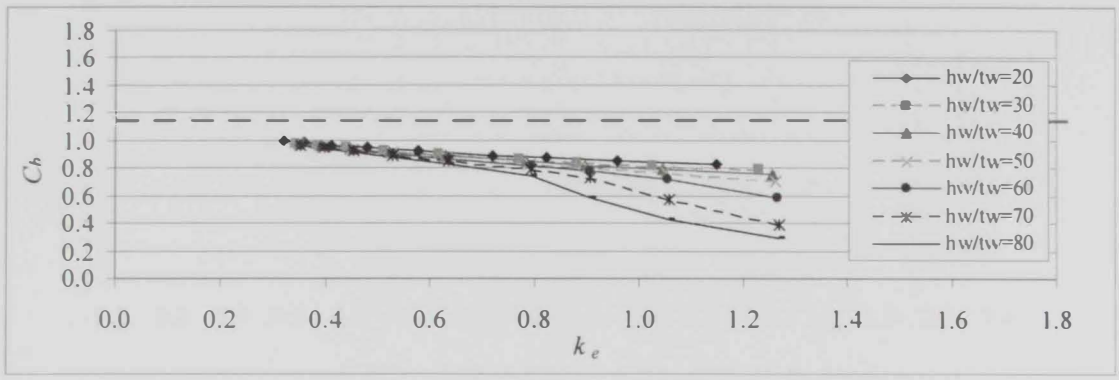

(b): Uniform Load Applied at Top Flange ($d_h/h_w = 0.6$)

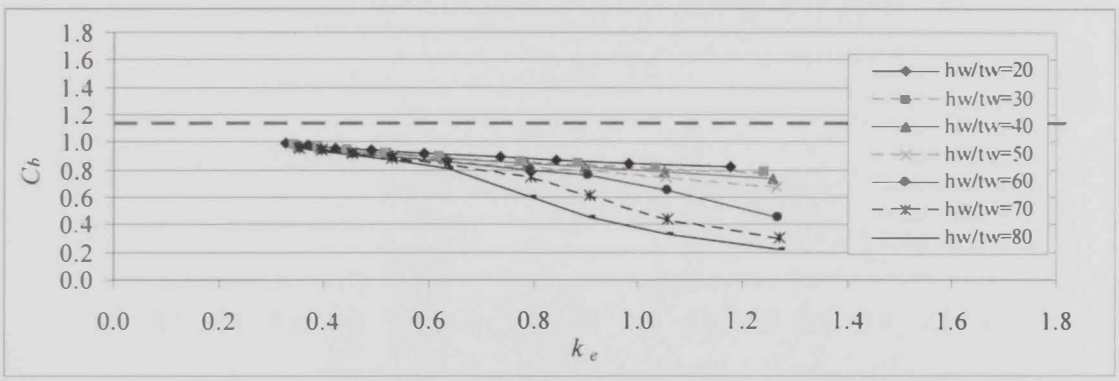

(c): Uniform Load Applied at Top Flange ($d_h/h_w = 0.7$)

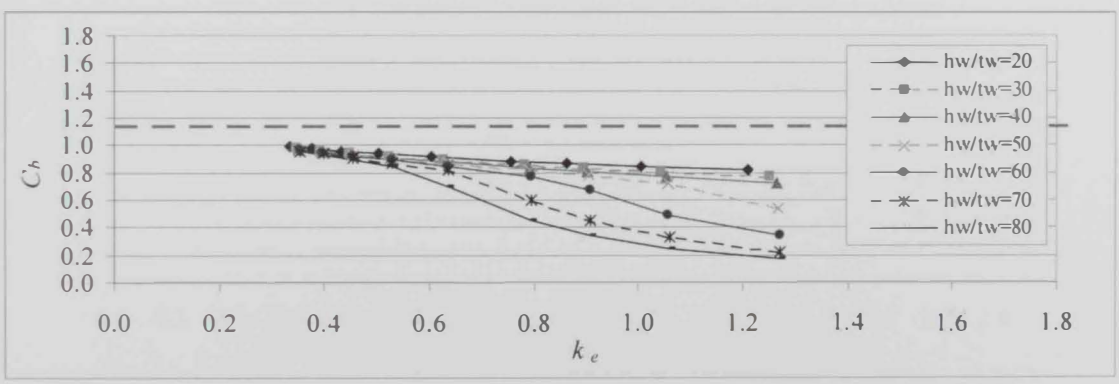

(d): Uniform Load Applied at Top Flange ($d_h/h_w = 0.8$)

Figure 4.23: Moment Gradient Factor for ($b_f/t_f = 10$ and $s/h_w = 1.05$)

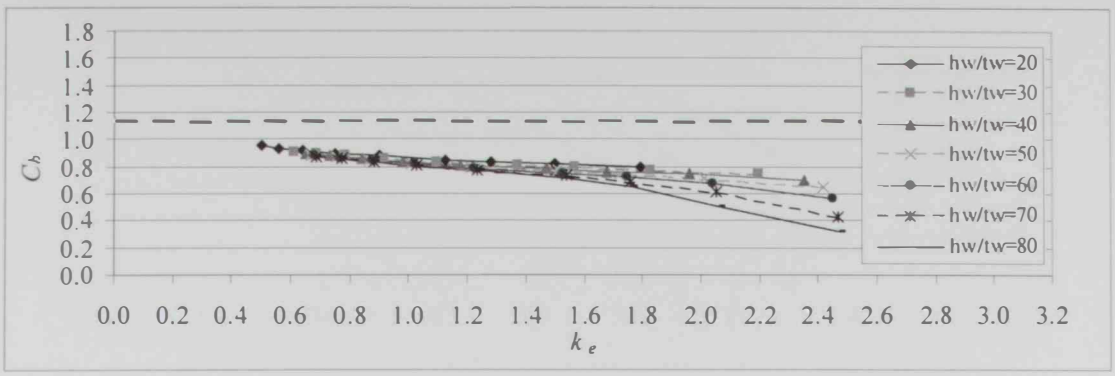

(a): Uniform Load Applied at Top Flange (d_h/h_w = 0.5)

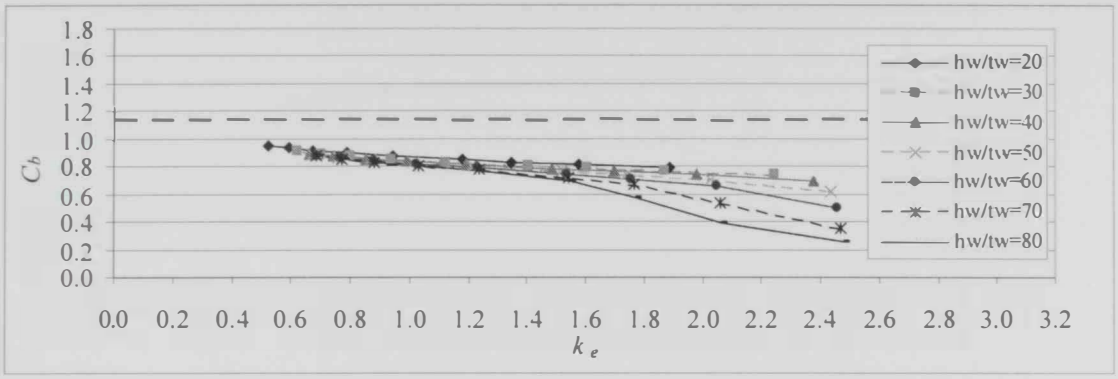

(b): Uniform Load Applied at Top Flange (d_h/h_w = 0.6)

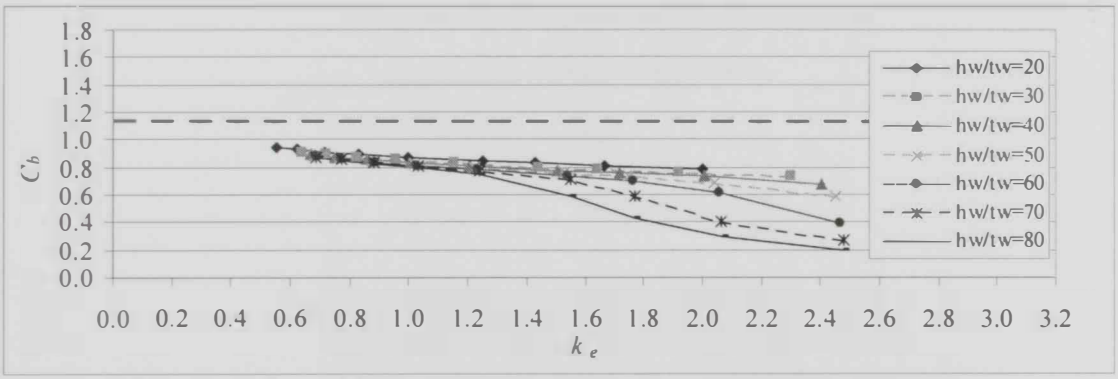

(c): Uniform Load Applied at Top Flange (d_h/h_w = 0.7)

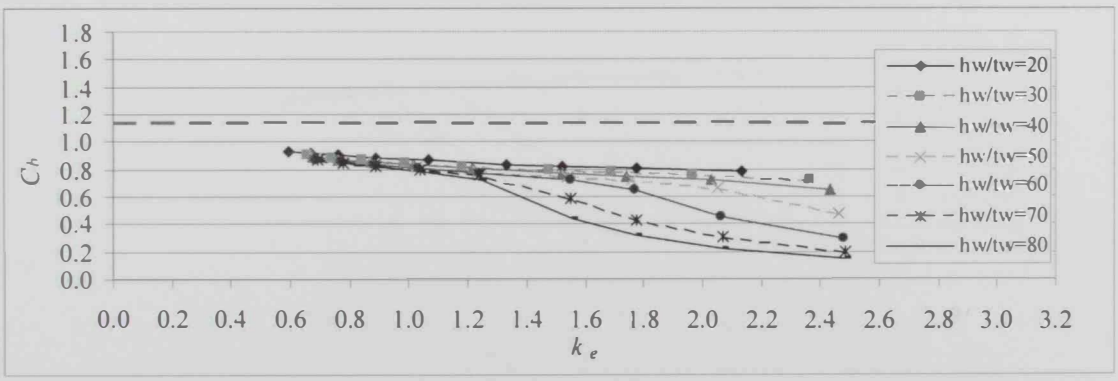

(d): Uniform Load Applied at Top Flange (d_h/h_w = 0.8)

Figure 4.24: Moment Gradient Factor for (b_f/t_f = 20 and s/h_w = 1.05)

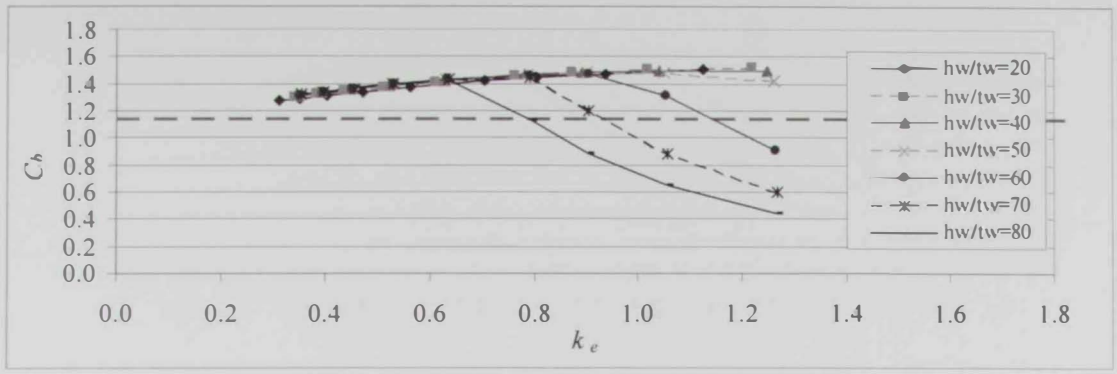

(a): Uniform Load Applied at Bottom Flange (d_h/h_w = 0.5)

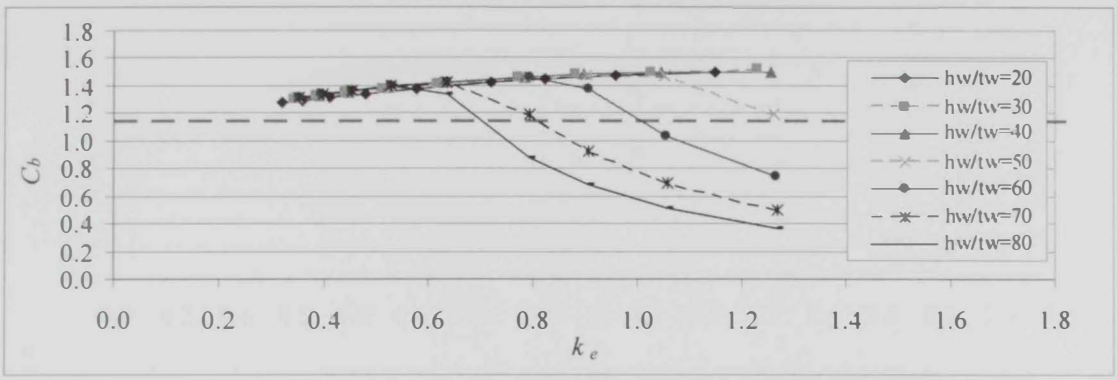

(b): Uniform Load Applied at Bottom Flange (d_h/h_w = 0.6)

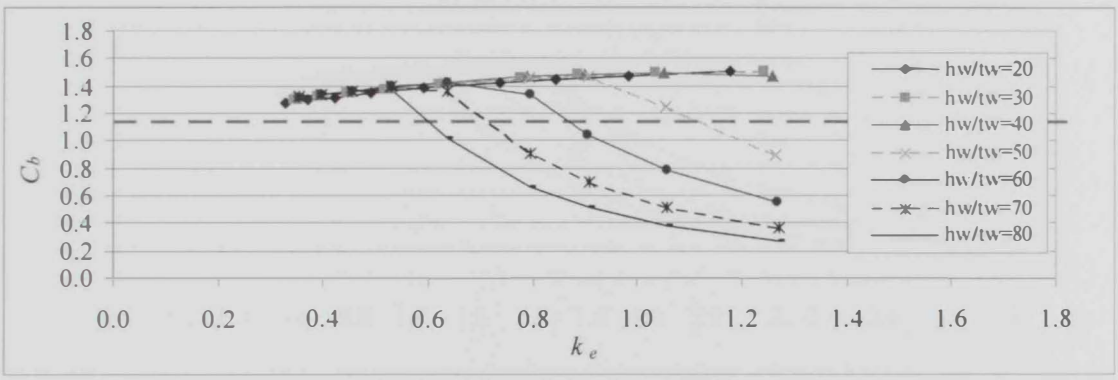

(c): Uniform Load Applied at Bottom Flange (d_h/h_w = 0.7)

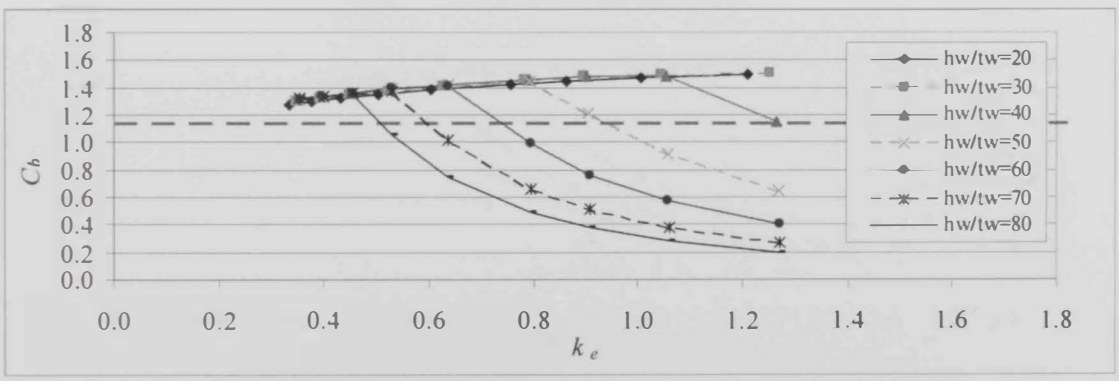

(d): Uniform Load Applied at Bottom Flange (d_h/h_w = 0.8)

Figure 4.25: Moment Gradient Factor for (b_f/t_f = 10 and s/h_w = 1.05)

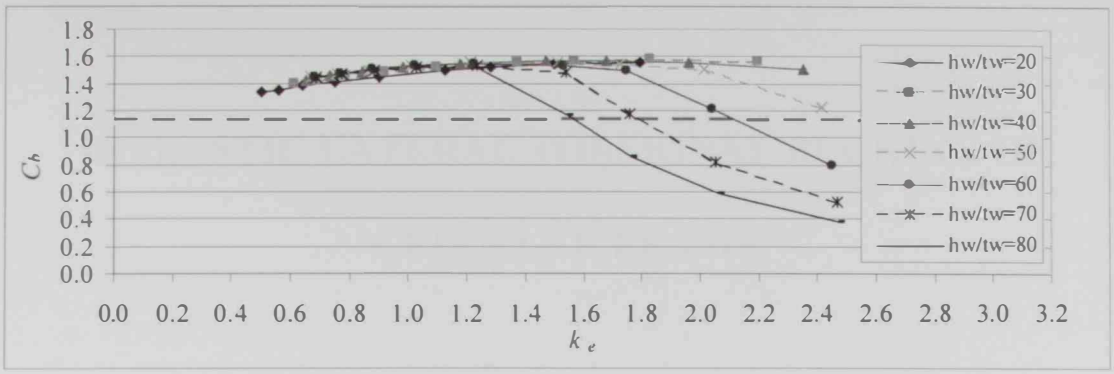

(a): Uniform Load Applied at Bottom Flange (d_h/h_w = 0.5)

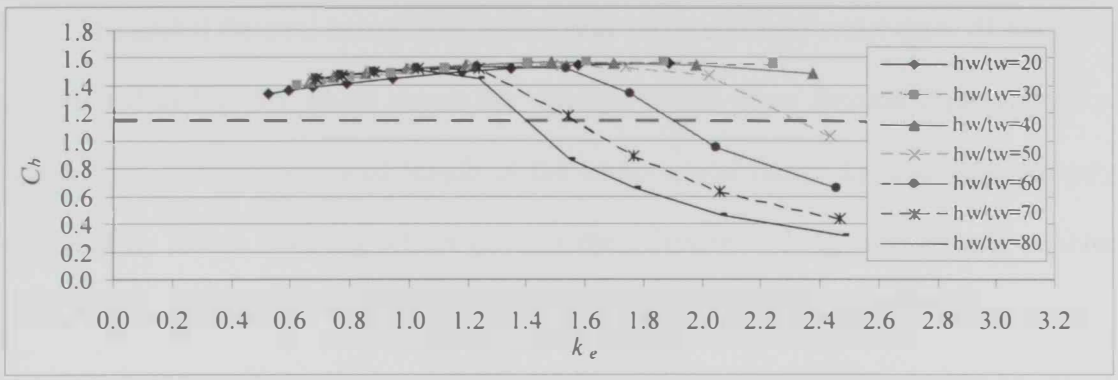

(b): Uniform Load Applied at Bottom Flange (d_h/h_w = 0.6)

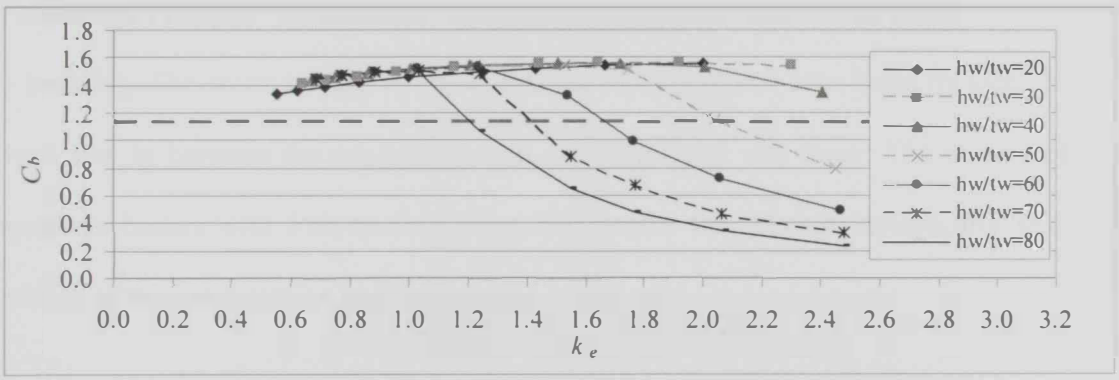

(c): Uniform Load Applied at Bottom Flange (d_h/h_w = 0.7)

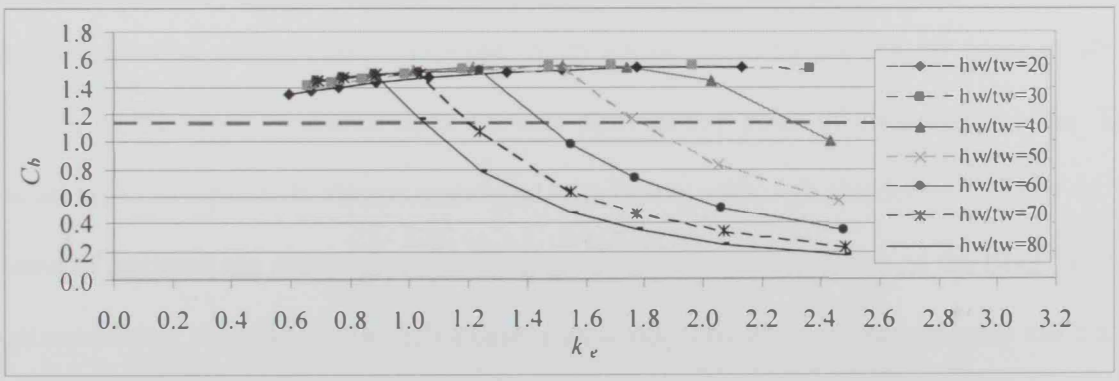

(d): Uniform Load Applied at Bottom Flange (d_h/h_w = 0.8)

Figure 4.26: Moment Gradient Factor for (b_f/t_f = 20 and s/h_w = 1.05)

CHAPTER 5

INELASTIC LATERAL TORSIONAL BUCKING OF CELLULAR BEAMS

5.1 INTRODUCTION

The global flexural behavior of beams may be categorized under three distinct ranges as illustrated in Fig. 5.1 which shows the variation of the beam flexural capacity, M_n, with respect to its laterally unbraced length of the compression flange L_b. The first category is dominated by elastic buckling which governs the behavior of long span laterally–unbraced beams. On the other hand, beams with adequate lateral bracing system are characterized by short unbraced length which causes yielding of the entire cross section to occur before onset of buckling. This type represents the third category that is dominated by plastic behavior with no buckling. The second category represents the most practical case faced by steel designers which lies in between the aforementioned categories one and three. The second category represents beams with intermediate unbraced lengths that buckle inelastically after some portions of the cross section have yielded.

The elastic buckling analysis and behavior presented in Chapter 4 are based on the basic assumption of full elastic response. Such elastic buckling applies for cases in which yielding of the beam's material does not take place at any point of the buckled beam. This special type of response is always associated with beams with high slenderness. However, for beams of intermediate slenderness, yielding occurs in the outmost fibers of the beam prior to commencement of buckling. In such a case, elastic buckling analysis that assumes full elastic behavior overestimates the buckling capacity of the beam. This is attributed to the fact that

only the elastic portions of the beam remain effective in resisting buckling action. Meanwhile, yielded parts possess reduced stiffness and, therefore, contribute less to the buckling resistance. As a result, the critical load associated with inelastic buckling is reduced. In practice, use of long spans steel beams without adequate bracing against lateral deflection and twisting (i.e.; high slenderness cellular steel beams) is relatively limited to the particular case of beams during erection (during the construction stage). This fact reveals that cases of elastic lateral torsional buckling may be relatively rare and, therefore, introduces the significance of studying inelastic buckling behavior of cellular steel beams, which is more likely to be faced in practice.

The literature review presented in Chapter 2 indicates that previous work completed for lateral torsional buckling of cellular steel beams is limited. The need to investigate these beams under lateral torsional buckling is imperative for understanding their behavior and improving their design. The current chapter concentrates on the inelastic lateral buckling behavior of cellular steel beams. The results of this study are expected to provide more insight into the behavior of cellular steel beams which would enhance the level of understanding of the influence of the circular web perforations on the global flexural stability of steel sections. In addition, the outcomes of this research will complement those obtained in Chapter 4 to enhance the effectiveness of the design of cellular steel beams in both the elastic and inelastic ranges of response.

5.2 GEOMETRICAL PARAMETERS FOR INELASTIC ANALYSIS

As a result of the wide variety in the size and configuration of web openings, it is crucial to investigate the influence of perforations on the behavior of this special type of members. The validated 3D finite element model is employed to conduct a parametric study

to identify the buckling characteristics of a wide range of cellular steel beams. A wide range of geometrical properties of analyzed sections is selected to cover, and extend beyond, the practical range of dimensions of such beams. An extensive survey is conducted to identify the commonly used dimensions in the European and North American markets. In addition, the survey considers the recommendations of the European Committee for Standardization (1994 and 2005). Based on the survey outcomes and due to numerous ranges of dimensions and perforation configurations of cellular steel beams, analyzed beams are designated through a set of dimensionless parameters such as the web aspect ratio denoted by its height–to–thickness ratio (h_w/t_w), the flange width–to–thickness ratio (b_f/t_f), and the beam's span length–to–web height ratio (L/h_w). Two main parameters are utilized to identify the perforation configuration namely; the hole diameter–to–web height ratio (d_h/h_w), and the hole spacing to web depth ratio (s/h_w).

The considered web height–to–thickness ratio (h_w/t_w) varies from 20 to 80 with an increment of 10 while the flange width–to–thickness ratio (b_f/t_f) is considered to vary from 10 to 20 with an increment of 5. The beam length to web height ratio (L/h_w) is assigned a wide range that includes long, intermediate and short span beams to allow all potential failure modes to be investigated. The considered (L/h_w) range extends from 10.5 to 37.8. As for the web openings configurations, the hole diameter–to–web height ratio (d_h/h_w) is taken as 0.5, 0.6, 0.7, and 0.8. In view of the results obtained in Chapter 4, which show that the most critical behavior is associated with closely spaced holes and given the significantly long time needed to execute inelastic cases of analysis, the current chapter considers a single value of 1.05 for the hole spacing to web height ratio (s/h_w). This value represents the case of closely spaced web holes and is associated with hole spacing–to–diameter ratios (s/d_h) of 2.1, 1.75, 1.5 and 1.3125 for hole diameter–to–web height ratios (d_h/h_w) of 0.5, 0.6, 0.7 and 0.8,

respectively. The above presented range of dimensions corresponds to a total of 2,268 cases of inelastic finite element analysis that are performed in this chapter. It is important to note that when selecting these specific values, a strict constraint is always achieved by having an integer value for the beam length to the hole spacing ratio (L/s) to allow for the generation of complete panels (i.e.; integer number of web holes or panels) during the modeling as explained in Chapter 3.

5.3 CONFIRMATION OF THE APPLICABILITY OF USING THE k_e PARAMETER FOR PRESENTING RESULTS

Similar to the process adopted in Chapter 4, each of the beams described in the previous section is analyzed under three different cases of loadings; namely uniform moment due to pure end moments, mid–span concentrated load and uniformly distributed load. For each beam, buckling moment values obtained from both cases of concentrated and uniform loading are used to calculate the moment gradient factor, C_b, through normalization with respect to the corresponding critical moment that results from a uniform moment case of loading:

$$C_b = \frac{M_{FE-P}}{M_{FE-M}} \quad \text{for the concentrated load case} \qquad (5.1(a))$$

$$C_b = \frac{M_{FE-W}}{M_{FE-M}} \quad \text{for the uniformly distributed load case} \qquad (5.1(b))$$

where

M_{FE-M} is the buckling moment at mid–span due to uniform moment distribution,

M_{FE-P} is the buckling moment at mid–span due to concentrated mid–span load, and

M_{FE-W} is the buckling moment at mid–span due to uniformly distributed load.

The typical procedure for evaluating the buckling moment M_{FE-M} is based on identifying the peak moment value from the nonlinear moment–lateral deformation relationship for a central point on the top flange of the mid–span cross section. Sample results are presented in Fig. 5.2(a) for a cellular beam with d_h/h_w = 0.6, h_w/t_w = 70, b_f/t_f = 15, s/h_w = 1.05, L/h_w = 25.2 and L = 22,932 mm subjected to pure end moments (uniform moment). Presented results indicate a buckling moment M_{FE-M} = 3517.35 kN.m at U_x = 106.11 mm. Meanwhile, the process of evaluating the buckling moment due to concentrated mid–span load M_{FE-P} involves two steps. First, the buckling load, P_{cr}, is identified from the nonlinear load–lateral deformation curve shown in Fig. 5.2(b) to be equal to 773.25 kN at U_x = 77.24 mm. Then, the corresponding buckling moment, M_{FE-P}, is calculated using

$$M_{FE-P} = \frac{P_{cr} L}{4} = 4433.03 \text{ kN.m} \qquad (5.2(a))$$

A similar process is adopted to evaluate the buckling moment due to uniformly distributed load, M_{FE-W}. The buckling load, W_{cr}, is identified from the nonlinear load–lateral deformation curve shown in Fig. 5.2(c) to be equal to 57.88 kN at U_x = 86.73 mm. Following that the corresponding buckling moment, M_{FE-W}, is obtained in accordance with the following equation

$$M_{FE-W} = \frac{W_{cr} L^2}{8} = 3805.05 \text{ kN.m} \qquad (5.2(b))$$

Consequently, the moment gradient factors, C_b, for the two cases of concentrated load and uniformly distributed load are calculated using Eqs. (5.1(a)) and (5.1(b)), respectively, as

$C_b = \frac{M_{FE-P}}{M_{FE-M}} = 1.260$ for the concentrated load case, and

$C_b = \frac{M_{FE-W}}{M_{FE-M}} = 1.082$ for the uniformly distributed load case.

For all analyzed cases, the variation of obtained C_b factor is presented with respect to a non–dimensional factor k_e that accounts for the major characteristics of the beam including, the beam length L, the torsional rigidity of the beam GJ, and the warping rigidity EC_w [AISC 360–05 (2005)]:

$$k_e = \frac{\pi}{L}\sqrt{\frac{EC_w}{GJ_{net}}} \tag{5.3}$$

where

E is Young's modulus of elasticity,

C_w is the warping torsional constant of the cross section given by Eq. (4.4),

G is the shear modulus of elasticity, and

J_{net} is the torsional constant of the net cross section as given by Eq. (4.5).

As discussed in Chapter 4, the main advantage in using the k_e factor is that different cellular beams having the same k_e value are shown to have the same C_b factor. The same k_e value can be attained for various sections with different dimensions as long as these beams have equal (b_f/t_f), (h_w/t_w), (A_f/A_w), (d_h/h_w), (s/h_w), and (L/h_w) ratios. A similar trend is observed for cellular beams undergoing inelastic lateral buckling. As such, the k_e factor is used to present the results obtained in the current chapter. In order to confirm this characteristic, sample verification results are presented in Tables 5.1 through 5.3. Table 5.1 shows three groups of cellular beams with five different beams in each group. All the beams listed in the table have h_w/t_w = 40, b_f/t_f = 20, A_f/A_w = 0.802, d_h/h_w = 0.7 and s/h_w = 1.05. In order to investigate the influence of L/h_w ratio on the k_e factor, a different L/h_w ratio is assigned to each group while the L/h_w value is kept constant within the same group. As presented in Table 5.1, L/h_w ratios of 21, 14.7 and 10.5 are used to represent different ranges of spans including long, medium and short spans, respectively. Tabulated results reveal constant C_b value for different beams within the same group (i.e.; having equal k_e fa ctor) under a

particular case of loading. On the contrary, the C_b value varies from one group to another as a result of changing the L/h_w ratio and consequently the k_e factor.

The effect of changing the flange aspect ratio (b_f/t_f) and the flange–to–web areas ratio (A_f/A_w) on the C_b factor is depicted in Table 5.2. All the beams shown in this table have h_w/t_w = 40, L/h_w = 14.7, d_h/h_w = 0.7 and s/h_w = 1.05. Meanwhile, the three tabulated groups of beams have b_f/t_f ratio of 10, 15, and 20. The results shown in Table 5.2 indicate the correlation between the k_e factor and the C_b value for the five different beams in each group with equal k_e factor. Comparison between these results confirms that different beams with equal k_e and the same perforation configuration (i.e.; same s/h_w, and d_h/h_w values) have the same C_b value as long as they are subjected to the same load pattern and buckling mode.

Similarly, the effect of changing (h_w/t_w) on the C_b factor is shown by the results of six groups of cellular beams summarized in Table 5.3. For all the beams included in this table, the L/h_w = 21, d_h/h_w = 0.7 and s/h_w = 1.05. Comparison between the results of each two consecutive groups reveals that, despite the fact that the (b_f/t_f) ratio is kept constant, changing the (h_w/t_w) ratio leads to variation in the k_e factor and, consequently, the C_b values.

For all the C_b values presented in Tables 5.1 through 5.3, it can be observed that tabulated values are relatively low compared to the ones recommended by the AISC 360–06 [AISC 360–05 (2005)] for solid beams. A detailed discussion of this critical observation is presented later in this chapter.

5.4 FINITE ELEMENT RESULTS AND DISCUSSION

The verified three–dimensional finite element model is utilized to investigate the elasto–plastic lateral torsional buckling characteristics of cellular steel beams. It is worth mentioning that the developed model is capable of capturing various buckling deformations including lateral buckling, and localized web distortion. An extensive parametric study is conducted to assess the impact of various design parameters on the elasto–plastic lateral torsional buckling of simply supported cellular steel beams. The study considers beams subjected to equal and opposite end moments in addition to two common transverse loading cases including mid–span concentrated load and uniformly distributed load applied at the shear centre of the cross section. The buckling load is calculated by obtaining the peak load from the nonlinear load–lateral deformation curve drawn for a central point on the top flange at mid–span as explained in details in Chapter 3. The studied parameters include a wide range of geometrical and perforation configurations defined by the dimensionless parameters (h_w/t_w, b_f/t_f, L/h_w, and d_h/h_w). A total number of 2,268 elasto–plastic cases of analyses are performed in this comprehensive parametric study. Outcomes of the study are expressed in terms of the moment gradient factor C_b that represents the ratio of the elasto–plastic buckling moment for non–uniform moment conditions (under transverse concentrated or uniformly distributed loading) and that for the basic case of equal moments applied at the ends of the beam. The variation of the C_b factor is presented with respect to the non–dimensional k_e factor that accounts for the beam slenderness in addition to its torsion and warping rigidities.

Figures 5.3(a) and (b) present sample results to demonstrate the variation of the C_b factor for cellular beams subjected to mid–span concentrated load and uniformly distributed load, respectively. These figures also show the variation of moment–gradient factor C_b relative to the standard values recommended by the AISC 360–05 (2005) for solid beams.

The results presented in these figures correspond to the particular case of cellular beams with b_f/t_f = 15, d_h/h_w = 0.6 and s/h_w = 1.05. Meanwhile, three representative web slenderness values h_w/t_w = 30, 50 and 70 are considered in these figures for illustrative purposes.

In general, the results shown in Figs. 5.3(a) and (b) reveal that the non–uniform moment distribution caused by transverse loading increases the elasto–plastic lateral buckling strength of cellular beams (i.e., $C_b > 1.0$) compared to the uniform moment case of loading especially for long–span beams (i.e.; with lower k_e values). Consequently, the higher the C_b factor value is, the more strength benefits are attained. The figures also indicate that cellular beams subjected to mid–span concentrated load (Fig. 5.3(a)) can sustain higher moments than those supporting uniformly distributed load (Fig. 5.3(b)). Similar behavior has been discussed in Chapter 4 and is attributed to spread of the high moment values (and consequently higher compressive stresses in the compression flange) over a longer portion of the beam's span in the case of uniformly distributed load. On the contrary, the influence of the high compressive stresses is significantly localized around the mid–span of beams carrying mid–span concentrated load. For both cases of loading, it can be seen that slender beams (i.e.; with lower k_e values) possess C_b values that are close to the recommended code values for solid beams [AISC 360–05 (2005)]. This behavior is limited by k_e values not exceeding about 0.7 (Fig. 5.3(a)) and 0.9 (Fig. 5.3(b)) for the beams carrying mid–span concentrated load and uniformly distributed load, respectively.

For the case of slender cellular beams (i.e.; with lower k_e values) subjected to mid–span concentrated load, finite element results indicate that the response of these beams is dominated by pure inelastic lateral torsional buckling mode (LTB) as shown in Fig. 5.4(a). It can be observed from Fig. 5.3(a) that this behavior is associated with C_b values that are close

to standard code value as they vary between 1.30 and 1.15 for h_w/t_w =30 and 50, while this range becomes 1.32 to 1.20 for h_w/t_w =70. As the beam slenderness decreases (i.e.; k_e value increases), the level of web distortion during lateral buckling increases leading to formation of lateral distortional buckling mode (LDB) where local web distortion and lateral torsional buckling occur simultaneously (Fig. 5.4(b)). This behavior becomes more apparent in beams with higher h_w/t_w values where localized web distortions are more pronounced. Formation of the (LDB) mode is associated with reduction in the C_b value that ranges between about 1.15 and 1.0 for h_w/t_w =30 and 50. Meanwhile, the C_b range is reduced to about 1.20 to 1.05 for h_w/t_w =70. Further reduction in the C_b factor corresponds to the interaction between the local buckling of the web post that accompanies the lateral buckling deformations as shown in Fig. 5.4(c). Such an interaction is characterized by C_b range of about 1.0 to 0.95 for beams having h_w/t_w =30 and 50. This range becomes 1.05 to 0.95 for beams with h_w/t_w =70. For all the beams having C_b factor less than 0.95, the response is mainly dominated by local buckling of the web post with no lateral deformations existing in the buckling mode as depicted by Fig. 5.4(d).

Similarly, for cellular beam subjected to uniformly distributed load buckling of slender beams is dominated by inelastic lateral torsional mode (LTB) as presented in Fig. 5.4(a). The corresponding C_b values vary between 1.11 and 1.04 for h_w/t_w =30 and 50, while this range becomes 1.12 to 1.06 for h_w/t_w =70. As the beam slenderness decreases (i.e.; k_e value increases), the level of web distortion becomes more pronounced in the dominating lateral buckling deformations leading to formation of lateral distortional buckling mode (LDB) as shown in Fig. 5.4(b). Similar to the behavior of beams subjected to concentrated loading, the (LDB) deformations are more apparent in beams with higher h_w/t_w values and take place with a reduced C_b factor that varies from 1.04 to 1.00 for h_w/t_w =30 and 50. The C_b

range bounds slightly increase to about 1.06 to 1.02 for h_w/t_w =70. Further reduction in the C_b factor takes place with simultaneous occurrence of local buckling deformations in the web post and lateral buckling deformations (Fig. 5.4(c)) where the C_b value ranges between 1.00 and 0.87 for beams having h_w/t_w =30 and 50. The C_b range extends to vary between 1.02 and 0.77 for beams with h_w/t_w =70. Further reduction in the C_b factor below 0.87 (h_w/t_w =30 and 50) and 0.77 (h_w/t_w =70) is always associated with non–lateral buckling mode dominated by local deformations in the web post as shown in Fig. 5.4(d).

The above discussion for the sample results shown in Figs. 5.3(a) and (b) implies that C_b factors provided by current design codes for solid steel beams may not provide accurate predictions for the moment carrying capacity of cellular beams. A constant C_b factor is recommended by AISC 360–05 (2005) (C_b = 1.32 for mid–span concentrated load and C_b = 1.14 for uniformly distributed load) independent of beam torsional slenderness (i.e., length and section geometry). These values seem to represent upper bound estimates of the moment gradient factor C_b that correspond to pure lateral torsional buckling (LTB) mode only. However, current code values do not account for the other potential buckling modes stated in the above discussion including lateral distortional buckling (LDB) and interaction between lateral deformations and localized web post buckling. As indicated by the above discussion, these modes always lead to a reduction in the moment carrying capacity of the beams as reflected by the reduced C_b values. This confirms the inadequacy of using the C_b factors provided by current design codes for designing cellular beams as this could result in unconservative estimates for the buckling capacity of such a special beam type.

Prior to providing further discussions to the rest of the finite element results, it is prudent to summarize the general flexural stability characteristics that have been observed in

the sample finite element results under the two transverse loading patterns; concentrated and uniformly distributed loads. The schematic shown in Fig. 5.5 illustrates the stability behavior of the analyzed beams due to three distinct buckling modes that have been noticed in most of the reported results. The buckling modes are mainly dependent on the value of the parameter k_e that relates, very closely, to the torsional stiffness of the beam. Fig. 5.5 shows that lateral buckling modes (LTB and LDB) take place at small values of k_e (i.e., for slender long beams). In these cases, the values of C_b are very close to the proposed values by the different design codes (e.g., AISC 360–05 (2005)). As the value of k_e increases due to beam's thicker flanges and/or web or due to shorter span, the torsional stiffness of the beam increases. This leads to lateral instability of the beam under interacting lateral distortional buckling and localized web buckling modes (i.e., LDB and WLB). As the beam becomes significantly short or the elements of the cross–section become very thick, k_e increases and the beam's torsional stiffness becomes very high leading to instability due to web post local buckling (WLB) only. This typical behavior is referred to in the following discussions.

Fig. 5.6 shows the effect of the web slenderness (presented as h_w/t_w) on the lateral stability behavior of the beam. The figure shows that as the web becomes thicker (i.e. less slender with smaller h_w/t_w), the entire C_b–k_e curve shifts to the right. In addition, the zones of LTB, LDB, LDB–WLB interaction, and WLB shift to the right, as well, with thicker webs. This behavior may be justified in the view of two simultaneous effects due to the variation in h_w/t_w. These effects are explained as follows:

1. As the web h_w/t_w increases, the lateral torsional stiffness of the beam increases leading to increased lateral stability and, consequently, higher values for C_b. This is very clear for long beams with small values of k_e.

2. Once the beam span length reduces (i.e., k_e increases) and the web slenderness increases (i.e., with higher h_w/t_w), the stability of the beam is completely controlled by the web post local buckling leading to a reduction in stability as reflected in the smaller C_b values. This behavior is pronounced in short beams with high k_e values.

The effect of the hole diameter (represented by d_h/h_w) on the lateral stability behavior of the beam is shown in Fig. 5.7. For beams with long spans (i.e., small k_e values), one may not notice any change in the behavior since it is completely controlled by lateral torsional/distortional buckling (LTB or LDB). It is clear that as the hole diameter increases, the slenderness of the web post decreases relative to the torsional stiffness of the beam. Therefore, the effect of the web local buckling (WLB) becomes more pronounced. As such, interaction between LDB and WLB modes or pure WLB mode control the response of cellular beams with smaller values of k_e relative to those beams with smaller web holes.

5.4.1 Effect of Web Slenderness (h_w/t_w) on the Moment Gradient Factor C_b

The influence of varying the slenderness of the web plate h_w/t_w on the inelastic lateral torsional buckling of cellular beams is discussed herein. Illustrations presented pertain to a representative set of cellular beams having b_f/t_f value of 15 with uniform web openings spaced at constant intervals of s/h_w = 1.05. Analyzed beams are assigned a wide range of web slenderness values h_w/t_w that varies between 20 and 80 with an increment of 10. Figs. 5.8(a), (b), (c) and (d) show the variation in the C_b factor for these cellular beams having web hole sizes of d_h/h_w = 0.5, 0.6, 0.7 and 0.8, respectively, under the effect of mid–span concentrated loading. These figures reveal a general trend of reduction in the C_b factor with the increase in the web slenderness (h_w/t_w). Long span beams (having low k_e factor) with different h_w/t_w ratios are shown to have C_b factors that are close to code recommended value for lateral

torsional buckling (LTB) failure. Meanwhile, beams with intermediate slenderness (intermediate k_e values) with slender web plates where h_w/t_w = 60, 70 and 80, experience shear deformations in their web plates and, therefore, are controlled by combined lateral–local buckling modes (Figs. 5.8(b), (c) and (d)). In this case, the dominant mode changes from lateral distortional buckling mode (LDB) to interaction between lateral deformations and web post localized buckling as the k_e value increases. Short span beams (characterized by high k_e values) are shown to be more sensitive to the increase in their web slenderness. For such beams, lateral deformations are more difficult to occur and web post shear deformations become significantly dominant leading to a non–lateral buckling failure due to local web post buckling. This behavior is associated with a significant reduction in the C_b, factor which becomes more pronounced in beams with intermediate to slender web plates where h_w/t_w = 60 to 80 as shown in Fig. 5.8(b) and h_w/t_w = 50 to 80 as shown in Figs. 5.8(c) and (d).

A similar trend is observed for long and intermediate span cellular beams subjected to uniformly distributed load as depicted in Figs. 5.9(a), (b), (c) and (d) for web hole sizes of d_h/h_w = 0.5, 0.6, 0.7 and 0.8, respectively. Meanwhile, the influence of web shear deformations is more pronounced in short span beams subjected to uniform load (Fig. 5.9) as compared to their counterparts under mid–span concentrated load (Fig. 5.8). This may be attributed to the spread of high compressive stresses, and consequently yielding, over longer portion of the span of beams under uniform loading than those carrying concentrated loading. As such, short span beams (with high k_e values) experience higher shear deformations in the web posts leading to a non–lateral deformations associated with local web buckling. This behavior is associated with a severe reduction in the C_b factor, which becomes more pronounced in beams with intermediate to slender web plates where h_w/t_w = 50 to 80 as shown in Figs. 5.9(a) and (b) and h_w/t_w = 40 to 80 as shown in Figs. 5.9(c) and (d).

5.4.2 Effect of Web Hole Size (d_h/h_w) on the Moment Gradient Factor C_b

The presence of circular perforations in the web plate of cellular beams may alter the dominant buckling modes of cellular beams and their buckling capacity. This influence is reflected in the reduction in the C_b factor of these beams. In other words, the response of this type of beam varies from being a lateral buckling mode (LTB or LDB) to a localized non–lateral buckling mode depending on its span length, the slenderness level of the web plate and the size of the web hole.

The effect of the hole size on the inelastic lateral torsional buckling of cellular beams is presented for representative beams with $b_f/t_f = 15$. Considered beams have h_w/t_w values that cover the range of 20 to 80 with an increment of 10. The variation in web hole size is taken into account through consideration of d_h/h_w = 0.5, 0.6, 0.7 and 0.8. Assessed C_b factors are presented in Figs. 5.8 and 5.9 for mid–span concentrated load and uniformly distributed loads, respectively.

As implied by Figs. 5.8(a), (b), (c) and (d) for beams subjected to mid–span concentrated load, the increase in the web hole size has insignificant influence on the C_b factor of slender cellular beams (with low k_e values) failing by lateral buckling (LTB or LDB). The ranges of C_b factors that correspond to LTB and LDB modes for different d_h/h_w and h_w/t_w values are shown in Table 5.4(a). Furthermore, introduction of larger holes in the webs of intermediate and short–span beams is shown to alter the failure mode and reduce the corresponding C_b value. This observation is more pronounced in beams with more slender web plates (i.e., high h_w/t_w values). This behavior results from two simultaneous effects; firstly lateral deformations of intermediate and short–span beams are not as easy to excite as in longer beams and thus, the response may be controlled by other modes of failure.

Secondly, slender webs with bigger perforations provide less shear stiffness and have high potential to encounter high shear deformations in the web post between successive holes. As a result, beams with intermediate span length (i.e., with intermediate k_e values) are found to respond by a combined action between lateral buckling and local web deformations. This behavior is always coupled with a considerable reduction in the C_b factor relative to beams failing by lateral buckling modes. The typical range of the C_b factors associated with the LDB–WLB interaction is presented in Table 5.4(a). Further decrease in the span length is associated with a significant reduction in the C_b value where failure is dominated by non–lateral local web buckling mode (WLB). Local buckling is characterized by C_b values that are less than the lower C_b–limits shown in the rightmost column of Table 5.4(a).

The effect of web hole size on the stability of cellular beams subjected to uniformly distributed load is analogous to those supporting mid–span concentrated load. Figs. 5.9(a), (b), (c) and (d) show the change in C_b values for cellular beams with d_h/h_w = 0.5, 0.6, 0.7 and 0.8, respectively. In general, a noticeable effect of the hole size on the C_b factor takes place in cellular beams with intermediate and short–spans, especially those with more slender web plates (i.e.; high h_w/t_w values). Similar to the mid–span concentrated load case, the response of beams with intermediate span length is controlled by interaction between lateral buckling and local web deformations. This behavior is always associated with a considerable reduction in the C_b factor relative to beams failing by lateral buckling modes. The typical range of the C_b factors associated with the various buckling modes is presented in Table 5.4(b). Beams with shorter spans (higher values of k_e) encounter a more severe reduction in their C_b value as a result of failure due to non–lateral local web buckling mode. Local buckling is characterized by C_b factor less than the lower C_b–limits shown for the LDB–WLB interaction mode in Table 5.4(b).

5.4.3 Effect of Flange Dimensions (b_f/t_f) on the Moment Gradient Factor C_b

The variation of the moment gradient factor C_b is investigated with respect to the non–dimensional factor k_e based on the results related to three sets of cellular beams with flange aspect ratio b_f/t_f = 10, 15 and 20. Figs. 5.8, 5.10 and 5.11 summarize the C_b results for cellular beams subjected to mid–span concentrated load with b_f/t_f = 15, 10 and 20, respectively. Comparison between these figures reveals insignificant change in the obtained C_b factor for different beams having equal k_e values. This observation applies only to slender beams (with low k_e values) experiencing lateral buckling failure mode (LTB or LDB). However, a clear reduction in the C_b factor takes place in short cellular beams (high k_e values) with flanges of smaller aspect ratio (b_f/t_f = 10) relative to those with higher flange aspect ratio (b_f/t_f = 20) as indicated by Figs. 5.10 and 5.11, respectively. This observation is attributed to the high level of web distortions developed in beams with shorter spans. In addition, smaller flange plates do not provide effective torsional restrains for the perforated webs leading to more reduction in the C_b factor.

The impact of changing the flange aspect ratio on the behavior of cellular beams subjected to uniformly distributed load is identical to that of beams carrying concentrated load. Similar observations to the ones stated above can be drawn from Figs. 5.9, 5.12 and 5.13 that show the obtained C_b factor for cellular beams subjected to uniformly distributed load with b_f/t_f = 15, 10 and 20, respectively.

5.5 SUMMARY AND CONCLUSIONS

The inelastic lateral buckling of cellular beams is investigated in this chapter. The investigation is carried out numerical using a three–dimensional non–linear finite element model that has been developed and verified in Chapter 3. The study considers a wide

spectrum of geometrical parameters that presents the practical range of dimensions of cellular steel beams. Analyzed beams are designated through a set of dimensionless parameters to describe the various geometrical aspects. The considered web height–to–thickness ratio (h_w/t_w) varies from 20 to 80 with an increment of 10 while the flange width–to–thickness ratio (b_f/t_f) is considered to vary from 10 to 20 with an increment of 5. The beam length to web height ratio (L/h_w) extends from 10.5 to 37.8. As for the web openings configurations, the hole diameter–to–web height ratio (d_h/h_w) is taken as 0.5, 0.6, 0.7, and 0.8. Analyzed beams assumes a single value of 1.05 for the hole spacing to web height ratio (s/h_w). This value represents the case of closely spaced web holes and is associated with hole spacing–to–diameter ratios (s/d_h) of 2.1, 1.75, 1.5 and 1.3125 for hole diameter–to–web height ratios (d_h/h_w) of 0.5, 0.6, 0.7 and 0.8, respectively. A comprehensive parametric analysis is conducted to evaluate the impact of various cross section dimensions, beam slenderness, and web openings size on the inelastic buckling capacity and associated modes of cellular steel beams. Outcomes of the analyses are presented through the variation of the moment gradient factor C_b with respect to the non–dimensional factor k_e that relates the warping rigidity to the torsional rigidity of cellular beams. The main conclusions that may be drawn based on the finite element results are:

- Long span cellular beams are shown to experience inelastic lateral buckling due to lateral torsional buckling (LTB) or lateral distortional buckling (LDB).
- Cellular beams with intermediate span length experience interaction between lateral deformations and local web shear buckling at failure. This mode of failure is associated with considerable reduction in the C_b value.
- Buckling of short span cellular beams is governed by high level of web distortion that results from the high shear stresses induced in the web. For these beams, no lateral buckling occurs and significant reduction in C_b values occurs.

- Obtained results indicate that intermediate cellular beams with slender web plates (i.e.: high h_w/t_w values) and/or big web holes (i.e.: high d_h/h_w values) fail by combined lateral–local buckling modes that are associated with low C_b factors. Moreover, cellular beams with short spans and slender web plates (high h_w/t_w values) and/or big web holes (high d_h/h_w values) are sensitive to shear deformations. Failure of these beams is governed by non–lateral buckling modes that are localized in the web posts and are associated with significantly low C_b values.
- Failure of cellular beams subjected to mid–span concentrated loads by a combined action between lateral buckling and local web deformations is characterized by a C_b range of about 1.05 to 0.95 for hole sizes of d_h/h_w = 0.5 and 0.6 and a range of 1.0 to 0.9 for hole sizes of d_h/h_w = 0.7 and 0.8. Failure of these beams that is dominated by non–lateral local web buckling mode is characterized by C_b factors that are less than the above mentioned lower bounds.
- Failure of cellular beams subjected to uniformly distributed loads by interaction between lateral buckling and local web deformations is characterized by a C_b range of about 1.02 to 0.85 for hole sizes of d_h/h_w = 0.5 and 0.6 and a range of 1.0 to 0.8 for hole sizes of d_h/h_w = 0.7 and 0.8. Lower C_b values are associated with failures that are dominated by non–lateral local web buckling mode.
- Cellular beams with relatively small flange plates experience more reduction in the moment gradient factor C_b than those with bigger flange plates. This is attributed to the fact that bigger flange plates provide more effective torsional restrains for the perforated webs which, consequently, minimizes the encountered reduction in the C_b factor.

Table 5.1: Effect of Changing (L/h_w) on the k_e and C_b Factors for Beams with d_H/h_w = 0.7, and s/h_w = 1.05

Beam Properties								k_e	C_b (Concentrated Load)	C_b (Uniform Load)
b_f (mm)	t_f (mm)	h_w (mm)	t_w (mm)	b_f/t_f	h_w/t_w	A_f/A_w	L/h_w			
228	11.4	360	9	20	40	0.802	21.0	1.178	1.197	1.036
304	15.2	480	12	20	40	0.802	21.0	1.178	1.197	1.036
380	19	600	15	20	40	0.802	21.0	1.178	1.197	1.036
456	22.8	720	18	20	40	0.802	21.0	1.178	1.197	1.036
532	26.6	840	21	20	40	0.802	21.0	1.178	1.196	1.036
228	11.4	360	9	20	40	0.802	14.7	1.682	1.079	1.048
304	15.2	480	12	20	40	0.802	14.7	1.682	1.078	1.050
380	19	600	15	20	40	0.802	14.7	1.682	1.078	1.054
456	22.8	720	18	20	40	0.802	14.7	1.682	1.078	1.051
532	26.6	840	21	20	40	0.802	14.7	1.682	1.078	1.054
228	11.4	360	9	20	40	0.802	10.5	10.00	2.355	0.973
304	15.2	480	12	20	40	0.802	10.5	10.00	2.355	0.972
380	19	600	15	20	40	0.802	10.5	10.00	2.355	0.969
456	22.8	720	18	20	40	0.802	10.5	10.00	2.355	0.971
532	26.6	840	21	20	40	0.802	10.5	10.00	2.355	0.971

Table 5.2: Effect of Changing (b_f/t_f) on the k_e and C_b Factors for Beams with $d_h/h_w = 0.7$, and $s/h_w = 1.05$

Beam Properties								k_e	C_b (Concentrated Load)	C_b (Uniform Load)
b_f (mm)	t_f (mm)	h_w (mm)	t_w (mm)	b_f/t_f	h_w/t_w	A_f/A_w	L/h_w			
170	17	320	8	10	40	1.129	14.7	0.894	1.067	1.037
212.5	21.25	400	10	10	40	1.129	14.7	0.894	1.068	1.034
255	25.5	480	12	10	40	1.129	14.7	0.894	1.069	1.033
297.5	29.75	560	14	10	40	1.129	14.7	0.894	1.070	1.034
340	34	640	16	10	40	1.129	14.7	0.894	1.069	1.036
192	12.8	320	8	15	40	0.960	14.7	1.305	1.067	1.038
240	16	400	10	15	40	0.960	14.7	1.305	1.067	1.038
288	19.2	480	12	15	40	0.960	14.7	1.305	1.067	1.038
336	22.4	560	14	15	40	0.960	14.7	1.305	1.067	1.038
384	25.6	640	16	15	40	0.960	14.7	1.305	1.067	1.038
228	11.4	360	9	20	40	0.802	14.7	1.682	1.077	1.049
304	15.2	480	12	20	40	0.802	14.7	1.682	1.077	1.048
380	19	600	15	20	40	0.802	14.7	1.682	1.077	1.054
456	22.8	720	18	20	40	0.802	14.7	1.682	1.077	1.049
532	26.6	840	21	20	40	0.802	14.7	1.682	1.077	1.049

Table 5.3: Effect of Changing (h_w/t_w) and (b_f/t_f) on the k_e and C_b factors for Beams with $d_h/h_w = 0.7$, and $s/h_w = 1.05$

Beam Properties								k_e	C_b (Concentrated Load)	C_b (Uniform Load)
b_f (mm)	t_f (mm)	h_w (mm)	t_w (mm)	b_f/t_f	h_w/t_w	A_f/A_w	L/h_w			
170	17	320	8	10	40	1.129	21	0.626	1.193	1.073
212.5	21.25	400	10	10	40	1.129	21	0.626	1.193	1.073
255	25.5	480	12	10	40	1.129	21	0.626	1.193	1.073
297.5	29.75	560	14	10	40	1.129	21	0.626	1.193	1.073
340	34	640	16	10	40	1.129	21	0.626	1.193	1.073
250	25	480	6	10	80	2.170	21	0.633	1.273	0.894
312.5	31.25	600	7.5	10	80	2.170	21	0.633	1.272	0.899
375	37.5	720	9	10	80	2.170	21	0.633	1.271	0.899
437.5	43.75	840	10.5	10	80	2.170	21	0.633	1.271	0.898
500	50	960	12	10	80	2.170	21	0.633	1.270	0.897
192	12.8	320	8	15	40	0.960	21	0.913	1.137	1.030
240	16	400	10	15	40	0.960	21	0.913	1.137	1.030
288	19.2	480	12	15	40	0.960	21	0.913	1.137	1.030
336	22.4	560	14	15	40	0.960	21	0.913	1.137	1.030
384	25.6	640	16	15	40	0.960	21	0.913	1.137	1.030
360	24	640	8	15	80	1.688	21	0.934	1.231	1.071
450	30	800	10	15	80	1.688	21	0.934	1.231	1.071
540	36	960	12	15	80	1.688	21	0.934	1.231	1.071
630	42	1120	14	15	80	1.688	21	0.934	1.231	1.071
720	48	1280	16	15	80	1.688	21	0.934	1.231	1.071
228	11.4	360	9	20	40	0.802	21	1.178	1.197	1.036
304	15.2	480	12	20	40	0.802	21	1.178	1.197	1.036
380	19	600	15	20	40	0.802	21	1.178	1.197	1.036
456	22.8	720	18	20	40	0.802	21	1.178	1.197	1.036
532	26.6	840	21	20	40	0.802	21	1.178	1.196	1.036
400	20	640	8	20	80	1.563	21	1.234	1.127	1.010
500	25	800	10	20	80	1.563	21	1.234	1.127	1.010
600	30	960	12	20	80	1.563	21	1.234	1.127	1.010
700	35	1120	14	20	80	1.563	21	1.234	1.126	1.009
800	40	1280	16	20	80	1.563	21	1.234	1.126	1.010

Table 5.4(a): Values of the C_b Factor Related to Various Buckling Modes under Mid–Span Concentrated Load

Beam Properties		C_b Range		
d_h/h_w	h_w/t_w	LTB Mode	LDB Mode	LDB–WLB Interaction
0.5 and 0.6	20 to 60	1.33–1.15	1.15–1.00	1.00–0.95
0.5 and 0.6	70 to 80	1.33–1.20	1.20–1.05	1.05–0.95
0.7	20 to 50	1.33–1.20	1.20–0.95	0.95–0.80
0.7	60 to 80	1.33–1.25	1.25–1.05	1.05–0.75
0.8	20 to 50	1.33–1.25	1.25–0.90	0.90–0.80
0.8	60 to 80	1.33–1.30	1.30–1.15	1.15–0.70

Table 5.4(b): Values of the C_b Factor Related to Various Buckling Modes under Uniform Load

Beam Properties		C_b Range		
d_h/h_w	h_w/t_w	LTB Mode	LDB Mode	LDB–WLB Interaction
0.5 and 0.6	20 to 60	1.14–1.04	1.04–1.00	1.00–0.87
0.5 and 0.6	70 to 80	1.14–1.06	1.06–1.02	1.02–0.77
0.7	20 to 50	1.14–1.06	1.06–1.01	1.01–0.77
0.7	60 to 80	1.14–1.08	1.08–1.04	1.04–0.67
0.8	20 to 50	1.14–1.08	1.08–1.02	1.02–0.72
0.8	60 to 80	1.14–1.10	1.10–1.06	1.06–0.60

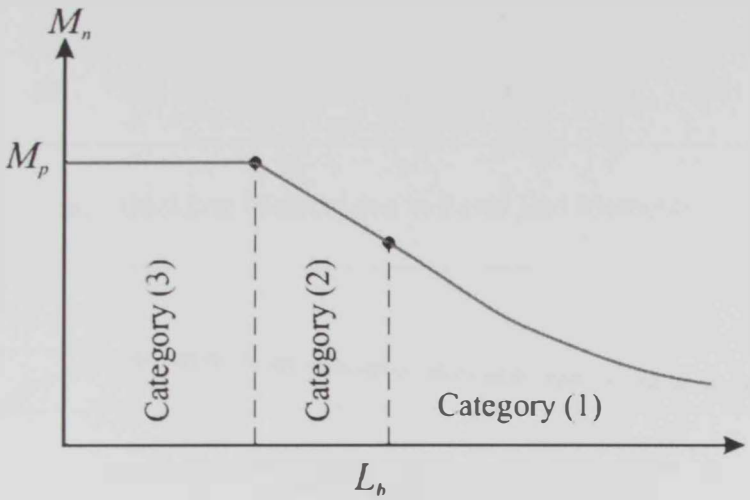

Figure 5.1: Beam Flexural Categories Including Elastic and Inelastic Buckling

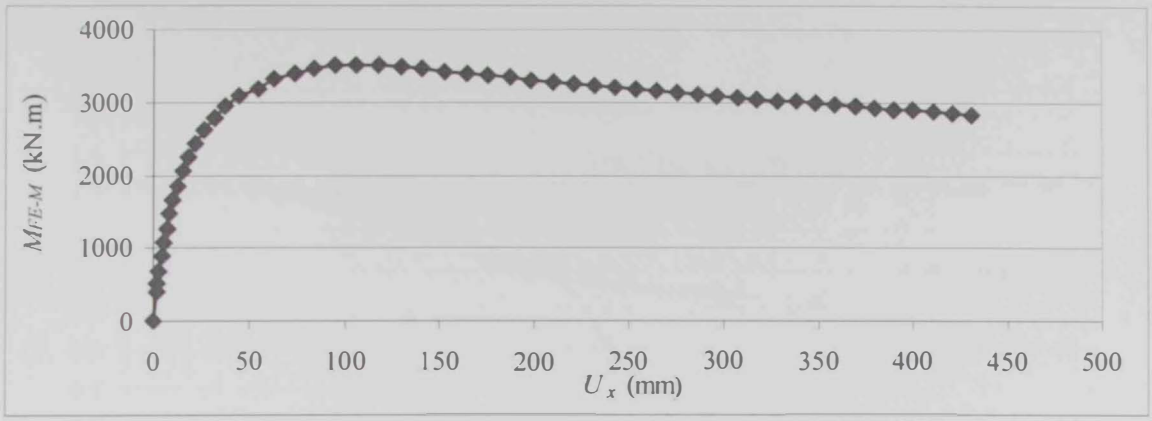

(a): Buckling Moment due to Equal End Moments

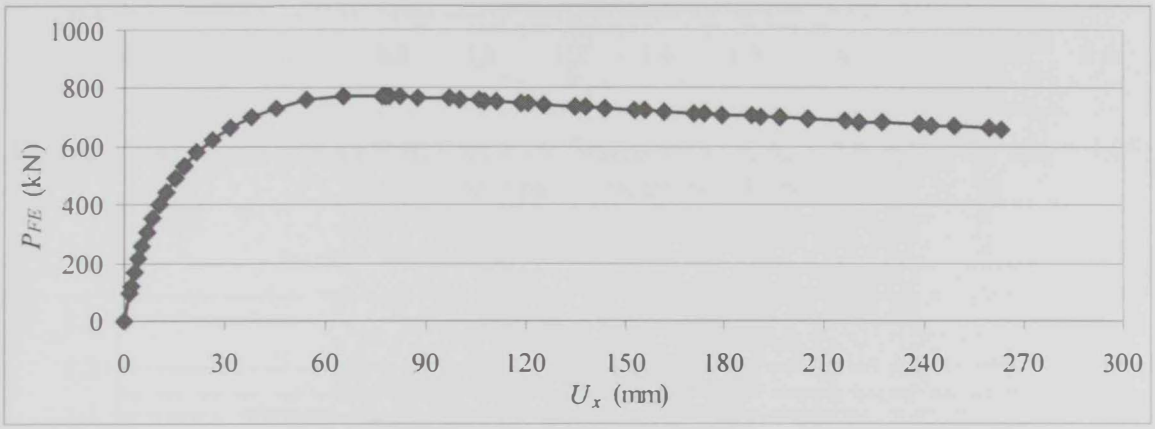

(b): Buckling Load due to Mid–Span Concentrated Load

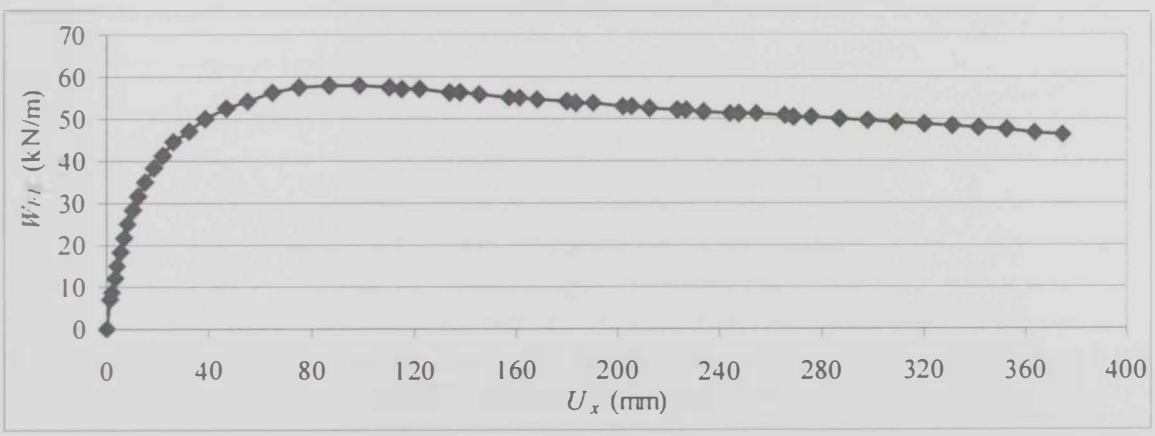

(c): Buckling Load due to Uniformly Distributed Load

Figure 5.2: Nonlinear Moment/Load–Lateral Deformation Curves at Mid–Span of a Cellular Beam with (d_h/h_w = 0.6, h_w/t_w = 70, b_f/t_f = 15, s/h_w = 1.05, and L/h_w = 25.2)

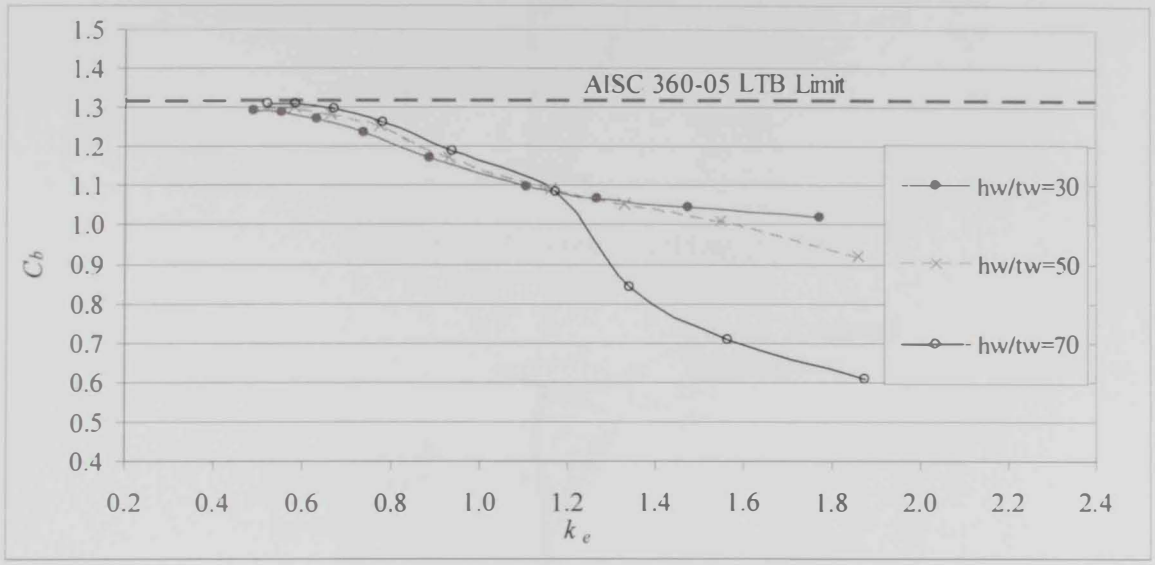

Figure 5.3(a): Moment Gradient Factor for Beams with (d_h/h_w = 0.6, b_f/t_f = 15, s/h_w = 1.05) under Mid–Span Concentrated Load

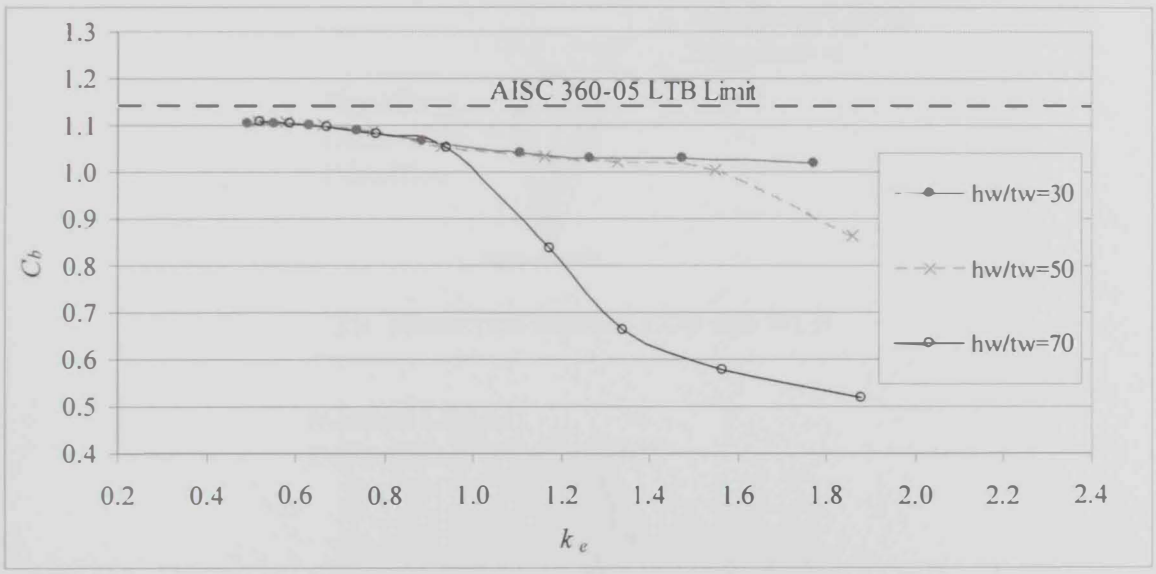

Figure 5.3(b): Moment Gradient Factor for Beams with (d_h/h_w = 0.6, b_f/t_f = 15, s/h_w = 1.05) under Uniformly Distributed Load

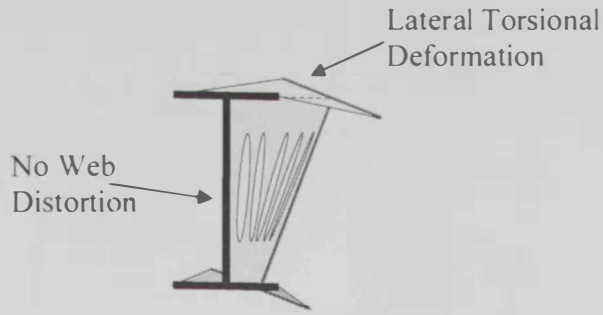

(a): Lateral Torsional Buckling (LTB)

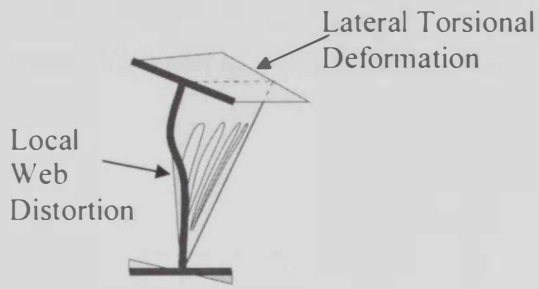

(b): Lateral Distortional Buckling (LDB)

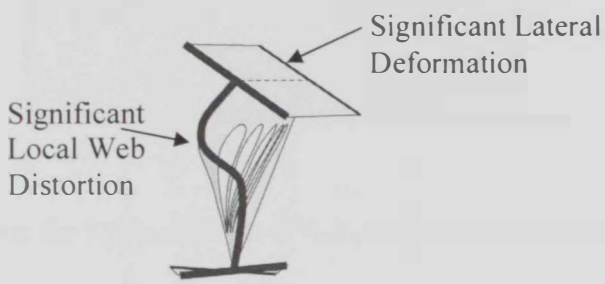

(c): Interaction between LDB and WLB

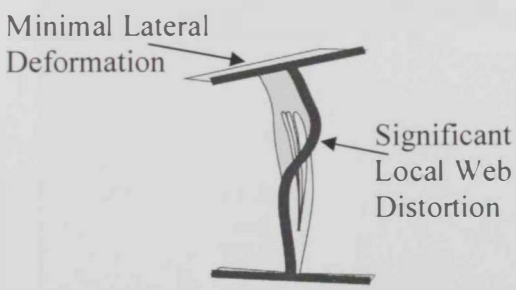

(d): Web Local Buckling (WLB)

Figure 5.4: View at Support Showing Different Inelastic Buckling Modes of Cellular Beams

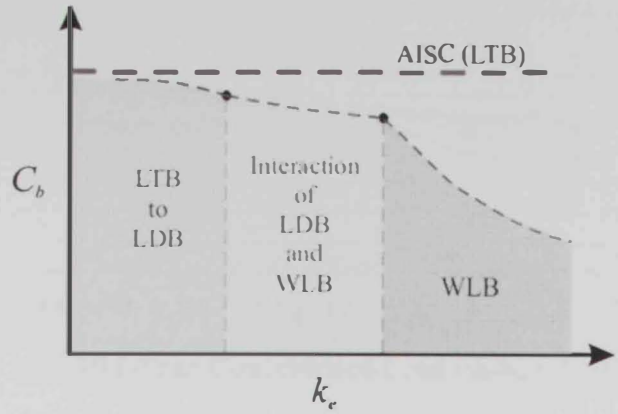

Figure 5.5: Schematic for Typical Variation of C_b with Various Buckling Modes of Beams

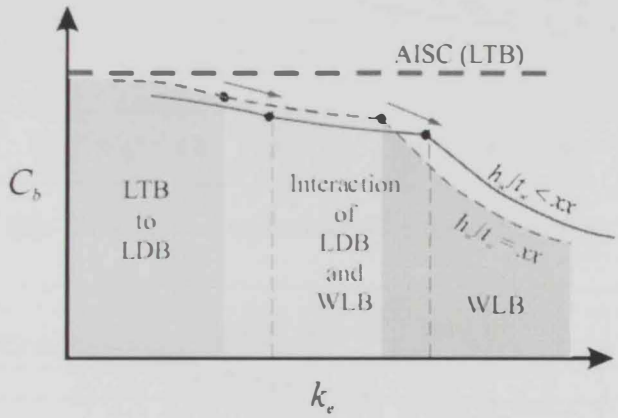

Figure 5.6: Schematic for Typical Effect of h_w/t_w on the Moment Gradient Factor C_b

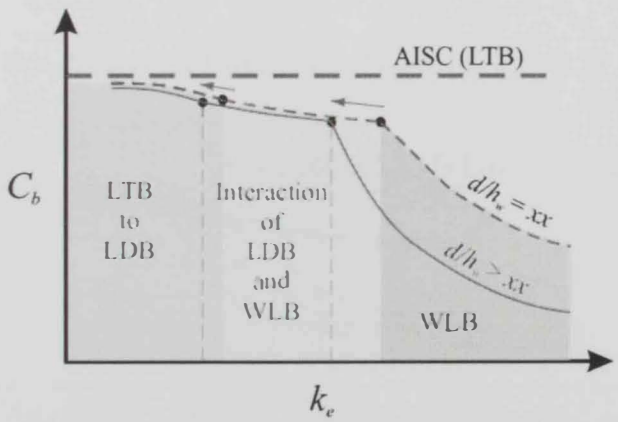

Figure 5.7: Schematic for Typical Effect of d_h/h_w on the Moment Gradient Factor C_b

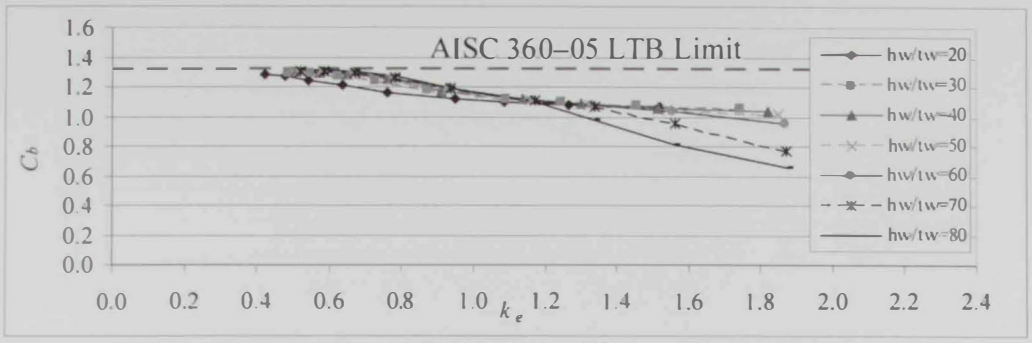

(a): Mid–Span Concentrated Load (d_h/h_w = 0.5)

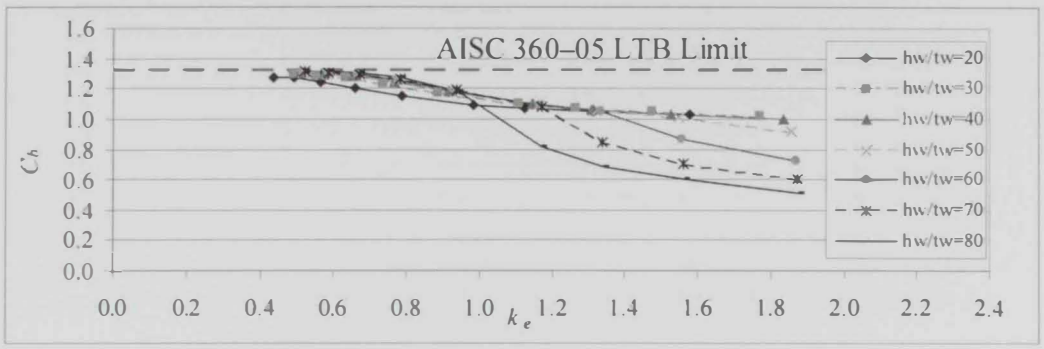

(b): Mid–Span Concentrated Load (d_h/h_w = 0.6)

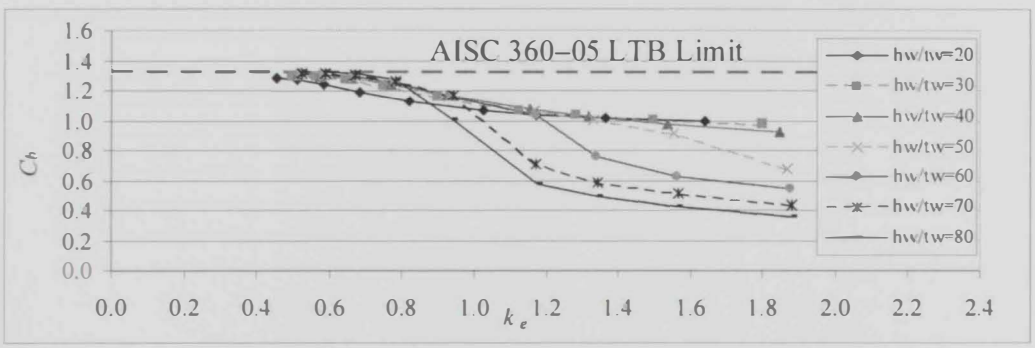

(c): Mid–Span Concentrated Load (d_h/h_w = 0.7)

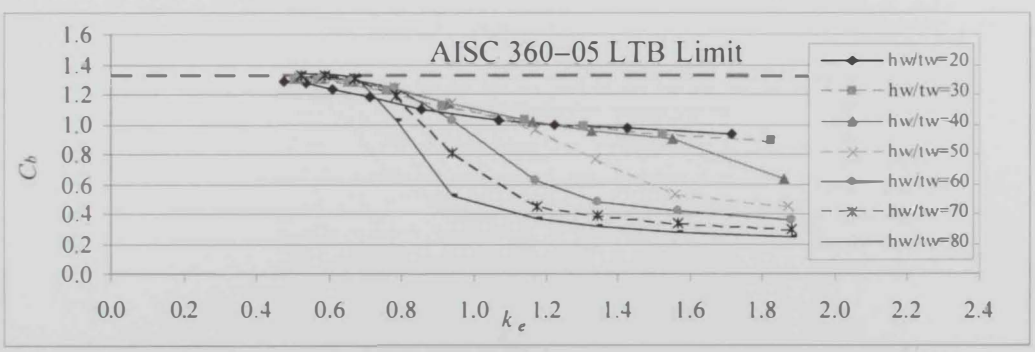

(d): Mid–Span Concentrated Load (d_h/h_w = 0.8)

Figure 5.8: Moment Gradient Factor for Beams with (b_f/t_f = 15 and s/h_w = 1.05)

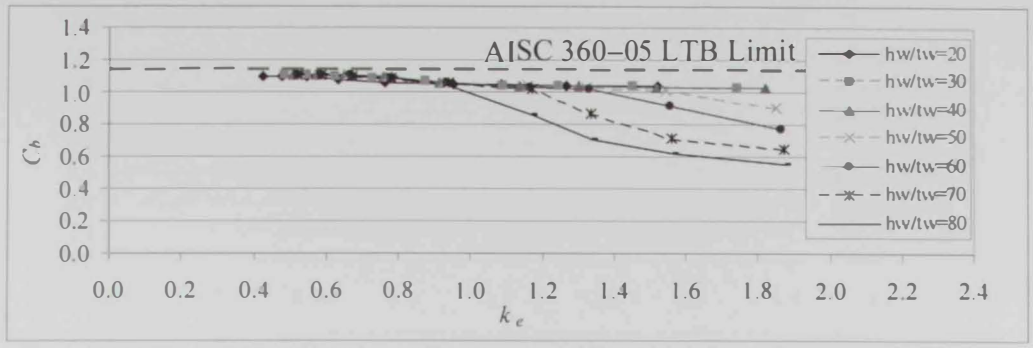

(a): Uniformly Distributed Load (d_h/h_w = 0.5)

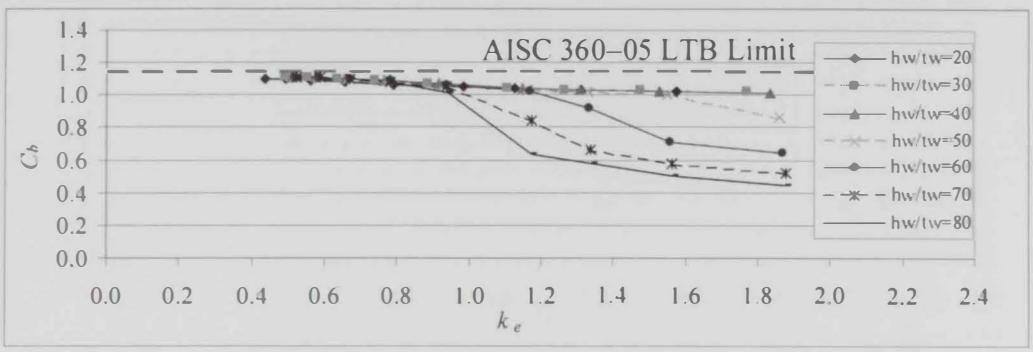

(b): Uniformly Distributed Load (d_h/h_w = 0.6)

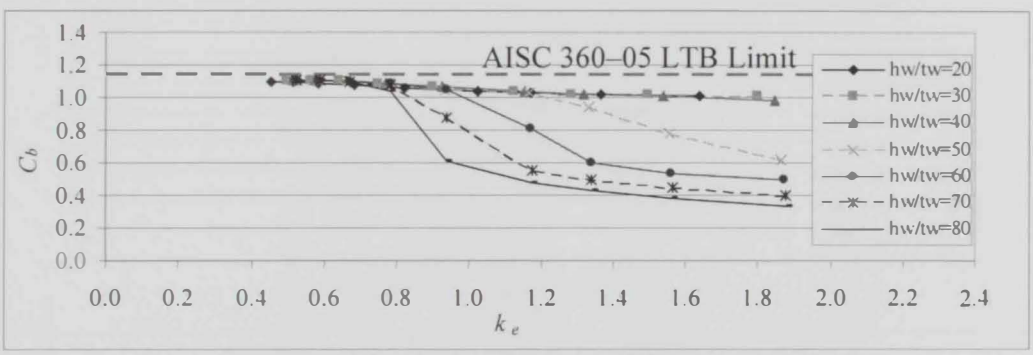

(c): Uniformly Distributed Load (d_h/h_w = 0.7)

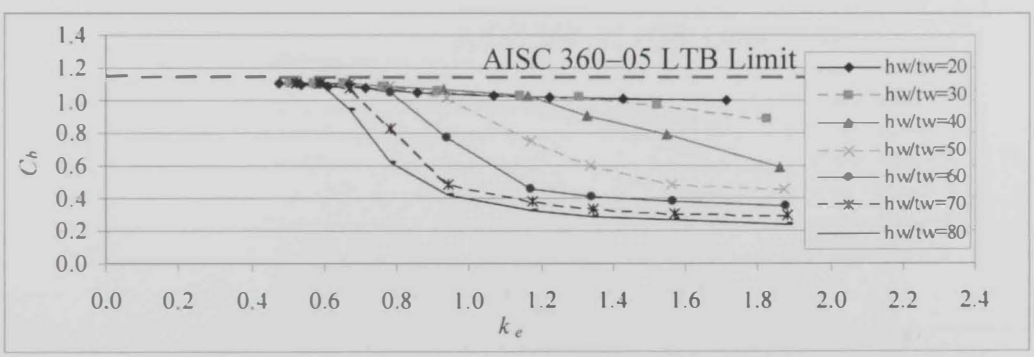

(d): Uniformly Distributed Load (d_h/h_w = 0.8)

Figure 5.9: Moment Gradient Factor for Beams with (b_f/t_f = 15 and s/h_w = 1.05)

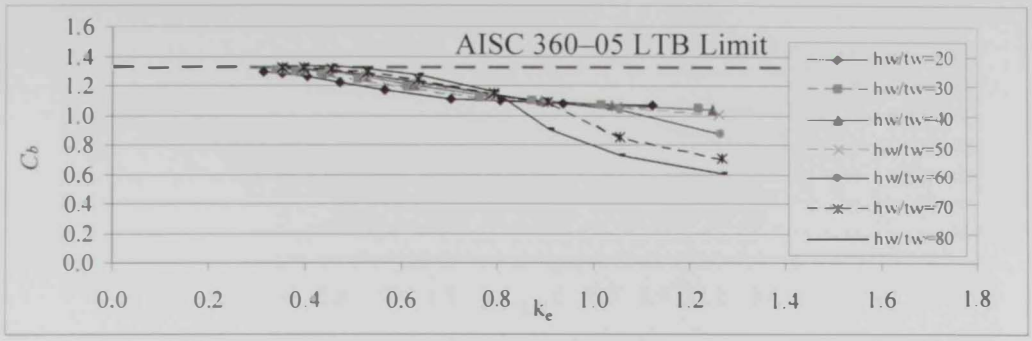

(a): Mid–Span Concentrated Load (d_h/h_w = 0.5)

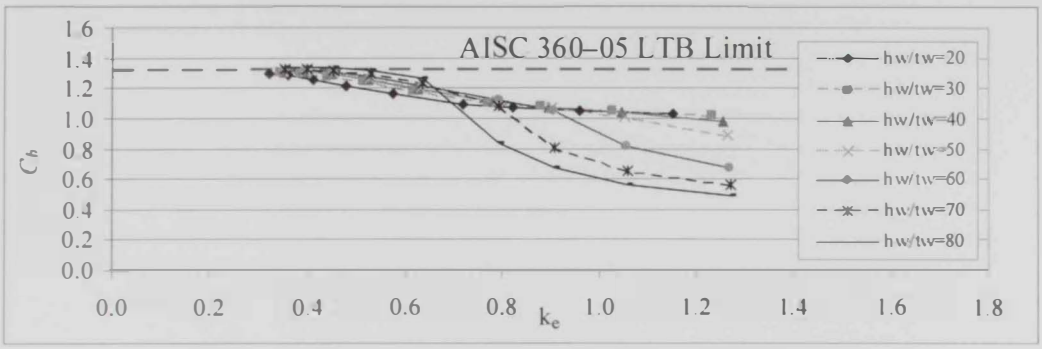

(b): Mid–Span Concentrated Load (d_h/h_w = 0.6)

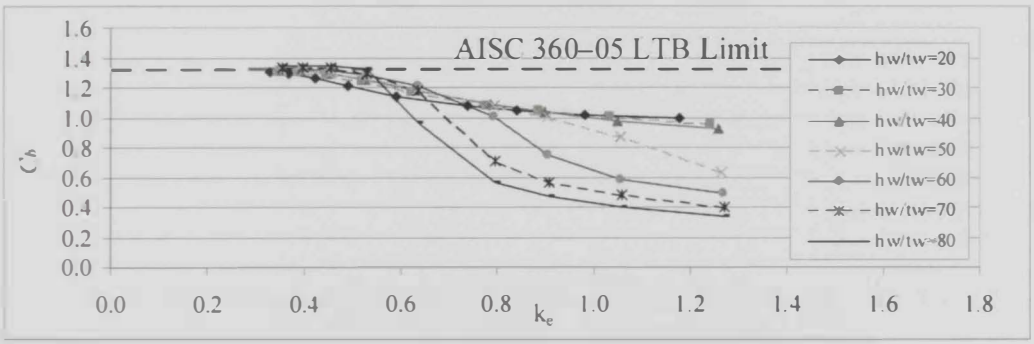

(c): Mid–Span Concentrated Load (d_h/h_w = 0.7)

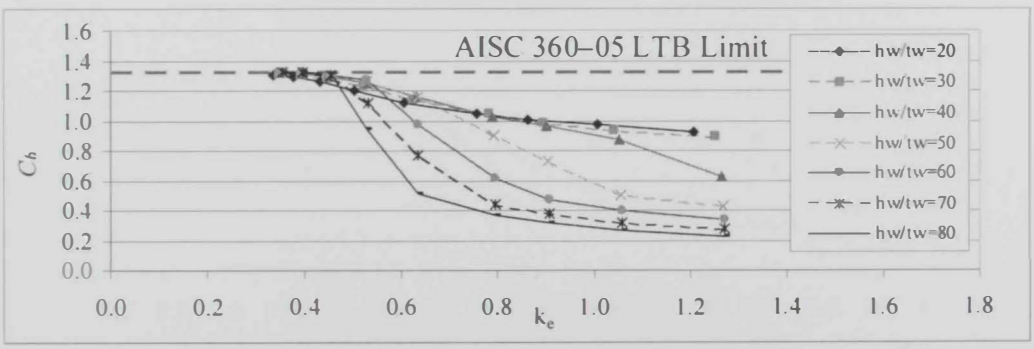

(d): Mid–Span Concentrated Load (d_h/h_w = 0.8)

Figure 5.10: Moment Gradient Factor for Beams with (b_f/t_f = 10 and s/h_w = 1.05)

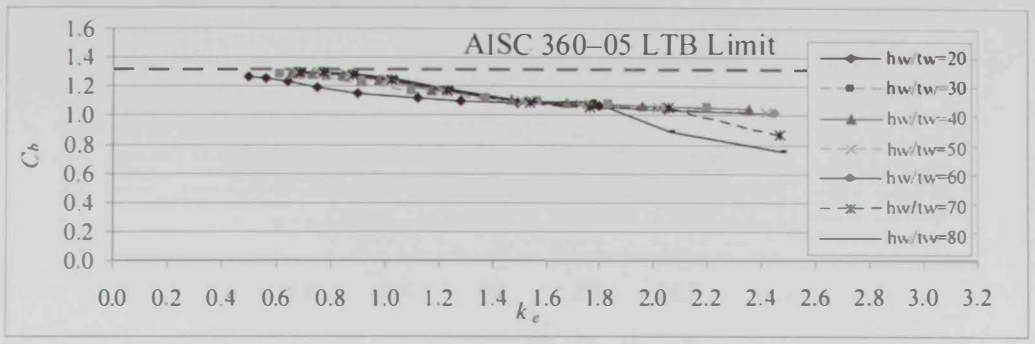

(a): Mid–Span Concentrated Load (d_h/h_w = 0.5)

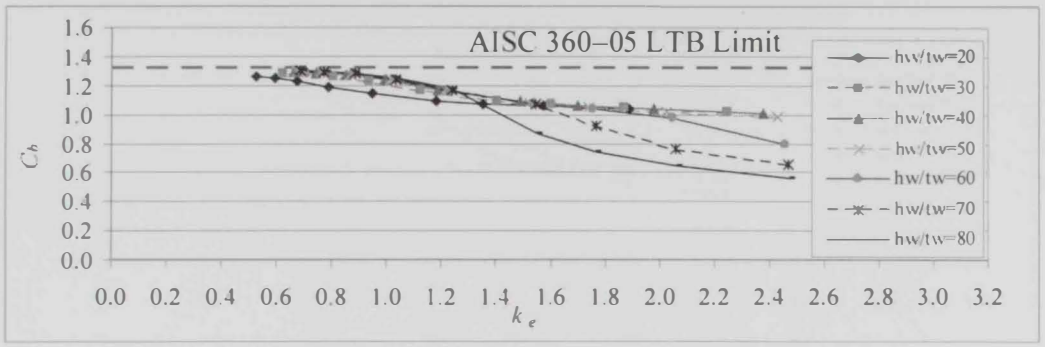

(b): Mid–Span Concentrated Load (d_h/h_w = 0.6)

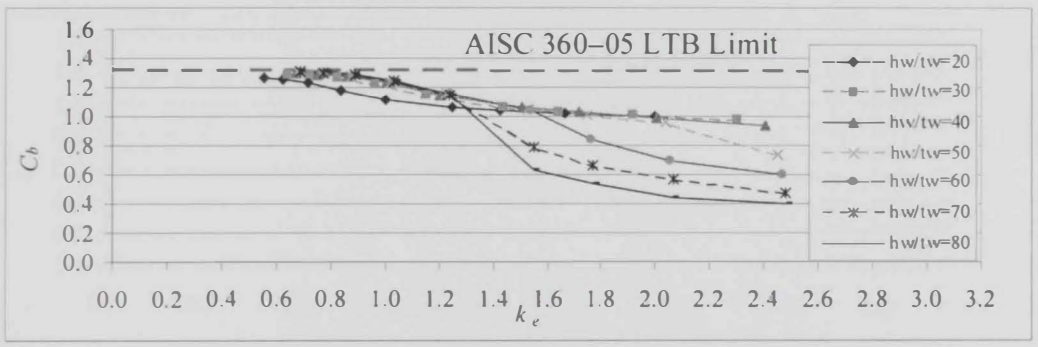

(c): Mid–Span Concentrated Load (d_h/h_w = 0.7)

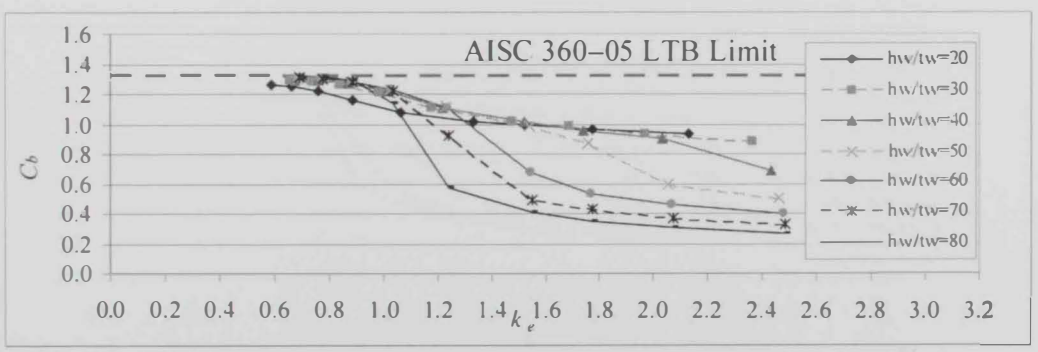

(d): Mid–Span Concentrated Load (d_h/h_w = 0.8)

Figure 5.11: Moment Gradient Factor for Beams with (b_f/t_f = 20 and s/h_w = 1.05)

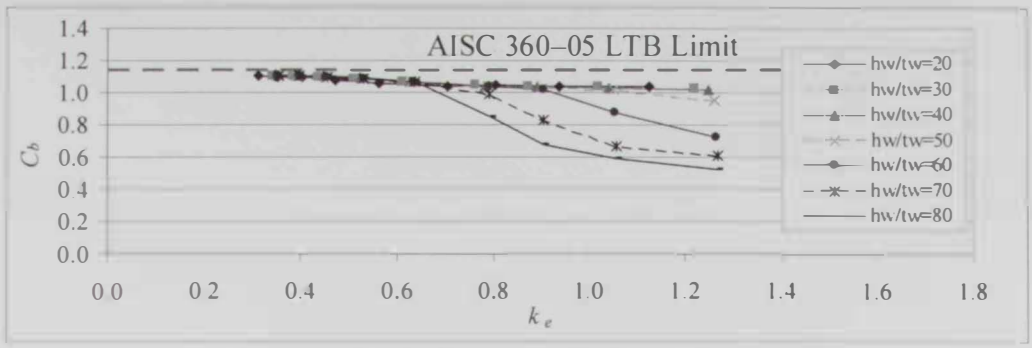

(a): Uniformly Distributed Load (d_h/h_w = 0.5)

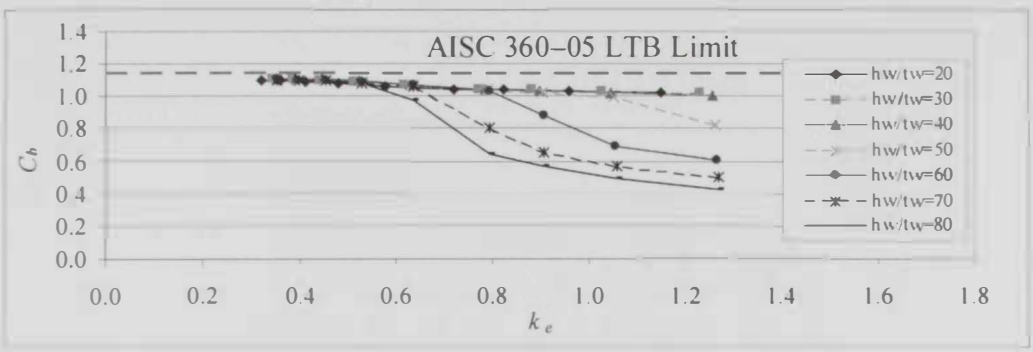

(b): Uniformly Distributed Load (d_h/h_w = 0.6)

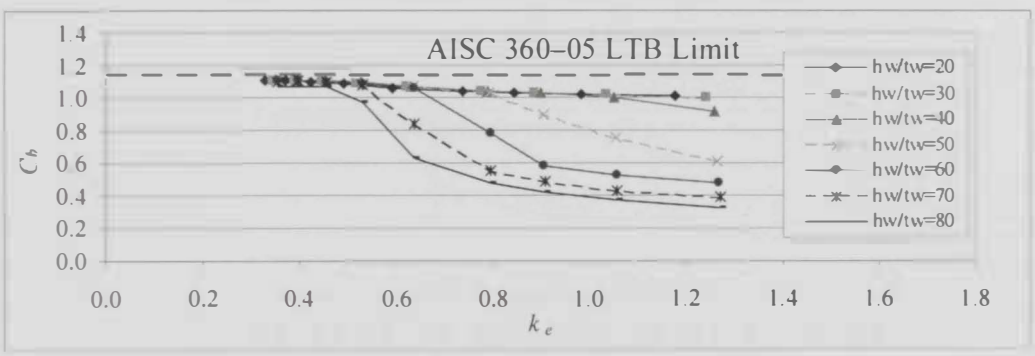

(c): Uniformly Distributed Load (d_h/h_w = 0.7)

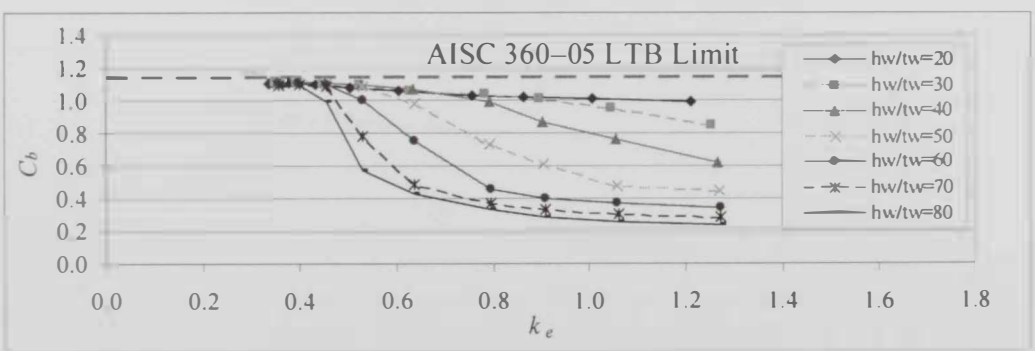

(d): Uniformly Distributed Load (d_h/h_w = 0.8)

Figure 5.12: Moment Gradient Factor for Beams with (b_f/t_f = 10 and s/h_w = 1.05)

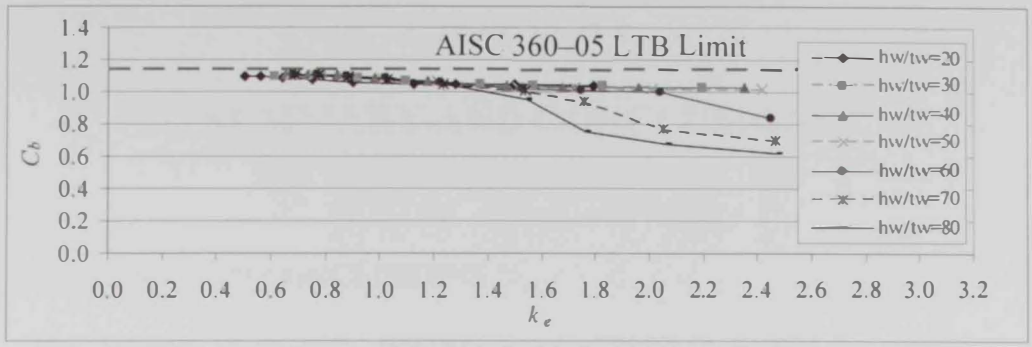

(a): Uniformly Distributed Load (d_h/h_w = 0.5)

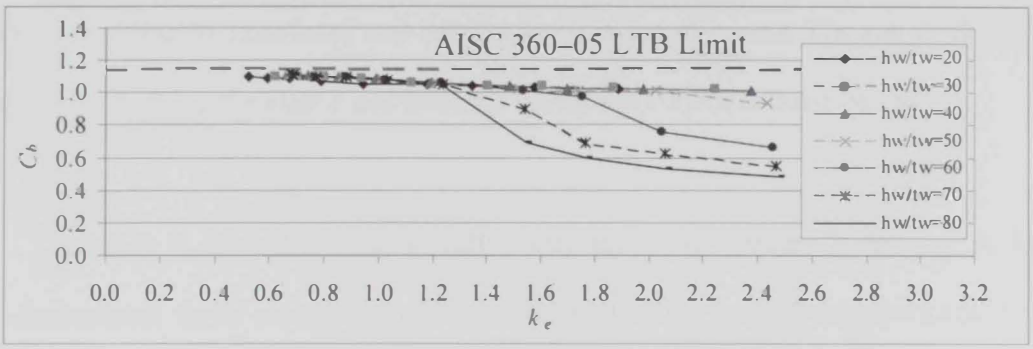

(b): Uniformly Distributed Load (d_h/h_w = 0.6)

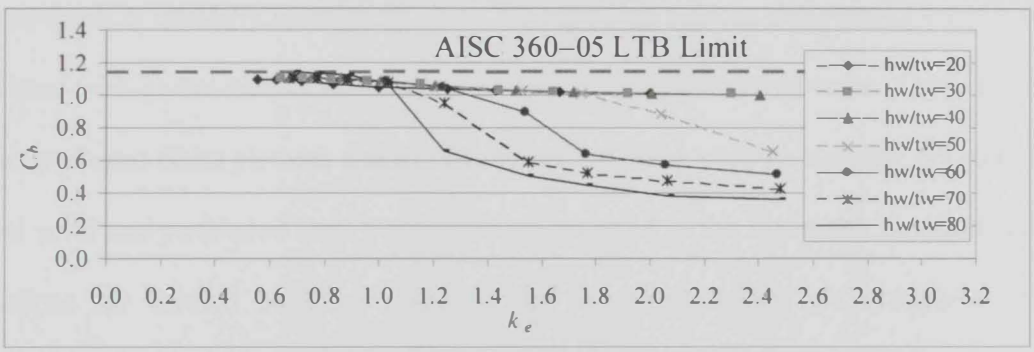

(c): Uniformly Distributed Load (d_h/h_w = 0.7)

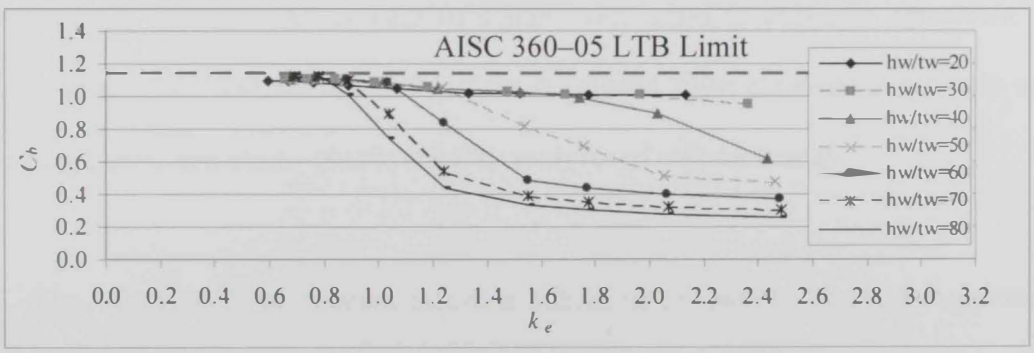

(d): Uniformly Distributed Load (d_h/h_w = 0.8)

Figure 5.13: Moment Gradient Factor for Beams with (b_f/t_f = 20 and s/h_w = 1.05)

CHAPTER 6

SUMMARY AND CONCLUSIONS

6.1 SUMMARY AND CONCLUSIONS

This research starts with presentation of a literature survey for experimental and numerical studies related to structural behavior of perforated steel beams with emphasis on the lateral buckling of castellated and cellular I–shaped steel beams. The rest of the research is devoted to studying the elastic and inelastic lateral stability of cellular beams.

The study is carried out numerically using the finite element technique. A detailed three dimensional finite element model is developed using the software package ANSYS. The developed model takes into consideration material and geometrical non–linearities. The adopted mesh is carefully selected to allow for capturing various deformations and rotations associated with global and local buckling modes of such perforated beams. The performance of the developed finite element model is validated by being used to simulate the response of several solid and perforated steel beams that are reported in the literature. The finite element predictions for critical buckling loads of the simulated beams are compared to their theoretical counterparts and to experimental findings and numerical outcomes that are reported in the literature. All comparisons show very good to excellent agreement which confirm the accuracy and the reliability of the developed finite element model to be used in performing elastic and elasto–plastic stability analyses of cellular beams.

The validated finite element model is subsequently used to conduct comprehensive buckling analyses of simply supported cellular steel beams under various loading conditions. Each beam is analyzed under three different cases of loadings including uniform moment due

to equal end moments, mid–span concentrated load, and uniformly distributed load. The study considers a wide spectrum of parameters that covers the potential range of practical geometric dimensions and perforation patterns of I–shaped cellular beams. Analyzed beams are designated through a set of dimensionless parameters to describe the various geometrical aspects. The considered web height–to–thickness ratio (h_w/t_w) varies from 20 to 80 with an increment of 10 while the flange width–to–thickness ratio (b_f/t_f) is considered to vary from 10 to 20 with an increment of 5. Circular web openings are expressed through a hole diameter–to–web height ratio (d_h/h_w) that varies between 0.5 and 0.8 with an increment of 0.1. In the elastic study, the holes are uniformly spaced with spacing to web height ratio s/h_w of 1.05 to 2.1 which corresponds to spacing to diameter ratio s/d_h that extends from 1.3 to 4.2. Moreover, a wide spectrum of beam span values is taken into consideration in the elastic study as expressed by span to web height ratio L/h_w which varies as: (1) from 10.50 to 37.8 for the case of s/h_w equals 1.05, (2) from 15.75 to 56.70 for s/h_w of 1.575, and (3) from 21.0 to 75.60 for s/h_w of 2.10. However, the inelastic study considers a representative s/h_w value of 1.05 that corresponds to closely spaced web holes.

A total of 11,340 cases of linear elastic analyses are performed to investigate the influence of load application location on the elastic lateral torsional buckling of I–shaped cellular beams under various loading conditions. The validated finite element model is used to identify the critical buckling load and the associated buckling modes of analyzed beams. A comprehensive parametric analysis is conducted to evaluate the impact of various cross section dimensions, beam slenderness, and web openings size and spacing on the flexural capacity and associated buckling modes of cellular steel beams. Results of conducted analyses are utilized to evaluate the variation of the moment gradient factor C_b relative to a non–dimensional factor k_e that relates the warping rigidity to the torsional rigidity of cellular

beams. Results are analyzed and discussed for loads applied at the top and bottom flange levels. Discussions include comparison of the results to those reported in the literature for loading at the shear center of beams.

The inelastic lateral buckling of cellular beams is investigated numerically by considering a wide range of cellular beams dimensions through 2,268 cases of analyses. A comprehensive parametric study is conducted to evaluate the impact of various cross section dimensions, beam slenderness, and web openings size on the inelastic buckling capacity and associated modes of cellular steel beams. Similar to the case of elastic buckling analyses, outcomes of the inelastic investigation are discussed by presenting the variation of the moment gradient factor C_b with respect to the non–dimensional factor k_e that relates the warping rigidity to the torsional rigidity of analyzed beams.

The major findings from this study could be categorized based on the outcomes of the elastic and inelastic analyses as presented herein.

6.1.1 Findings of the Elastic LTB Study

- Cellular beams subjected to mid–span concentrated loads provide higher moment–carrying capacity than those supporting uniformly distributed loads. This behavior is similar to that of conventional beams with solid webs.
- Loads applied at the top flange level of cellular beams result in destabilizing effect on the elastic response of cellular beams. This effect results from the additional torque exerted by applied loads which produces additional twisting of the beam leading to earlier instability failure of the beam.

- Loads applied at the bottom flange level enhance the elastic lateral stability of cellular beams. This is attributed to the load–related torque that counteracts the original lateral deformation of the beam. Consequently, buckling of these beams occurs at higher load value than its counterpart for beams loaded above the shear center.
- Long span cellular beams are shown to buckle elastically with pure lateral torsional buckling mode (LTB). Meanwhile, buckling of intermediate span beams is controlled by lateral distortional buckling mode (LDB) where web distortion occurs simultaneously with lateral deformations. Buckling of short span beams is dominated by the high level of web distortion associated with the high shear stresses induced in the web and significant reduction in C_b value.
- Non–lateral elastic buckling failure of cellular beams loaded at the top flange level is associated with C_b values that are less than 0.8 and 0.7 for mid–span concentrated loading and uniformly distributed loading, respectively. Meanwhile, C_b values of 1.6 and 1.3 provide upper limits for non–lateral elastic buckling failure of cellular beams loaded at their bottom flange level.
- Cellular beams with slender web plates (i.e.; high h_w/t_w values) and cellular beams with closely–spaced big holes (i.e.; low s/h_w and high d_h/h_w values) are more sensitive to shear deformations and, therefore, are mostly governed by local web buckling. Such beams are less likely to experience lateral buckling modes (LTB or LDB) unless having significantly long spans.
- Cellular beams with relatively small b_f/t_f experience more reduction in the moment gradient factor C_b than those with higher b_f/t_f values. Higher values of b_f/t_f provide more effective torsional restrains of the perforated webs which, consequently, minimizes the encountered reduction in the C_b factor.

6.1.2 Findings of the Inelastic LTB Study

- Similar to the observed elastic buckling response, long span cellular beams are shown to experience inelastic lateral buckling due to lateral torsional buckling (LTB) or lateral distortional buckling (LDB). Cellular beams with intermediate span length experience interaction between lateral deformations and local web shear buckling at failure. Meanwhile, buckling of short span cellular beams is governed by high level of web distortion that results from the high shear stresses induced in the web. In such a case, no lateral buckling is noticed and significant reduction in C_b values occurs.
- Inelastic buckling results indicate that intermediate spans cellular beams with slender web plates (i.e.; high h_w/t_w values) and/or big web holes (i.e.; high d_h/h_w values) are prone to combined lateral–local buckling modes that are associated with low C_b factors. Moreover, cellular beams with short spans and slender web plates (high h_w/t_w values) and/or big web holes (high d_h/h_w values) are sensitive to shear deformations. Instability of these beams is governed by non–lateral buckling modes that are localized in the web posts and are associated with significantly low C_b values.
- For cellular beams subjected to mid–span concentrated loads, the inelastic buckling due to the combined lateral buckling–local web deformations is characterized by a C_b range of about 1.05 to 0.95 for hole sizes of d_h/h_w = 0.5 and 0.6 and a range of 1.0 to 0.9 for hole sizes of d_h/h_w = 0.7 and 0.8. Buckling of these beams is dominated by non–lateral local web buckling mode and is characterized by C_b factors that are less than the above mentioned lower bounds.
- Inelastic failure of cellular beams subjected to uniformly distributed loads that is dominated by interaction between lateral buckling and local web deformations is characterized by a C_b range of about 1.02 to 0.85 for hole sizes of d_h/h_w = 0.5 and 0.6

and a range of 1.0 to 0.8 for hole sizes of d_h/h_w = 0.7 and 0.8. Lower C_b values are associated with failures that are dominated by non–lateral local web buckling mode.

- Similar to the case of elastic stability of cellular beams with relatively small flange plates, these beams experience a greater reduction in the moment gradient factor C_b than those with bigger flange plates. This is attributed to the more effective torsional restrains for the perforated webs that is provided by bigger flange plates. As such, less reduction in the C_b factor is observed.

6.2 RECOMMENDATIONS FOR FUTURE RESEARCH

The recent increase in usage of cellular beams highlights the need for additional research. The literature review presented in this thesis indicates that scarcity of research work on the design and behavior of cellular steel beams. The need to continue investigations for these beams is imperative for understanding their behavior and improving their design. More experimental and numerical researches are needed to investigate the following areas:

1. Experimental investigation of the elasto–plastic lateral buckling of cellular beams.
2. Numerical and/or experimental evaluation of the critical buckling load of cellular beams with various boundary conditions subjected to various cases of loading that are different from the particular ones considered in the current study.
3. Numerical and/or experimental investigation of the elasto–plastic local buckling of web plates in cellular beams.
4. Numerical investigation of the effect of varying web hole spacing and/or vertical alignment on the elasto–plastic lateral buckling of cellular beams.
5. Numerical and/or experimental evaluation of the influence of load application level on the elasto–plastic lateral buckling of cellular steel beams.

REFERENCES

[1] Aglan. A. A., Redwood, R.G. (1974). "Web Buckling in Castellated Beams.", Proceedings of the Institution of Civil Engineers, ICE, London, U.K., Part 2, Vol. 57, 307-320.

[2] Aloi, N. (2002), "Experimental Tests of Singly and Doubly Symmetric Non-Composite Castellated Beams." Villanova University, PA, USA.

[3] Altfillisch, M. D., Cooke, B. R., Toprac, A. A. (1957). "An Investigation of welded open-web expanded beams." Journal of the American Welding Society, Welding Research Supplementary, February, 77-88.

[4] American Institute of Steel Construction (AISC). "*ANSI/AISC 360-05 Specification for Structural Buildings", 13th edition*", Chicago, USA, 2005.

[5] ANSYS User's Manual Release 12.0.1 (2009), Canonsburg, Pennsylvania, USA.

[6] Barbarito, F. J. (1963). "Photoelastic Analysis of Circularly Perforated Beaming in Pure Bending." Polytechnic Institute of Brooklyn, NY.

[7] Bazile, A., Texier, J. (1968). "Essais de Pouters Ajourees." Constr. Metallique, Paris, France, 5 (3), 12-25.

[8] Boyer, J. P. (1964). "Castellated Beams - New Developments." *AISC Engineering Journal*, Second Quarter, 104-108.

[9] British Standards Institution (BSI). "*BS5950-1 Structural Use of Steelwork in Buildings-Part 1, Code of Practice for Design Rolled and Welded Sections*", England, 2000.

[10] Chen, W. F., Lui, E. M. Structural Stability, Theory and Implementation, P T R Prentice Hall, Upper Saddle River, New Jersey, 1987.

[11] Crisfield, M. A., (1981). "A Fast Incremental-Iterative Solution Procedure That

Handles Snap-Through.", *Computers and Structures*, Vol 13, pp. 55–62.

[12] Chung, K.F., Liu, T.C.H., Ko, A.C.H. (2000). "Investigation on Vierendeel Mechanism in Steel Beams with Circular Web Openings." *Journal of Constructional Steel Research*; (57): 467–490.

[13] Chung, K.F., Liu, T.C.H., Ko, A.C.H. (2003). "Steel Beams with Large Web Openings of Various Shapes and Sizes: an Empirical Design Method using a Generalised Moment-Shear Interaction Curve." *Journal of Constructional Steel Research*; (59): 1177–1200.

[14] Darwin, D. (1990), "Steel and Composite Beams with Web Openings", Steel Design Guide Series No. 2, American Institute of Steel Construction, Chicago.

[15] Dougherty, B. K. (1993). "Castellated Beams: A state of the art report", Technical Report, Journal of South African Institution of Civil Engineers, Vol. 35, No 2, 12-20.

[16] European Committee for Standardization, EN 1993-1-1 Eurocode 3 (EC3). "*Design of Steel Structures – Part 1-1: General Rules and Rules for Buildings*", 2005.

[17] Galambos TV. Structural Members and Frames, Englewood Cliffs, NJ: Prentice-Hall, 1968.

[18] Gerald, C. F., Gren, C. J., and Wheatley, P. O. Applied Numerical Analysis, 7th Ed., Addison Wesley Longman, California, USA, 2003.

[19] Hagen, N. Chr. (2004). "On the Shear Capacity of Steel Plate Girders with Large Web Openings" Ph.D. thesis, Norwegian University of Science and Technology. Trondheim.

[20] Halleux, P. (1967). "Limit Analysis of Castellated Beams." Acier-Stahl-Steel, No. 3, 133-144.

[21] Hennessey, J., Dinehart, D., Hoffman, R., Gross, S., Yost, J. (2004), "Effect of Cope Geometry on the Strength and Failure Behavior of Non-Composite Open Web

Expanded Beams" Research Report 7 to SMI Steel Products, Villanova University, PA., USA.

[22] Hosain, M.U., Speirs, W.G. (1973). "Experiments on Castellated Steel Beams" Journal of the American Welding Society, Vol. 52, pp 329-342.

[23] Kerdal, D., Nethercot, D. A. (1984). "Failure Modes for Castellated Beams." *Journal of Constructional Steel Research*; 4(4): 295–315.

[24] Knowles, P.R. (1991). "Castellated Beams", Proceeding of the Institution of Civil Engineers, ICE, London, U.K., Part 1, No. 90, pp 521-536.

[25] Kohnehpooshi, O. and Showkati, H. (2009). "Numerical Modeling and Structural Behavior of Elastic Castellated Section." European Journal of Scientific Research; 31(2): 306–318.

[26] Lawson, R. M. (1987), "Design for Openings in the Webs of Composite Beams", CIRIA Special Publication and SCI Publication 068, CIRIA/Steel Construction Institute.

[27] Liu, T.C.H., Chung, K.F. (2003). "Steel Beams with Large Web Openings of Various Shapes and Sizes: Finite Element Investigation." *Journal of Constructional Steel Research*; (59): 1159–1176.

[28] Mathews, J. H., and Kurtis, F. D. Numerical Methods using Matlab, 4th Ed., Pearson Prentice Hall Publishers, Upper Saddle River, New Jersey, USA, 2004.

[29] Mohebkhah, A. (2004). "The Moment-Gradient Factor in lateral-Torsional Buckling on Inelastic Castellated Beams." *Journal of Constructional Steel Research*; (60): 1481–1494.

[30] Nethercot, D.A., Kerdal, D. (1982). "Lateral-Torsional Buckling of Castellated Beams." *Journal of the Institution of Structural Engineers, Part A: Design and Construction*; 60B (3): 53–61.

[31] Nethercot, D. A., Trahair, N. S. (1976). "Inelastic Lateral Buckling of Determinate Beams." Journal of the Structural Division, ASCE, 102 (ST4), 701-717.

[32] Okubo, T., Nethercot, D. A. (1985). "Web Post Strength in Castellated Steel Beams", Proceedings of the Institution of Civil Engineers, ICE, London, U.K., Part 2, 79, 533-557.

[33] Redwood, R. G., Cho, S. H. (1993), "Design of Steel and Composite Beams with Web Openings." Journal of Constructional Steel Research, Vol.25, pp 23-41.

[34] Redwood, R, Demirdjian, S. (1998). "Castellated Beam Web Buckling in Shear." Journal of Structural Engineering, 10: 1202-1207.

[35] Redwood, R., Zaarour, W. (1996). "Web Buckling in Thin Webbed Castellated Beams." Journal of Structural Engineering, 08: 860-866.

[36] Reiter, M. (2002), "Experimental Testing of Non-Composite Cellular Beams." Villanova University, PA., USA.

[37] Reither, J., Dinehart, D., Hoffman, R., Gross, S., Yost, J. (2005), "Effect of Single Angle End Connection on the Strength and Failure Behavior of Castellated and Cellular Beams with End Copes" Research Report No. 13 to SMI Steel Products, Villanova University, PA., USA.

[38] Ritto-Correa, M., and Camotim, D. (2008). "On the Arc-Length and other Quadratic Control Methods: Established, Less Known and New Implementation Procedures." *Computers and Structures,* Vol 86, pp. 1353–1368.

[39] Salmon, C. G., Johnson, J. E., and Malhas, F. A. Steel Structures: Design and Behavior, Emphasizing Load and Resistance Factor Design, 5th Ed., Pearson Prentice Hall Publishers, Upper Saddle River, New Jersey, 2009.

[40] Shanmugam, N. E., Lian, V. T., and Thevendran, V. (2002). "Finite Element Modeling of Plate Girders with Web Openings", Thin-Walled Structures, 40(5): 443–

464.

[41] Sherbourne, A. N. (1966). "The Plastic Behaviour of Castellated Beams." Proceedings of the 2nd Commonwealth Welding Conference, Institute of Welding, London, No. C2, 1-5.

[42] Standards Australia (SA). *"AS 4100 Steel Structures"*, Sydney, Australia, 1998.

[43] Surtees, J. O., Liu, Z. (1995), Report of Loading Tests on Cellform Beams, Research Report, University of Leeds, UK.

[44] Sweedan, A.M.I. (2011). "Elastic Lateral Stability of I-Shaped Cellular Steel Beams." *Journal of Constructional Steel Research*; 67 (2): 151–163.

[45] Timoshenko, S. P., and Gere, J. M. Theory of Elastic Stability, 2nd Ed., McGraw-Hill Book Company, New York, N.Y., 1961.

[46] Toprac, A. A., Cooke, B. R. (1959). "An Experimental Investigation of Open-Web Beams." Welding Research Council Bulletin Series, 47.

[47] Trahair, N. S., Kitipornchai, S. (1972). "Buckling of Inelastic I-Beams under Uniform Moment." Journal of the Structural Division, ASCE, 98 (ST11), 2551-2566.

[48] Ward, J. K. Design of Composite and Non-Composite Cellular Beams, Steel Construction Institute, Ascot, Berks, England, 1990.

[49] Watson, J., R. O'neil, R. Barnoff, and E. Mead (1974). "Composite Action without Shear Connectors." *AISC Engineering Journal*. Second Quarter, 29-33.

[50] Zirakian, T. (2008). "Lateral-Distorsional Buckling of I-Beams and the Extrapolation Techniques." *Journal of Constructional Steel Research*; (64): 1–11.

[51] Zirakian, T., Showkati, H. (2006). "Distorsional Buckling of Castellated Beams." *Journal of Constructional Steel Research*; (62): 863–871.

العددية. ويأخذ هذا التصنيف في الاعتبار التداخل المحتمل بين أشكال الانبعاج الكلي والتشوهات الموضعية لعناصر المقطع العرضي.

الكلمات الرئيسية: عوارض إنشائية دائرية الثقوب، عوارض إنشائية سداسية الثقوب، وترة مثقبة، انبعاج التوائي جانبي، انبعاج تشوهي جانبي، انبعاج مرن، انبعاج لدن، سعة العزم للمحور الرئيسي، عامل معدل تدرج العزم، طريقة العنصر المحدد، أشكال الانبعاج، مكان التحميل.

يكون انبعاج العوارض الإنشائية متوسطة الطول محكوما بالانبعاج التشوهي الجانبي إذ يحصل تشوه في الوترة مع حدوث انحرافات جانبية في آن واحد. وأما انبعاج العوارض الإنشائية قصيرة الباع فيغلب عليه تشوه كبير في الوترة نتيجة الإجهادات المرتفعة للقص والمتولدة في الوترة. ويَظهَر هذا السلوك الخاص مقترنا دوما بانخفاض كبير في قيمة عامل معدل تدرج العزم (C_b).

تمتد الدراسة لتشمل الانبعاج الجانبي اللدن وذلك في حالة التحميل عند مركز قص العوارض الإنشائية الحديدية المحتوية على ثقوب دائرية في الوترة. وتتناول الدراسة نوعية واحدة من مادة الحديد تسمّى السبيكة 36 (A36)، وذلك وفقا لمقاييس الهيئة الأمريكية للإنشاءات الحديدية (AISC 360–05). وتُجرى الدراسة البارامترية الشاملة والتي تضم 2,268 حالة تحليل لتقييم تأثير أبعاد المقطع العرضي المختلفة ونحافة العارضة وأنواع الأحمال المختلفة وحجم الفتحات في الوترة على سعة الانبعاج اللدن لتلك العوارض وأشكال الانبعاج المصاحبة. وتُناقش نتائج الدراسة اللدنة بتوافق مع حالة الانبعاج المرن وذلك بعرض التغير في عامل معدل تدرج العزم (C_b) بالنسبة إلى العامل (k_e) عديم الوحدة. وبشكل مماثل لما لوحظ من سلوك الانبعاج المرن تتعرض العوارض الإنشائية طويلة الباع والمحتوية على ثقوب دائرية في الوترة لانبعاج جانبي لدن ناشئ عن انبعاج التوائي جانبي أو انبعاج تشوهي جانبي. أما العوارض الإنشائية متوسطة الطول فيكون سلوكها متداخلا ما بين الانبعاج الجانبي وتشوهات القص الموضعية للوترة عند الانبعاج. بينما يكون انبعاج العوارض الإنشائية قصيرة الباع محكوما بتشوه كبير في الوترة ناتج عن الإجهادات المرتفعة للقص والمتولدة في الوترة. ولا يحصل انبعاج جانبي في هذه الحالة، بل يحدث انخفاض كبير في قيمة عامل معدل تدرج العزم (C_b). وتحدد عدة مجالات لمختلف قيم عامل معدل تدرج العزم (C_b) وما يقابلها من أشكال الانبعاج المختلفة، وذلك لمجال واسع من الأبعاد الهندسية المستخدمة في الدراسة

الحالات التحليلية والعملية التي أوردت في استعراض الدراسات السابقة. ويُستخدم النموذج المجهز بعد اختباره في إجراء تحليل الانبعاج الشامل للعوارض الإنشائية الحديدية ذات الثقوب الدائرية في الوترة والتي تستند على ركائز بسيطة، وذلك تحت تأثير عزوم طرفية متساوية، وحمل مركز عند منتصف العارضة، وحمل منتظم التوزيع على طول العارضة. كما تغطي تحاليل الانبعاج المنفذة للعوارض الإنشائية الحديدية ذات الثقوب الدائرية في الوترة مجالا واسعا من الأبعاد الهندسية وأنماط التثقيب المستخدمة بشكل عملي.

تستكشِف الدراسة تأثير مكان التحميل على الانبعاج الالتوائي الجانبي المرن للعوارض الإنشائية التي تأخذ شكل الحرف I وتحتوي على ثقوب دائرية في الوترة وذلك عن طريق إجراء 11,340 حالة تحليل مختلفة. وتتناول التحاليل المنفذة عدة حالات من التحميل عند مستويي الشفتين العلوية والسفلية للعارضة. كما تستكشِف الدراسة تأثير أبعاد المقطع العرضي المختلفة ونحافة العارضة وأنواع الأحمال المختلفة وحجم الفتحات في الوترة والمسافة بين تلك الفتحات على سعة الانبعاج المرن لتلك العوارض. وتستخدَم نتائج التحاليل المنفذة في تقييم التغير في عامل معدل تدرج العزم (C_b) بالنسبة إلى العامل (k_e) عديم الوحدة والذي يربط صلابة الاعوجاج بصلابة الالتواء للعوارض الإنشائية ذات الثقوب الدائرية في الوترة. كما تقارَن هذه النتائج مع تلك التي أوردت في الدراسة الخاصة بالتحميل عند مركز القص للعوارض الإنشائية المحتوية على ثقوب دائرية في الوترة. تُظهر المقارنة أثرا واضحا لإضعاف الاستقرار في حالة التحميل عند مستوى الشفة العلوية للعارضة. وعلى النقيض من ذلك، فإن التحميل عند مستوى الشفة السفلية للعارضة يُعَزِّز الاستقرار الجانبي لتلك للعوارض. علاوة على ذلك، عندما تنبعِج العوارض الإنشائية طويلة الباع والتي تحتوي على ثقوب دائرية في الوترة؛ فإنها تأخذ شكل الانبعاج الالتوائي الجانبي الصِّرف. بينما

حصول انهيار قبل بلوغ سعتها الانثنائية الكاملة. كما يُتوقع أيضا أن تؤثر تلك الثقوب على سلوك هذه العوارض وعلى أشكال الانهيار المحتملة المرتبطة بسلوكها. وعادة ما يكون الاستقرار الجانبي المرن للعوارض الإنشائية الحديدية ذات الثقوب الدائرية في الوترة موضع اهتمام خلال مرحلة التشييد والبناء إذ تكون عناصر التربيط الجانبي للعوارض غير مركبة بعد. أما سلوك الانبعاج الجانبي اللدن لتلك العوارض فهو الأكثر شيوعا من ناحية عملية؛ وذلك بسبب بلوغ الألياف الخارجية للعارضة حد المرونة قبل بدء الانبعاج. وتتأثر السعة الحِملية لهذه العوارض بالانبعاج الكلي للعارضة، والانبعاج الموضعي لعناصر المقطع العرضي للعارضة، كما تتأثر أيضا بوجود الفجوات في المقطع العرضي والناشئة عن ثقوب الوترة. ولسوء الحظ فإن مجموعات قواعد التصميم الحالية لا تعطي إرشادات صريحة عن كيفية التعامل مع الانبعاج الالتوائي الجانبي للعوارض الإنشائية الحديدية المثقبة.

يَهتم البحث العلمي المقدم بنقص المعلومات المتعلقة بالاستقرار الجانبي للعوارض الإنشائية الحديدية ذات الثقوب الدائرية في الوترة وذلك تحت تأثير الانثناء. كما يستعرض هذا البحث الدراسات السابقة العملية والعددية المتعلقة بالسلوك الإنشائي للعوارض الإنشائية الحديدية المثقبة مع التركيز على سلوك الانبعاج للعوارض الإنشائية الحديدية التي تأخذ شكل الحرف I وتحتوي على ثقوب سداسية أو دائرية في الوترة. وتجرَى الدراسة عدديا باستعمال النمذجة المفصلة وذلك بتطوير نموذج العنصر المحدد ثلاثي الأبعاد باستخدام برنامج التصميم الشامل "ANSYS". ويُؤخذ بعين الاعتبار موضوع اللاخطية في المادة والشكل الهندسي للنموذج المجهز. كما يَتم اتخاذ شبكة مختارة للنموذج المستخدم لتسمح بتشكل مختلف الانحرافات والدورانات المصاحبة لأشكال الانبعاج الكلي والموضعي لتلك العوارض. ويُختبر النموذج المجهز عن طريق استخدامه في محاكاة مختلف

ملخص الرسالة

تمثل العناصر الإنشائية الحديدية التي تأخذ شكل الحرف I المُكوِّن الإنشائي الرئيسي في معظم المنشآت الحديدية. وقد استخدمت المقاطع الحديدية التي تأخذ شكل الحرف I وتحتوي على وترة مثقبة كعناصر إنشائية منذ الحرب العالمية الثانية في محاولة لتحسين السلوك الانثنائي للمقاطع الحديدية التقليدية ذات الوترة المصمتة بدون زيادة في كلفة مادة الحديد. وفي الممارسات الهندسية عموما يُستخدَم نوعان من ثقوب الوترة على نحو شائع، وهما السداسية والدائرية. وتهدف عملية التثقيب أساسا إلى إنتاج مقاطع أقوى وذلك بزيادة ارتفاع الوترة وبالتالي تحقيق سعة انثنائية أعلى للمحور الرئيسي لتلك المقاطع مقارنة مع المقاطع ذات الوترة المصمتة التي لها نفس الوزن. ولا يقتصر الأمر على ذلك، فهي تسمح بمرور التمديدات الخدمية عبر تلك الثقوب وبالتالي تحقق الاستخدام الأمثل لمادة الحديد الإنشائية المكلفة. كما أن المظهر الجمالي لتلك العناصر الإنشائية ذات الوترة المثقبة يُغري باستخدامها ويجعلها مكونات جوهرية في تشييد المنشآت الحديدية المكشوفة. وقد انضم إلى هذه الميزات التطورُ الهائل في معدات التصنيع المحوسبة مما أدى إلى الانتشار الواسع في استخدام العناصر الإنشائية الحديدية ذات الوترة المثقبة بأشكالها المتنوعة لتناسب حالات التحميل المتعددة في مختلف التطبيقات الإنشائية.

في الواقع دوما ما تُجذب التصاميمُ الإنشائية بزيادة ارتفاع المقطع المحتوي على ثقوب دائرية في الوترة مقارنة مع نظيره المحتوي على وترة مصمتة مما يُحَسِّن خصائصه الإنشائية. ومع ذلك تجب ملاحظة أن عدم التماثل بين المقاطع العرضية للعارضة الإنشائية نتيجة وجود الثقوب الدائرية في الوترة قد يؤدي إلى أثر عكسي على السعة الانثنائية لتلك العوارض وذلك في حالة

جامعة الإمارات العربية المتحدة
United Arab Emirates University

UAEU

برنامج ماجستير الهندسة المدنية
قسم الهندسة المدنية والبيئية
كلية الهندسة
جامعة الإمارات العربية المتحدة

عنوان الرسالة:

الانبعاج الالتوائي الجانبي المرن–اللدن للعوارض الإنشائية الحديدية المحتوية على ثقوب في الوترة

اسم الباحث: **محمد إقبال محمد هشام مارتيني**

أسماء المشرفين:

د. عمرو محمود سويدان
الأستاذ المساعد في الهندسة الإنشائية
قسم الهندسة المدنية والبيئية بكلية الهندسة
جامعة الإمارات العربية المتحدة
الإمارات العربية المتحدة

د. خالد محمود الصاوي
الأستاذ المشارك في الهندسة الإنشائية
قسم الهندسة المدنية والبيئية بكلية الهندسة
جامعة الإمارات العربية المتحدة
الإمارات العربية المتحدة